SURFACTANTS IN NONPOLAR OILS: AGENTS OF ELECTRIC CHARGING AND NANOGEL TEMPLATES

A Dissertation
Presented to
The Academic Faculty

By

Qiong Guo

In Partial Fulfillment
Of the Requirements for the Degree
Doctor of Philosophy in the
School of Chemical & Biomolecular Engineering

Georgia Institute of Technology

May 2012

SURFACTANTS IN NONPOLAR OILS: AGENTS OF ELECTRIC CHARGING AND NANOGEL TEMPLATES

Approved by:

Dr. Sven Behrens, Advisor
School of Chemical & Biomolecular Engineering
Georgia Institute of Technology

Dr. Yulin Deng
School of Chemical & Biomolecular Engineering
Georgia Institute of Technology

Dr. William Koros
School of Chemical & Biomolecular Engineering
Georgia Institute of Technology

Dr. Carson Meredith
School of Chemical & Biomolecular Engineering
Georgia Institute of Technology

Dr. Elisa Riedo
School of Physics
Georgia Institute of Technology

Date Approved: February 14th, 2012

To my lovely daughter, Cecilia Sun.

ACKNOWLEDGEMENTS

I would like to express my sincere gratitude to my advisor Dr. Sven Behrens for his invaluable guidance and support. His continuous encouragement helped me to be creative and innovative at research. I always admire his enthusiasm, solid knowledge, strong work ethic, and personal attitude that will continue as a great inspiration source for me. I could not have imagined having a better advisor and mentor for my Ph.D. life and research. I would like to thank Dr. Yulin Deng, Dr. William Koros, Dr. Carson Meredith, and Dr. Elisa Riedo for serving on my committee and providing insightful comments and valuable suggestions. The funding support from the Camille and Henry Dreyfus New Faculty Awards Program is also greatly appreciated.

I am grateful to all the past and present members, Dr. Virendra Singh, Dr. Adriana San Miguel, Carlos Espinosa, Hongzhi Wang, Ishtiaque Ahmed, and Joohyung Lee, for their great insights and generous help. They are labmates, more like friends and family, making my graduate life a wonderful learning experience.

I would also like to thank Dr. Niren Murthy, and Dr. Xinghai Ning and Dr. Scott Wilson in Murthy Group for discussions, research guidance, excellent advices, and chemicals support during the collaboration of nanogel synthesis.

My special thanks belong to my family for their love and support. None of this would have been possible without endless patience, encouragement, and understanding of my husband, Zhi Sun, and my parents in China.

TABLE OF CONTENTS

LIST OF TABLES

LIST OF FIGURES

SUMMARY

The formation of mobile and surface-bound electric charges in aqueous environments has been widely studied; by contrast, charge formation in nonpolar media is far from understood. The existence of charged mobile species and significant surface charging in nonpolar solutions of ionic surfactants are well documented, but there is no consensus about the mechanisms of charging, and very few studies acknowledge that even nonionic, non-dissociable surfactants can promote charging in nonpolar liquids. The present work primarily aims at expanding ourunderstanding of surfactant mediated electric charging in nonpolar liquids. This task is approached by comparing the electrostatic effects of an ionic and nonionic surfactant that form very similar micelles. The surfactants' ability to raise the conductivity in low dielectric media is analyzed first. Next, the tendency of both types of surfactants to impart surface charges on polymer particles in nonpolar liquids is studied by electrophoresis for particles of different material and surface functionalization. Independent evidence both for particle charging and for the formation of screening ions in solution is obtained by analyzing the pair interaction energy of suspended polymer particles. The results of this study provide valuable clues about the mechanisms of charge separation in the nonpolar liquid bulk and on particle surfacesat surfactant concentrations above and below the critical micelle concentration.

Besides the fundamental understanding the charging phenomena in nonpolar oils associated with surfactants, self-assembled spherical reverse micelles are described as a

novel tool to synthesize nano-sized hydrogel particles, highly crosslinked networks of water-soluble polymers. In order to achieve good reproducibility and particle size control, the hydrophilic cores of reverse micelles/microemulsions are utilized as templates for the polymerization process. More excitingly, copper-free Click chemistry is introduced in synthesizing nanogels templated by swollen reverse micelles. This nanogel synthesis allows for even better control of the particle size while avoiding metal catalysts and free radicals that are considered hazardous for most biomedical applications.

CHAPTER 1

INTRODUCTION

1.1 Overview and concepts

The possibility to introduce and control electric charge and to understand charging mechanisms in nonpolar media has great relevance to scientific studies and industrial applications, for examples, in the prevention of explosion hazards in petroleum handling due to the flow electrification [1-3], in the context of asphaltene deposition in crude oil processing [4], in the design of electrophoretic displays [5, 6], liquid toners [7], and drug delivery systems [8], or for the development of detergents [9] and novel crystalline materials [10].

Electric charges are ubiquitous in aqueous environments and their formation mechanisms are widely studied and reasonably well understood. In very nonpolar solvents, by contrast, the separation of opposite charges requires a prohibitively large energetic cost that thermal forces cannot provide [9]. Yet, stable mobile charges are nonetheless found in the presence of ionic surfactant additives [11-19], a phenomenon often ascribed to the disproportionation of reversed micelles [20, 21]; a process in which two neutral micelles exchange a charge to form a pair of oppositely charged micelles. Important details, such as the role of the ionic surfactant headgroups in micellar charging or the electrostatic behavior of surfactant solutions upon crossing the critical micelle concentration (CMC) still remain unclear. Moreover, recently reported charging phenomena caused by nonionizable surfactants have not yet been widely acknowledged

and much less explained. Prior to this work, controversial claims had been published that nonionizable surfactants can promote charging in nonpolar media as effectively as ionic ones, but no study had ever compared the charging effect of an ionic surfactant and a surfactant without ionizable headgroup, but similar aggregation behavior.

Liquids that support the mobile electric charges typically also promote the net electric charging of wetted solid surfaces. In polar solvents, solid surfaces can acquire charges via the dissociation of surface-bound groups [22-26], similar to the generation of small ions from a bulk dissociation reaction, via partial dissolution of a crystalline solid [27-32] or through the adsorption of charged species [33-35]. In all cases, the charging of colloidal particles is affected by the surface chemistry and the surrounding liquid phase in ways that are generally understood. Surface and particle charging has also been observed in nonpolar surfactant solutions, but here our knowledge is almost purely empirical. Several mechanisms of surfactant-mediated surface charging in nonpolar media have been proposed that typically require the presence of reverse surfactant micelles. In one case these micelles act as acceptors of counterions from a surface dissociation [36]; in another case, micelles charged independently of the surface by disproportionation carry charges to the surfaces via competitive adsorption [16]. Yet another tentative explanation invokes charge transfer driven by acid-base interactions between the solid surface and the surfactant. Neither of these mechanisms has yet been verified conclusively, nor has the presence of micelles been firmly established as a prerequisite for surface charging. Some clarification is obviously needed.

Recent interest in reverse surfactant micelles has been sparked not just by their role in generating electric charges in nonpolar media, but also by their use as “nano-

reactors" for aqueous reactants and templates for nano-sized hydrogel particles. These "nanogels" are networks of water-soluble polymers, that can be conveniently assembled and crosslinked in the hydrophilic core of swollen reverse micelles. Such nanogels have great promise for applications in biomedical engineering [37-39], drug delivery [40-42], consumer products [43], and the development of novel materials and technologies [44-47].

Polymerization in reverse microemulsion droplets (swollen reverse micelles) potentially allows the control of the hydrogel dimension and size distribution, thus avoiding the variations in particle morphology associated with alternative methods relying on polymer self-assembly [48-51] and the low throughput of microfluidics methods [52-54]. We pioneer the use of microemulsion templates for nanogel preparation by copper-free azide-alkyne cycloaddition ("click" reaction). The ring-strain promoted "click" reaction avoids the toxicologically undesirable use of free radicals and metal catalysts in the polymerization process, and guarantees a fast reaction rate and improved size control.

1.2 Motivation and objectives

Although the observed charging effects induced by surfactants in nonpolar media can be dramatic, the underlying mechanisms are far from understood. The lack of understanding motivates us to investigate the role of nonionizable surfactants as "charge control agents" and any distinction from the behavior of ionic surfactants. A part of this investigation involves relating the size, shape and composition of water-swollen micelles to their electrostatic properties. We see an opportunity to further apply the gained experience with swollen micelles toward their use as polymerization reactors in a novel type of nanogel synthesis with unique advantage for biomedical applications.

Our objectives are to understand the mechanisms, in which the surfactant additives can

a) Introduce mobile ions in nonpolar liquids;
b) Promote surface charging and charge screening of suspended particles in nonpolar dispersions;
c) Provide a template for nanogel particles synthesized via copper-free click reaction.

So far, scientific studies of charging in nonpolar solvents mostly focus on solutions of ionic surfactants. We aim to compare the electric phenomena caused by nonionic surfactants with the better-known behavior of aqueous electrolytes and ionic surfactants. The findings in a) and b) will help us understand the intriguing and commonly ignored role played by nonionizable surfactants. Not limited to the nonionic surfactants, the participation of surfactants in c) realizes the novel pathway to obtain controllable synthesis of nanogels.

1.3 Thesis organization

Systematic experimental studies of surfactant mediated conductivity in alkane-based solutions, and a detailed analysis of the charge formation promoted by a nonionic surfactant will be presented in *Chapter 2* (Objective a).

The surfactant mediated charging of polymer particles in alkanes will be discussed in *Chapter 3* (Objective b). A careful analysis of electrophoretic particle mobilities in electric fields of different magnitude is used to study the particles' electrostatic surface potential and compare it with the potential of the same particles in aqueous media. Systematic variation of the surfactant type and concentration, the particle material, and the functional surface groups, make it possible to estimate the relative importance of surface dissociation, acid-base interactions between the surfactant and the particle material, and charge screening by the mobile ions responsible for the solution conductivity. Measurements of the pair interaction energy for PMMA sulfate particles in hexane solutions of the nonionic surfactant Span 85 suggest a screened Coulomb interaction with particle charges and Debye screening lengths that corroborate both the particle charging observed by electrophoresis and the presence of mobile ions seen by conductometry in the previous chapter.

Chapter 4 introduces the procedure of preparing nanogels in reverse microemulsion via "click" reaction (Objective c), and compares the process to the formation of nanogels by free radical polymerization of acrylate-terminated prepolymers.

Chapter 5 summaries the primary contribution of this research and presents recommendations for further investigation.

1.4 References

1. Kinkenberg, A. & van der Minne, J.L. *Electrostatics in the Petroleum Industry*. *Elsevier, New York* (1958).

2. Touchard, G. Flow electrification of liquids. *Journal of Electrostatics* **51-52**, 440-447 (2001).

3. Tolpekin, V.A., van den Ende, D., Duits, M.H.G. & Mellema, J. Flow Electrification in Nonaqueous Colloidal Suspensions, Studied with Video Microscopy. *Langmuir* **20**, 8460-8467 (2004).

4. Leon, O., Rogel, E., Espidel, J. & Torres, G. Asphaltenes: Structural characterization, self-association, and stability behavior. *Energy & Fuels* **14**, 6-10 (2000).

5. Comiskey, B., Albert, J.D., Yoshizawa, H. & Jacobson, J. An electrophoretic ink for all-printed reflective electronic displays. *Nature* **394**, 253-255 (1998).

6. Chen, Y. *et al.* Flexible active-matrix electronic ink display. *Nature* **423**, 136-136 (2003).

7. Pearlstine, K., Page, L. & Elsayed, L. Mechanism of Electric Charging of Toner Particles in Nonaqueous Liquid with Carboxylic-Acid Charge Additives. *Journal of Imaging Science* **35**, 55-58 (1991).

8. Jones, S.A., Martin, G.P. & Brown, M.B. Manipulation of beclomethasone-hydrofluoroalkane interactions using biocompatible macromolecules. *Journal of Pharmaceutical Sciences* **95**, 1060-1074 (2006).

9. van der Hoeven, P.H.C. & Lyklema, J. Electrostatic Stabilization in Nonaqueous Media. *Advances in Colloid and Interface Science* **42**, 205-277 (1992).

10. Leunissen, M.E. *et al.* Ionic colloidal crystals of oppositely charged particles. *Nature* **437**, 235-240 (2005).

11. Morrison, I.D. Electrical charges in nonaqueous media. *Colloids and Surfaces A: Physicochemical and Engineering Aspects* **71**, 1-37 (1993).

12. Hamada, K., Ikeda, T., Kawai, T. & Kon-No, K. Ionic Strength Effects of Electrolytes on Solubilized States of Water in AOT Reversed Micelles. *Journal of Colloid and Interface Science* **233**, 166-170 (2001).

13. Briscoe, W.H. & Horn, R.G. Direct Measurement of Surface Forces Due to Charging of Solids Immersed in a Nonpolar Liquid. *Langmuir* **18**, 3945-3956 (2002).

14. Michel, E., Baur, R. & Macholdt, H.T. Charge stabilizers: properties and applications. *Journal of Electrostatics* **51-52**, 91-96 (2001).

15. Sainis, S.K., Merrill, J.W. & Dufresne, E.R. Electrostatic Interactions of Colloidal Particles at Vanishing Ionic Strength. *Langmuir* **24**, 13334-13337 (2008).

16. Roberts, G.S., Sanchez, R., Kemp, R., Wood, T. & Bartlett, P. Electrostatic Charging of Nonpolar Colloids by Reverse Micelles. *Langmuir* **24**, 6530-6541 (2008).

17. Morrison, I.D., Thomas, A.G. & Tarnawskyj, C.J. A method to measure the average charge to mass ratio of particles in low-conductivity media. *Langmuir* **7**, 2847-2852 (1991).

18. Kornbrekke, R.E., Morrison, I.D. & Oja, T. Electrophoretic Mobility Measurements in Low Conductivity Media. *Langmuir* **8**, 1211-1217 (1992).

19. Shen, Y. & Duhamel, J. Micellization and Adsorption of a Series of Succinimide Dispersants. *Langmuir* **24**, 10665-10673 (2008).

20. Denat, A., Gosse, B. & Gosse, J.P. Electrical conduction of solutions of an ionic surfactant in hydrocarbons. *Journal of Electrostatics* **12**, 197-205 (1982).

21. Strubbe, F., Verschueren, A.R.M., Schlangen, L.J.M., Beunis, F. & Neyts, K. Generation current of charged micelles in nonaqueous liquids: Measurements and simulations. *Journal of Colloid and Interface Science* **300**, 396-403 (2006).

22. Diaz, A., Fenzelalexander, D., Wollmann, D. & Barker, J.A. IMPORTANCE OF DISSOCIATED IONS IN CONTACT CHARGING. *Langmuir* **8**, 2698-2706 (1992).

23. de Groot, J., Koper, G.J.M., Borkovec, M. & de Bleijser, J. Dissociation behavior of poly(maleic acid): Potentiometric titrations, viscometry, pulsed field gradient NMR, and model calculations. *Macromolecules* **31**, 4182-4188 (1998).

24. Chatelier, R.C., Hodges, A.M., Drummond, C.J., Chan, D.Y.C. & Griesser, H.J. Determination of the Intrinsic Acid-base Dissociation Constant and Site Density of Ionizable Surface Groups by Capillary Rise Measurements. *Langmuir* **13**, 3043-3046 (1997).

25. Vinod, M.P., Mandle, A.B., Sainkar, S.R. & Vijayamohanan, K. Effect of gelling on the surface structure of a porous lead electrode in sulfuric acid. *Journal of Applied Electrochemistry* **27**, 462-468 (1997).

26. Behrens, S.H., Christl, D.I., Emmerzael, R., Schurtenberger, P. & Borkovec, M. Charging and aggregation properties of carboxyl latex particles: Experiments versus DLVO theory. *Langmuir* **16**, 2566-2575 (2000).

27. Franks, G.V. & Gan, Y. Charging behavior at the alumina-water interface and implications for ceramic processing. *Journal of the American Ceramic Society* **90**, 3373-3388 (2007).

28. Brown, G.E. *et al.* Metal oxide surfaces and their interactions with aqueous solutions and microbial organisms. *Chemical Reviews* **99**, 77-174 (1999).

29. Brown, G.E. Surface science - How minerals react with water. *Science* **294**, 67-+ (2001).

30. Hiemstra, T., Venema, P. & VanRiemsdijk, W.H. Intrinsic proton affinity of reactive surface groups of metal (hydr)oxides: The bond valence principle. *Journal of Colloid and Interface Science* **184**, 680-692 (1996).

31. Rosenqvist, J., Persson, P. & Sjoberg, S. Protonation and charging of nanosized gibbsite (alpha-Al(OH)(3)) particles in aqueous suspension. *Langmuir* **18**, 4598-4604 (2002).

32. Kosmulski, M. The pH-dependent surface charging and the points of zero charge. *Journal of Colloid and Interface Science* **253**, 77-87 (2002).

33. Sefcik, J., Verduyn, M., Storti, G. & Morbidelli, M. Charging of Latex Particles Stabilized by Sulfate Surfactant. *Langmuir* **19**, 4778-4783 (2003).

34. Lee, E.M. & Koopal, L.K. Adsorption of cationic and anionic surfactants on metal oxide surfaces: Surface charge adjustment and competition effects. *Journal of Colloid and Interface Science* **177**, 478-489 (1996).

35. Iruthayaraj, J. *et al.* Adsorption of low charge density polyelectrolyte containing poly(ethylene oxide) side chains on silica: Effects of ionic strength and pH. *Macromolecules* **38**, 6152-6160 (2005).

36. Hsu, M.F., Dufresne, E.R. & Weitz, D.A. Charge Stabilization in Nonpolar Solvents. *Langmuir* **21**, 4881-4887 (2005).

37. Christensen, L.H., Breiting, V.B., Aasted, A., Jørgensen, A. & Kebuladze, I. Long-Term Effects of Polyacrylamide Hydrogel on Human Breast Tissue. *Plastic and Reconstructive Surgery* **111**, 1883-1890 1810.1097/1801.PRS.0000056873.0000087165.0000056875A (2003).

38. Langer, R. & Vacanti, J.P. Tissue Engineering. *Science* **260**, 920-926 (1993).

39. Brandl, F., Sommer, F. & Goepferich, A. Rational design of hydrogels for tissue engineering: Impact of physical factors on cell behavior. *Biomaterials* **28**, 134-146 (2007).

40. Langer, R. Perspectives: Drug delivery - Drugs on target. *Science* **293**, 58-59 (2001).

41. Missirlis, D., Tirelli, N. & Hubbell, J.A. Amphiphilic hydrogel nanoparticles. Preparation, characterization, and preliminary assessment as new colloidal drug carriers. *Langmuir* **21**, 2605-2613 (2005).

42. Huang, G. *et al.* Controlled drug release from hydrogel nanoparticle networks. *Journal of Controlled Release* **94**, 303-311 (2004).

43. Jones, L. *et al.* Lysozyme and Lipid Deposition on Silicone Hydrogel Contact Lens Materials. *Eye & Contact Lens* **29**, S75-S79 (2003).

44. Okay, O. & Oppermann, W. Polyacrylamide-clay nanocomposite hydrogels: Rheological and light scattering characterization. *Macromolecules* **40**, 3378-3387 (2007).

45. Peppas, N.A., Hilt, J.Z., Khademhosseini, A. & Langer, R. Hydrogels in biology and medicine: From molecular principles to bionanotechnology. *Advanced Materials* **18**, 1345-1360 (2006).

46. Miyazaki, S., Endo, H., Karino, T., Haraguchi, K. & Shibayama, M. Gelation mechanism of poly(N-isopropylacrylamide)-clay nanocomposite gels. *Macromolecules* **40**, 4287-4295 (2007).

47. Haraguchi, K. & Song, L.Y. Microstructures formed in co-cross-linked networks and their relationships to the optical and mechanical properties of PNIPA/clay nanocomposite gels. *Macromolecules* **40**, 5526-5536 (2007).

48. Nishikawa, T., Akiyoshi, K. & Sunamoto, J. Macromolecular complexation between bovine serum albumin and the self-assembled hydrogel nanoparticle of hydrophobized polysaccharides. *Journal of the American Chemical Society* **118**, 6110-6115 (1996).

49. Nishikawa, T., Akiyoshi, K. & Sunamoto, J. Supramolecular assembly between nanoparticles of hydrophobized polysaccharide and soluble-protein complexation between the self-aggregate of cholesterol-bearing pullulan and alpha-chymotrypsin. *Macromolecules* **27**, 7654-7659 (1994).

50. Lee, I. & Akiyoshi, K. Single molecular mechanics of a cholesterol-bearing pullulan nanogel at the hydrophobic interfaces. *Biomaterials* **25**, 2911-2918 (2004).

51. Akiyoshi, K. *et al.* Controlled association of amphiphilic polymers in water: Thermosensitive nanoparticles formed by self-assembly of hydrophobically modified pullulans and poly(N-isopropylacrylamides). *Macromolecules* **33**, 3244-3249 (2000).

52. Zhang, H., Tumarkin, E., Sullan, R.M.A., Walker, G.C. & Kumacheva, E. Exploring microfluidic routes to microgels of biological polymers. *Macromolecular Rapid Communications* **28**, 527-538 (2007).

53. Zhang, H. *et al.* Microfluidic production of biopolymer microcapsules with controlled morphology. *Journal of the American Chemical Society* **128**, 12205-12210 (2006).

54. De Geest, B.G., Urbanski, J.P., Thorsen, T., Demeester, J. & De Smedt, S.C. Synthesis of monodisperse biodegradable microgels in microfluidic devices. *Langmuir* **21**, 10275-10279 (2005).

CHAPTER 2

IONIZATION IN NONPOLAR LIQUIDS INDUCED BY SURFACTANTS

2.1 Backgrounds and theories

2.1.1 Surfactants and their self-assembled aggregates

2.1.1.1 Basic properties of surfactants

Surfactants are amphiphilic organic compounds containing both hydrophilic, oil insoluble heads, and hydrophobic, oil soluble tails.

Surfactants are widely used to lower the surface tension of a liquid and the tension of liquid-liquid or liquid-solid interfaces, with the applications including emulsifiers, detergents, dispersants, and wetting agents, among others. Because of their amphiphilic nature, surfactants will migrate to the water-air or water-oil interfaces, where the hydrophilic head groups remain in water while the hydrophobic tail groups extend out of the water phase into the air or oil phase. This interfacial assembly is responsible by the reduction in interfacial tension.

Above a threshold surfactant concentration known as the critical micelle concentration (CMC), self-assembly of surfactant molecules also takes place in the solution bulk. Driven by the unfavorable interaction of solvent molecules with the surfactant's solvophobic part, surfactant molecules form aggregates with a solvophobic core and a solvophilic shell. These aggregates are referred as (direct) micelles when

surfactants assemble in water, and reverse micelles when they assemble in oil, which will be described in the next section.

Surfactants are often classified according to the composition of their hydrophilic head groups. Ionic surfactants are the ones whose head carries an electric charge: if the head group is negatively charged, the surfactant is called anionic (sulfate, sulfonate, phosphate, carboxylate, etc.); if the head group is positively charged, the surfactant is called cationic (primary, secondary, or tertiary amines, etc.); and if the head groups contain two opposite charges, the surfactant is called zwitterionic (both anionic and cationic groups). Nonionic surfactants are the ones without charged heads. This includes surfactants with a very low ionization tendency in water, such as fatty alcohols, and surfactants without any ionizable groups, such as sorbitan alkyl esters or many ethoxylates. The research reported in this thesis focuses on comparing the behavior of ionic surfactants and nonionic surfactants without ionizable groups.

2.1.1.2 Micelles

In aqueous solution, surfactants form micelles in which the hydrophobic hydrocarbon groups tend to stick together and the hydrophilic head groups form a shield to protect the aggregates of hydrophobic tails from external interaction with the surrounding water. These surfactant micelles are usually formed above the critical micellar concentration (CMC), a narrow concentration window separating the low concentration regime, in which the surfactant dissolves molecularly, from the micellar regime, in which added surfactant predominantly gets incorporated into micelles without significantly raising the concentration of unaggregated molecules. Near the CMC, the

surfactant micelles tend to have spherical shape, whereas at higher concentrations spherical, rod-like or lamellar structures can form, depending on the surfactant architecture [1, 2].

Surfactants in nonpolar solutions assemble into the corresponding inverse structures (reverse micelles), exposing the hydrophobic tails to the solvent and burying the hydrophilic polar heads in the micelle core. (Reverse) micellization in nonpolar media thus mirrors the formation of the (direct) micelles in water-based system, but there are two subtle differences observed empirically: the CMC in nonpolar solutions tends to be higher and less sharply defined than in aqueous system, meaning that the transition between the dilute and micellar concentration regime is typically somewhat more gradual in nonpolar than in aqueous solutions, and values for the aggregation number, i.e. the average number of surfactant molecules per aggregate, are typically lower for nonpolar systems.

Thermodynamic characterizations of surfactant solutions are very important to help us better understand and study the behaviors of surfactants in liquid [3]. The CMC and aggregation number are two key characteristics for the surfactant solution. Various properties, such as interfacial tension, structure and dimension of self-assembled entities, and viscosity, would change as the surfactant concentration crosses the CMC. These changes in surfactant solutions provide different CMC determination methods by measuring a change in, for instance, the UV-vis spectrum, the fluorescence emission spectrum, the electrical conductivity [4, 5], the size of growing surfactant aggregates, and the interfacial tension, etc. [6-8] Typical experiments to determine the mean aggregation number involve luminescence quenching [9, 10], surface tension isotherm [11], light

scattering [12, 13], etc.

2.1.1.3 Microemulsions

Micelles in aqueous solutions present as a hydrophobic core and hydrophilic shell structure. Nonpolar oils, immiscible with bulk water, can be solubilized through uptake by the hydrophobic micelle cores, thus swelling the micelles. Solutions of swollen micelles are often referred to as microemulsions. The defining difference between microemulsion droplets and surfactant-covered droplets of a regular emulsion is that the former are thermodynamically stable. Similarly, water can be solubilized in nonpolar surfactant solutions by the incorporation in the hydrophilic cores of the reverse micelles, thereby increasing the micelle size and turning a nonpolar surfactant solution into a reverse microemulsion.

Because of their thermodynamic stability, microemulsions form spontaneously upon mixing their constituents, whereas are ordinary emulsions generally require vigorous agitation for droplets to form. Because of their typically small (submicron) droplet size, microemulsions tend to be transparent. The basic types of microemulsions are direct (oil dispersed in water, o/w) and reverse (water dispersed in oil, w/o) based on the ratio of oil-and-water liquid phases and self-assembly of amphiphilic surfactants.

2.1.2 Electric charges in low dielectric media

2.1.2.1 Electric charge formation and stabilization in liquids

In aqueous and other polar liquids environments, the mechanisms of charge formation and stabilization haven been widely studied and are reasonably well-

understood [14-16]. Ionogenic compounds (molecules, salts, or complexes) can dissociate into smaller charged entities. The polar solvent molecules form a "solvation layer" around the charged species, which keeps the oppositely charged centers at a distance where the Coulombic attraction is balanced or outweighed by the random forces of thermal motion. Thus, the protection from "solvation layer" allows the separation of opposite sign of charges and further stabilizes them.

In very non-polar environments, by contrast, the low dielectric constant makes the energetic cost of separating charges prohibitively large [17]. A medium's electrostatic resistance to ion separation is often quantified by the liquid's Bjerrum length [18],

$$\lambda_B = e^2/4\pi\varepsilon\varepsilon_0 kT \ . \qquad \text{Equation 2-1}$$

The Bjerrum length, as expressed in Equation 2-1, is the separation distance at which two embedded opposite elementary charges attract each other with energy kT , or alternatively, the effective diameter of a monovalent ion with Born energy kT . Thanks to its large dielectric constant ($\epsilon \approx 80$), water has a low Bjerrum length ($\lambda_B = 0.7$ nm), supporting the dissociation of small ions, the amount of which is directly linked to the conductivity of fluid. In contrast, very nonpolar liquids generally have dielectric constants around 2 and the corresponding Bjerrum lengths over 28 nm, which is much larger than a typical salt ion.

The Born energy [14],

$$U_B = (Ze)^2/8\pi\varepsilon\varepsilon_0 a \ , \qquad \text{Equation 2-2}$$

is the cost in free energy of introducing an ion of radius *a* and charge *Ze* in a medium of dielectric constant ε. Here, *e* is the elementary charge, *Z* the ion valency with the value of

1 for the case of monovalent ions, which will be considered the default situation in the following, and ε_0 the dielectric permittivity in vacuum. In an aqueous environment, the Born energy is typically smaller than or comparable to the available thermal energy kT [17], which makes dissociation happen spontaneously. The effective ion radius a increases in solution due to a protective solvation shell. This reduces the Born energy and keeps the oppositely charged ions apart. However, the Born energy of common oppositely charged ions in low dielectric media typically far exceeds the available thermal energy [17]. Therefore, nonpolar liquids are a very charge-hostile environment with very low conductivity, usually about five orders of magnitude lower than that of pure water.

2.1.2.2 Electric conductivity raised by surfactants in nonpolar liquids

For the reasons discussed above mobile ions are generally considered to play no role in nonpolar liquids at room temperature. This conventional wisdom, however, is often contradicted in the presence of surfactant additives, which can, in some cases, induce strong electric charging effects and electrostatic interaction in nonpolar media [19-31]. While experiment evidence for such surfactant-mediated charging abounds, their scientific explanation is still a matter of ongoing research.

Morrison [19] firmly established for the first time that surfactant additives (or impurities) can give rise to electric charging effects. This was followed by great efforts dedicated to finding the existence of mobile charges in the presence of surfactants and to understand the charging effects on the suspended solid surfaces by such mobile charged species. To date, numerous ionic surfactants [19, 25, 31-34] and some select nonionic

surfactants with ionizable functional groups [24, 35, 36] have been identified as powerful "charge control agents" [33, 37-39]. It has been shown that these surfactants can raise the conductivity of nonpolar liquids by many orders of magnitude [34] and cause surface charging and charge screening for suspended particles [22, 24-26].

Three different charge formation mechanisms have been suggested, based on data gathered from conductivity studies. The first mechanism considers the injection of charge into the bulk liquid by the electrodes used to probe the conductivity [40]. However, this mechanism cannot explain the raise of conductivity in the case of applying sufficiently low field strength. The second proposed mechanism concerns the spontaneous dissociation of ionic surfactant molecules [34],

$$A^+B^- \leftrightarrow A^+ + B^-, \qquad \text{Equation 2-3}$$

which is so strongly suppressed by the unfavorable balance of electrostatic and thermal energy as discussed before.

The third and most important hypothetical charging mechanism is the disproportionation of reversed micelles [29, 41],

$$2A \longrightarrow A^+ + A^-, \qquad \text{Equation 2-4}$$

and typically this mechanism is suggested for the micelles of ionic surfactants.

Strubbe [29] proposec a general scheme for the generation of charges by disproportionation of reversed micelles (seen in Figure 2-1). A hypothetical intermediate structure forms via the collision of two neutral reverse micelles and then splits up into two oppositely charges micelles. In the context of water-in-oil micro-emulsions, the

exchange of charge between neutral entities explains the dependence of conductivity on droplet size and volume fraction [42, 43]. The comparably large size of the microemulsion droplets provides the necessary separation to keep the charge species apart by reaching the Bjerrum length of nonpolar liquids. Thus, thermal motion is enough to keep the separated ions fairly stable. This charging pathway may also apply to reverse micelles of surfactants, especially since there is always some amount of water in the hydrophilic core. Figure 2-2 illustrates the common view of the surfactant hydrophilic core as a counterions reservoir in the microemulsion droplet or swollen micelle. This reservoir of mobile charge would appear crucial for the ability of micelles to exchange charges. The counterions to ionic surfactant headgroups are the suggested origin of the charge in the reverse micelles according to the disproportionation pathway sketched in Figure 2-1.

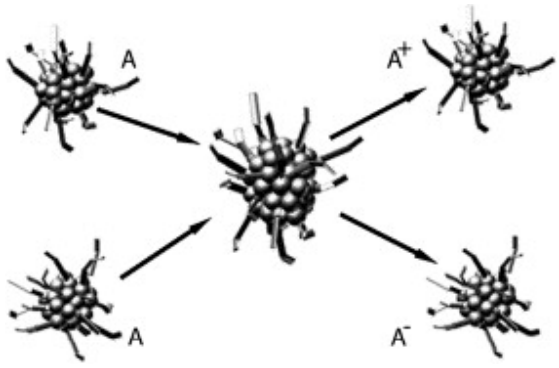

Figure 2-1 Schematic of reversed micelle disproportionation via a hypothetical intermediate structure [29].

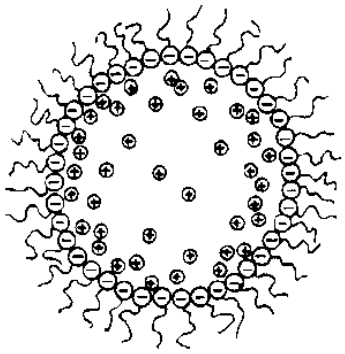

Figure 2-2 An aqueous microemulsion droplet stabilized by anionic surfactant [42].

Clues as to whether bulk charging occurs via charge dissociation (Equation 2-3) or disproportionation (Equation 2-4) can be inferred from conductivity measurements. The conductivity increase observed by Sainis [34] involves the regions both below and above the CMC of AOT (sodium bis(2-ethylhexyl) sulfosuccinate) in hexadecane, as shown in Figure 2-3. The conductivity vs. concentration in region I scales like

$$\sigma \sim [AOT]^{1/2} \qquad \text{Equation 2-5}$$

which is consistent with the mass action law for the dissociation of individual surfactant molecules; by contrast, the relationship

$$\sigma \sim [AOT] \qquad \text{Equation 2-6}$$

found in regime III (above the CMC), is consistent with the mass action law for the charge disproportionation of reverse micelles (RM).

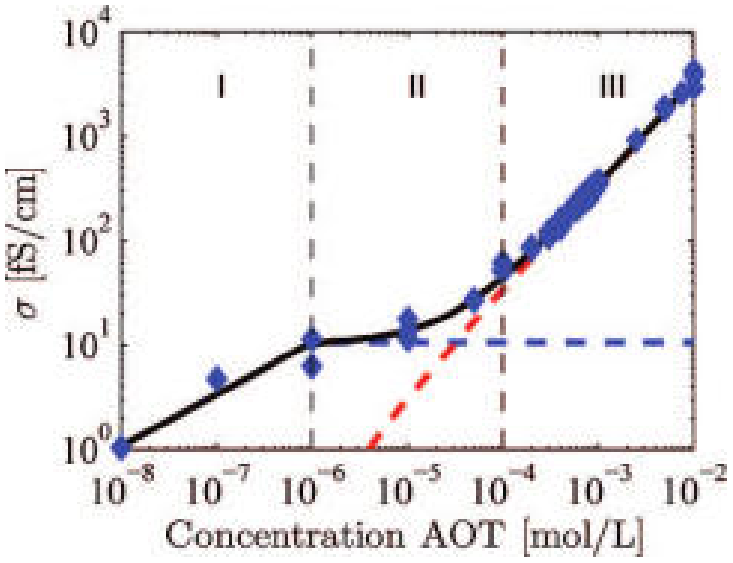

Figure 2-3 Conductivity of AOT/hexadecane solutions [34].

Both the dissociation of ionic/ionizable functional group as well as the charge exchange in reverse micelles by disproportionation would seem to involve the ionic component of the surfactants' hydrophilic head. Yet, when Bumajdad et al. [44] studied nonpolar solutions with mixtures of ionic and nonionic surfactant, they found no systematic dependence of conductivity on the fraction of ionic surfactant used. The authors nonetheless never questioned the need for some ionic surfactants in the mixture to generate the observed conductivity and never investigated purely nonionic surfactant solutions.

The first and to our best knowledge, the only study focused on electric charging in solutions of nonionizable surfactant (prior to our own work), published by Duhkin and Goetz in rarely cited article [45], comes to a surprising conclusion that challenges the traditional understanding of surfactant mediated charging. The study suggests that

nonionic surfactants (sorbitanoleate surfactants as shown in Figure 2-4) can enhance the conductivity and ion stability in nonpolar liquids as effectively as ionic surfactants do. The authors speculate that the observed charges are "sterically stabilized" ionic impurities, but do not provide a detailed analysis to further substantiate this claim.

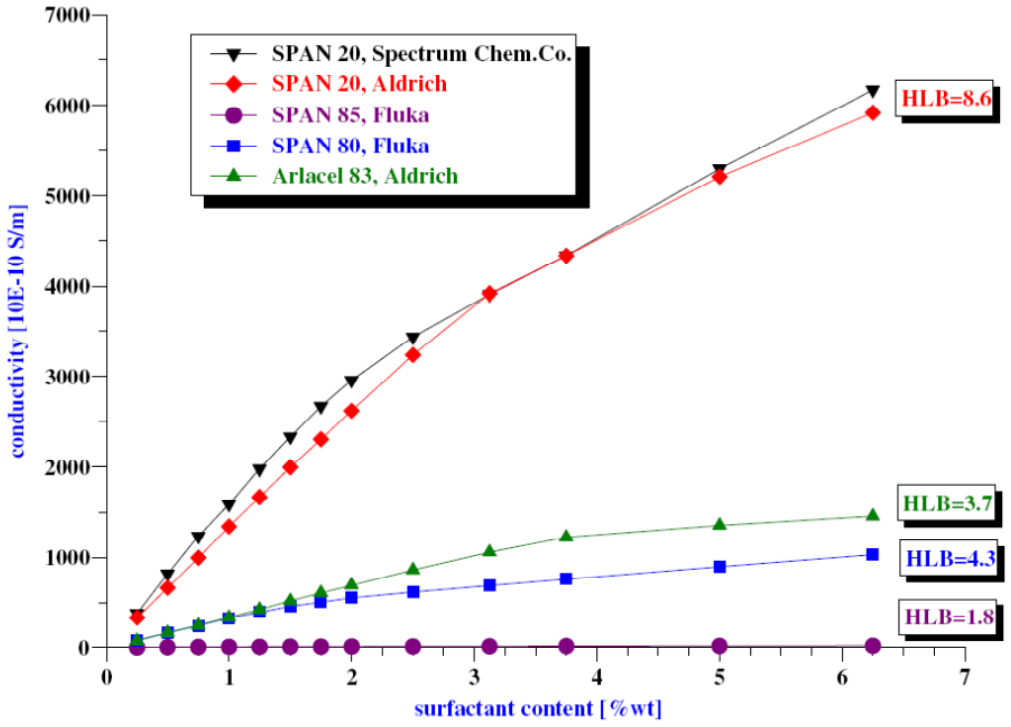

Figure 2-4 Conductivity of the kerosene solutions with various nonionic surfactants [45].

This study does not answer the question whether charging occurs by direct dissociation of the hypothesized impurities or whether micelle disproportionation can still take place, and if so, whether the concept of an ion reservoir in the micelle core might still apply even in the absence of ionic surfactant head groups and their counterions. Even if micellar disproportionation was possible for both ionic and nonionic surfactants, no such similarity can be expected below the CMC, where dissociation of the surfactant

headgroup is the alleged primary charging mechanism in solutions with ionic surfactants. The mechanism is clearly unavailable to surfactants with a non-dissociable hydrophilic head group. Since no CMC values are pointed in Figure 2-4 and the source article, it is unknown whether any charging effects are caused by the *molecularly dissolved* non-dissociable surfactants. Without a connection to the concentration and the aggregation state of surfactant additives, such questions remain unanswered.

2.1.2.3 Charge fluctuation model

Theoretically, the occurrence of a net charge in nonpolar liquids can be understood as a matter of equilibrium fluctuations around a zero average charge [42]. Eicke and co-workers originally proposed the charge fluctuation model for large droplets [42]. Hall [43] modified this model by explicitly accounting for the discreteness of electric charge, which allowed him to explain experimental data on the conductivity of water-in-oil microemulsions as a function of the droplet size. Recently the charge fluctuation model has been used to describe charging effects caused by reverse micelles in solutions of ionic surfactants [31] or surfactant mixtures [44]. However, the model has not been applied to systems with nonionic surfactants, arguably because the ability of these additives to promote charge formation is not (yet) widely acknowledged. A detailed study and thermodynamic modeling in the regions both below and above the CMC are needed to achieve a better understanding of the mechanism responsible for the formation of mobile charges in nonpolar liquids. In this thesis, we systematically investigate the electrostatic behaviors of nonionic surfactants in nonpolar solutions and theoretically understand the electric charges formation predicted by the charge fluctuation model.

2.2 Materials and methods

2.2.1 Surfactant solutions

Surfactant solutions are prepared by precisely measuring the weight of the surfactants and the volume of the solvents and simply mixing them on a magnetic stirring plate overnight. The well dissolved solutions are thermodynamically stable and transparent. Most types of solutions are colorless, but Span 85 in nonpolar oil solution is slightly yellowish due to the color of surfactant. All surfactant solutions are allowed to equilibrate for 1 day prior to use. All experiments are performed in a thermostatted environment at 22 ± 0.5 ℃.

2.2.1.1 Solvents

In order to capture the effects related to very nonpolar liquids, we focus our attention on alkane solutions with a high degree of purity.

Hexane (BDH, ACS grade) was chosen because of its very low dielectric constant ($\epsilon \approx 1.89$). Compared to longer chain alkanes, it also offers the advantage of better optical contrast with the surfactants used in this study, but it has the slight disadvantage of being more volatile. Small material losses observed gravimetrically correspond to an increase in concentrations of up to 1% over the course of our experiments; the reported concentrations are averages of initial and final values.

Ultrapure water with a resistivity of $18.3 M\Omega \cdot cm$ (Barnstead) is used for swelling reverse micelles and for interfacial tension measurements.

2.2.1.2 Surfactants

To find out the similarities and differences between nonionic and ionic surfactant in inducing charging effect in nonpolar liquids, we compare the results with the well-known ionic charge control agent AOT (sodium bis(2-ethylhexyl)sulfosuccinate). Two members in the Span family are selected for the nonionic surfactant without any ionizable functional group: Span 80 (Sorbitanmonooleate, HLB value 4.3), and Span 85 (Sorbitantrioleate, HLB value 1.8); the latter resembles AOT in its branched structure and micelle size. Sorbitanoleates are widely used as food emulsifiers, for cosmetic and pharmaceutical preparations, and for protein separation. AOT, Span 80, and Span 85 are all purchased from Sigma-Aldrich and used without further purification. The nominal structures of these surfactants are shown in Figure 2-5, but it is important to mention that all Span surfactants are truly mixtures of mono-, di-, tri- and tetra-oleates [46, 47]. All of these lack ionizable groups and thus seem unlikely vehicles for electric charges, but as mentioned before, the findings by Duhkin and Goetz [45] had already suggested the counterintuitive possibility of controlling the conductivity and ion composition of non-polar liquids with precisely this type of surfactant.

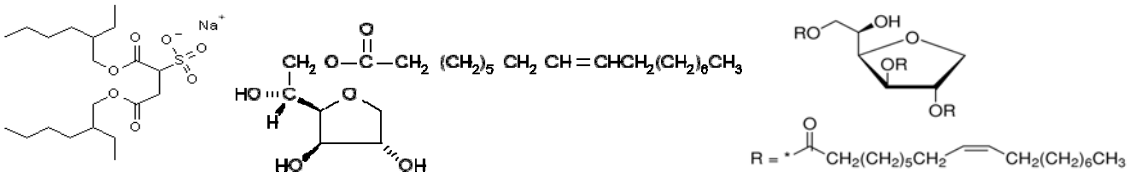

Figure 2-5 Structure of AOT (left), Span 80 (middle), and Span 85 (right).

The results and discussion sections will describe our study of the surfactant/non-polar oil solutions with regard to aggregate size and architecture, the influence of

impurities on electrostatic properties, and the theoretical analysis.

2.2.2 Dynamic light scattering

The characterization by dynamic light scattering (DLS) uses a precision goniometer setup (ALV/DLS/SLS-5022F). In the technique of DLS as implemented in this study, the intensity autocorrelation function is computed using a digital correlator, and the collective diffusion coefficient is determined from the measured correlation function using the second-order cumulant fit [48]. The selection of the scattering angle depends on the intensity of scattered light. If the surfactant micelles are too small to exhibit significant angular dependence of the scattered light intensity, the measurements can be made at a fixed scattering angle of $\theta = 90°$. Diffusion of the micelles changes their relative position and thus the relative phase with which light scattered by different micelles superimposes on the detector; the ensuing decorrelation rate for the scattered intensity reflects the average diffusivity of the micelles. From this, the hydrodynamic radius of the micelles can be determine using the Stokes-Einstein relation [49]

$$R_h = kT/6\pi\eta D, \qquad \text{Equation 2-7}$$

where η is the solvent viscosity. The scattering intensity from non-aggregated surfactant molecules is negligibly small.

2.2.3 Static light scattering

The characterization by static light scattering (SLS) is performed on the same instrumental setup. While the DLS measurements yield the average micellar hydrodynamic radius, R_h, the SLS measurements yield the weight-averaged micelle

aggregation number, *N*, which provides more information of the micellar configuration.

To simply introduce the technique of SLS, the angle dependent Rayleigh ratio, a quantity used to characterize the scattered intensity as a function of scattering angle, is calculated based on the intensity of scattered light from the micellar solution and from a reference solvent. The difference in Rayleigh ratio between the micellar solution and the reference solvent in the absence of micelles, $\Delta R_\theta = R_\theta - R_\theta^0$, is related to the apparent molecular weight of the micelles M_{app}, via [13]

$$\lim_{C_S \to CMC} \left(\frac{K_0 (C_S - CMC)}{\Delta R_\theta} \right) = \frac{1}{M_{app}} \qquad \text{Equation 2-8}$$

with the optical constant

$$K_0 = \frac{4\pi^2 n_0^2 (dn/dc)^2}{N_A \lambda^4}, \qquad \text{Equation 2-9}$$

where n_0 is the refractive index of the solvent, (dn/dc) the refractive index increment of the solution, N_A Avogadro's number, and λ the wavelength of light used. As seen in equation 2-9, the value of K_0 depends sensitively on the refractive index increment $\left(\frac{dn}{dc}\right)$, which is measured with an Abbé refractometer. The increment is calculated by fitting *n* as a function of concentration to a linear function. Equation 2-8 only features the surfactant concentration in excess of the critical micelle concentration (CMC) because only this excess effectively contributes to the micelles. The determination of the CMC will be described in the following section. Finally the aggregation number (the number of surfactant molecules per micelle) is obtained by dividing the average molecular weight of micelles by the known molecular weight of the individual surfactant molecule.

2.2.4 Interfacial tensiometry

The interfacial tension of drops of pure water in hexane solutions of Span 85 are measured with a drop volume tensiometer (TVT-2, Lauda). This instrument allows the determination of the interfacial tension of liquids at the moment of drop separation, from the volume of the drop growing in an immiscible second fluid. When air is chosen as the surrounding phase, this method yields the surface tension of the pending liquid drop. The densities of the concerned phases need to be known in order to calculate the surface/interfacial tension from the measured drop volume.

Drops of a liquid with a high density, e.g. water, are generated in a liquid with low density, e.g. hexane (with surfactant solution). As soon as the droplet weight, corrected for buoyancy, reaches the same magnitude as the tension-mediated holding force, the drop will fall. Mathematically, once the volume of the falling drop is measured, the interfacial/surface tension can be calculated by

$$\sigma = \frac{g(\rho_1 - \rho_2)V}{2\pi r f_{HB}}, \qquad \text{Equation 2-10}$$

where σ is the interfacial tension, ρ_1 and ρ_2 are the density of specific heavier or lighter phase, g is the acceleration due to gravity, and f_{HB} is the correction factor for the dimension of the droplet injector. When the lighter phase is air, the density of air can be neglected compared to the liquid drop phase. Thus, Equation 2-10 gives the surface tension of the drop pending phase.

2.2.5 High-precision conductometry

Conductivity measurements were taken with a high-precision conductivity meter (model 1154, Emcee Electronics).

Prior to the measurements, the sample cell is carefully cleaned in a multi-step procedure with hot water, DI water, acetone, toluene/isopropyl alcohol mixture, dried with nitrogen, and rinsed with sample solution.

A specific volume (around 100 mL, doesn't have to be exact amount) of test sample solution is placed in the conductivity cell between two concentric electrodes. The measuring cell is then connected using a triaxial cable to a sensitive DC ammeter in the Console. A series of DC voltage source is then applied between the two electrodes.

Due to the physical geometry of the cell, the cell constant is stable and calculable. The conductivity is calculated by Ohm's law from the cell characteristics, the voltage across the cell, and the almost instantaneous peak current reading. Then the resultant peak current is readily transformed and digitally displayed as picosiemens per meter (pS/m), or commonly known as conductivity units (CU, 1 CU = 1 pS/m).

2.2.6 Karl Fischer titration

The water content of our solutions was determined using Karl Fischer titration (TitroLine KF, SCHOTT).

HYDRANAL® Karl Fischer Titration Reagents is used by the titration instrument to react with water in the test sample solution. Methanol is used as the alcohol solvent

because it is miscible with both base reagents and sample solution. The net reaction as shown below in Equation 2-11 is oxidation of SO_2 by I_2, and one mole of I_2 is consumed for each mole of H_2O,

$$CH_3OH + SO_2 + RN \rightarrow [RNH]SO_3CH_3 \qquad \text{Equation 2-11}$$

$$I_2 + [RNH]SO_3CH_3 + 2RN + H_2O \rightarrow [RNH]SO_4CH_3 + 2[RNH]I$$

where RN is the base reagents using imidazole or diethanolamine as a base.

In the measurement process, a pair of Pt electrodes is immersed in the methanol solution with a constant current between them during titration measurement. At the beginning of titration, only I^- but little I_2 is in the solution; at the equivalence point, excess I_2 appears and an abrupt voltage drop below the pre-set threshold indicates the end point. The amount of consumed titration reagents can then be used to calculate the amount of water in the test sample. By giving the mass or volume of the original test sample to the system, the percentage of water containing is digitally displayed and recorded for further discussion.

2.3 Results and discussions

To better understand the electric charging phenomena in nonpolar solution, we focused on studying the nonionic surfactant without any ionizable functional groups, and explored the previously neglected possibility of introducing mobile charge by such additives in non-polar liquids.

The thermodynamic properties of nonionic surfactants were obtained by characterization of the critical micellar concentration and the micellar configuration. By observing the raise of electric conductivity with surfactant concentration in nonpolar solution, we aim to differentiate the behavior of individual surfactant molecules from reverse micelles and ultimately to establish the pathway of charge formation with the association of surfactants.

2.3.1 Self-assembly of surfactants

It has been confirmed that the electric properties of nonpolar media can be dramatically changed in the presence of surfactant additives, thus the surfactant concentration should be one factor to affect the electric property of the nonpolar solvent. Dynamic light scattering (DLS) allows the measurement of the micelles' hydrodynamic size and provides the information on the surfactant critical micellar concentration (CMC) and micellar shape [50, 51]. We also use static light scattering (SLS) to determine the average aggregation number of micelles [51], N, which is important to calculate the number of reverse micelles in the bulk phase.

2.3.1.1 Hydrodynamic size of surfactant aggregates

Commercial AOT being a well-known charge control agent, its composition, the critical micelle concentration, and the structure of AOT micelle have been studied in the past 30 years by light and X-ray scattering [52], photon correlation spectroscopy (PCS) [51], small angle neutron scattering (SANS) [53]. Especially, it is well established that AOT can form spherical structures of a well-defined size at concentrations above the CMC in nonpolar solvents. This constant micellar size makes it convenient to study the (micelle) concentration dependence of electric properties, with the assumption of a disproportionation pathway [34]. The connection between micellar configuration and electrostatic phenomenon induced by surfactants in nonpolar solution motivates to study the size and shape of the nonionic surfactant reverse micelles to compare with the better-known AOT, and thus DLS will be a good way to obtain such information.

Dynamic light scattering (DLS) is applied to measure the apparent hydrodynamic size of surfactant aggregates in non-polar oils. The results of AOT in hexane solution are shown in Figure 2-6, where the data marked by open symbols suffer from poor signal-to-noise ratio. Each data point is averaged from three independently measurements and standard deviation is calculated. The corresponding error bars would be in the size range of the data markers.

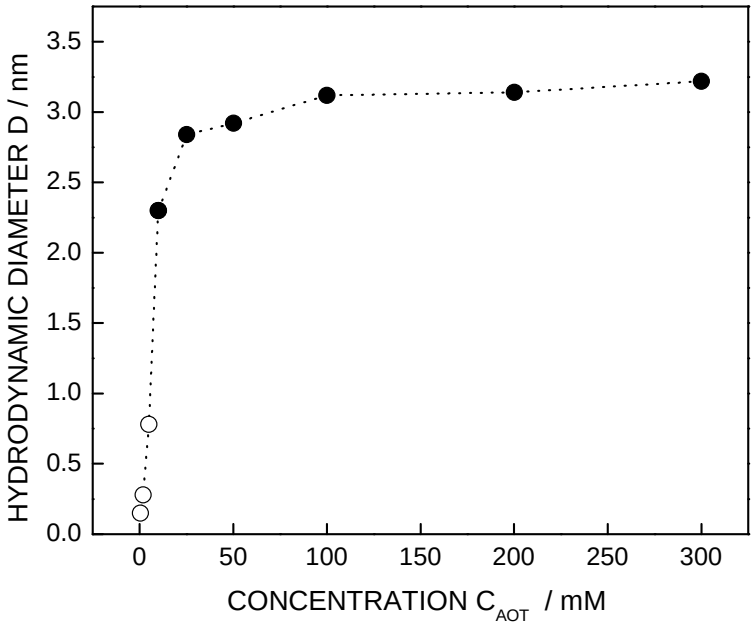

Figure 2-6 Apparent hydrodynamic diameter of AOT in hexane measured with DLS.

The hydrodynamic size of AOT aggregates in hexane initially increases with AOT concentration, and then remains roughly constant around 3 nm in diameter over a wide range of concentration till the highest one in the measurements. The DLS results of AOT in hexane confirm that AOT forms spherical micelles at high concentration, and the size is consistent with the published result in literature [54, 55].

According to the literature, relatively larger microstructures are formed by Span 80 and the shape is worm-like [56], which is consistent with our DLS data shown in Figure 2-7. With increasing concentration of Span 80 in hexane beyond the CMC, the average hydrodynamic size of Span 80 aggregates keeps rising. This size increase is expected for worm-like micelles, which tend become increasingly elongated and

polydispersed as more surfactant is added.

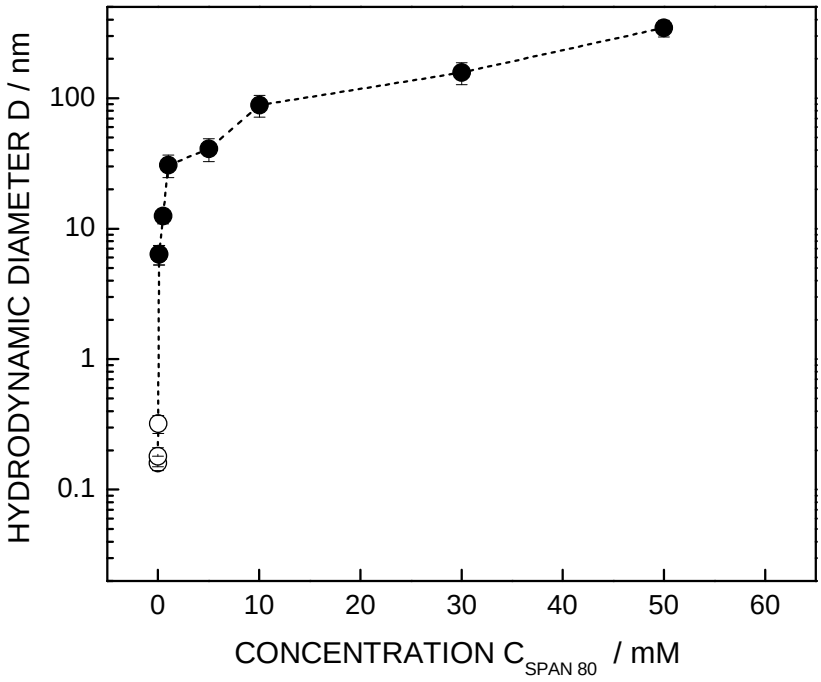

Figure 2-7 Apparent hydrodynamic diameter of Span 80 in hexane measured with DLS.

In contrast with the single hydrophobic tail of Span 80, Span 85 molecules have highly branched structure, and would therefore be expected to favor aggregates with high curvature, similar to AOT. Our DLS results (Figure 2-8) confirm the insensitivity of micelle size (a plateau value above the CMC) indicative of spherical micelles. Again, the open symbols are not reliable because the scattering intensity drops sharply, making the experimental uncertainty prohibitively large for the very low concentration.

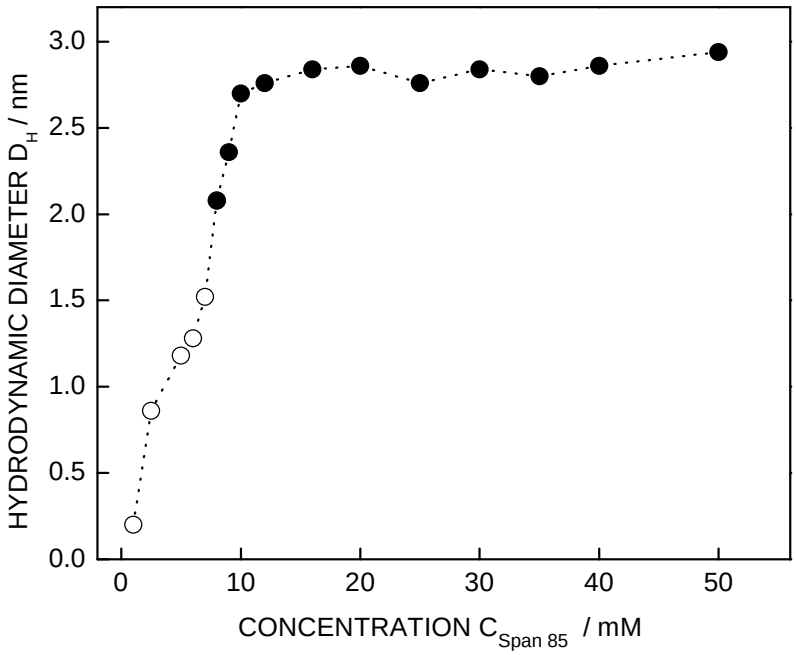

Figure 2-8 Apparent hydrodynamic diameter of Span 85 in hexane measured with DLS.

We conclude that Span 85 forms small, spherical reverse micelles with a roughly constant size, much like the widely studied ionic surfactant AOT [54, 55]. A value around 2.8 nm for the hydrodynamic diameter for Span 85 micelles in hexane can be inferred from the plateau in Figure 2-8.

Besides the size and shape of surfactant aggregates, the critical micellar concentration (CMC) is another important aspect to understand the self-assembly properties of surfactants in nonpolor media; the CMC measurement is discussed in the following section.

2.3.1.2 Critical micellar concentration

For a surfactant solution, the dissolved surfactant molecules present below the CMC scatter too little light for a meaningful DLS analysis. Once a sufficient number of micelles have formed (around and above the CMC) the scattering intensity increases significantly and the autocorrelation function yields a robust value for the hydrodynamic size. Thus the onset of the size plateau roughly indicates the CMC of surfactant.

Compared to Span 85 with no reported CMC information, AOT is widely studied, although the reported values differ in orders of magnitude [54, 55], and Span 80 forms worm-like micelles with the complication of polydispersity and unclear micelle number concentration [56]. We targeted the nonionic surfactants Span 85 to study the CMC and aggregation number of a well-defined spherical micelle.

The hydrodynamic diameter results of Span 85 in hexane in Figure 2-8 indicate the formation of Span 85 aggregates. The concentration around 10 mM above which the hydrodynamic size remains roughly constant is the CMC of Span 85 in hexane.

Interfacial tension (IFT) provides an alternative way to measure the CMC. Below the CMC, the IFT decreases with increasing surfactant concentration and correspondingly increasing surfactant adsorption to the water-and-oil interface. Above the CMC, the bulk concentration of molecularly dissolved surfactant remains almost constant, and so does the interfacial coverage, and, by extension, the interfacial tension. Therefore, the transition of IFT can also be used to determine the CMC of surfactant in nonpolar liquids, which will prove useful in the following sections for estimating and studying the water content in an individual micelle and participation of surfactant (molecules or micelles) in

forming charged species.

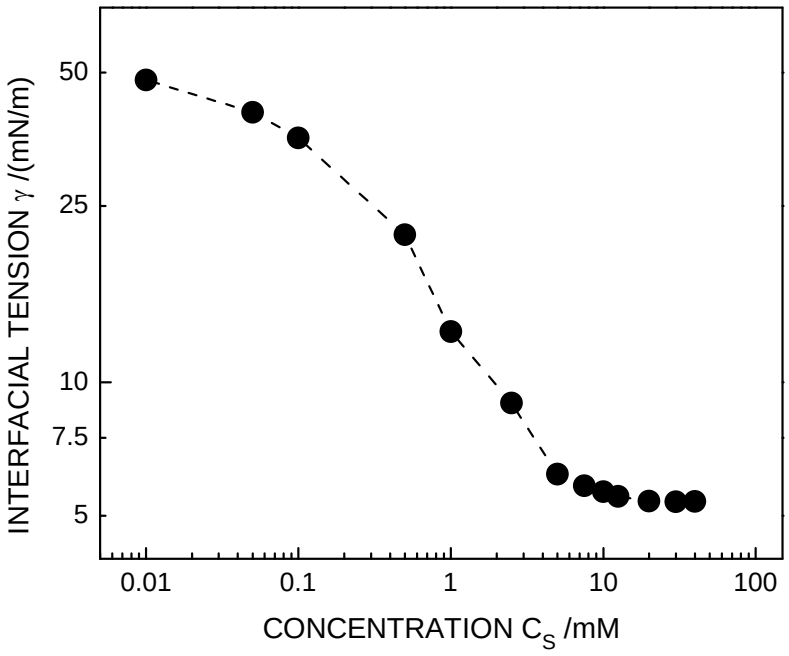

Figure 2-9 The interfacial tension of Span 85 in hexane solution when contact with DI water with the concentration of Span 85.

The interfacial tension results in Figure 2-9 indicate that the CMC of Span 85 in hexane is about 10 mM, above which the interfacial tension remains constant. The CMC obtained from this independent method is consistent with the one confirmed from the DLS method. A CMC of ~10 mM is large, but not surprising for Span 85, which features three or four hydrocarbon tail groups around a weak hydrophilic head group. We can also expect that the aggregation number of Span 85 micelle is low due to its large lipophilic component [57].

2.3.1.3 Aggregation number

The aggregation number of surfactant in nonpolar solution is obtained from the interpretation of SLS results. With the confirmed CMC and the principles described in Equation 2-8 and Equation 2-9, the refractive index increment $(\mathrm{dn/dc})$ of the surfactant solution is necessary to calculate the optical constant K_0, by extension, the aggregation number. The refractive index results of Span 85 in hexane solution are measured by an Abbe refractometer and shown in Figure 2-10. The value of refractive index depends on the concentration of Span 85 linearly, with a slope of $(\mathrm{dn/dc}) = 0.1572\ \mathrm{mL/g}$.

According to Equation 2-8, the limit value of the Rayleigh ratio difference between the micellar solution and the reference solvent in the absence of micelles, "excess Rayleigh ratio" ΔR_θ, is related to the apparent molecular weight of the micelle. In the interpretation of the SLS data, we used the slope of 0.1572 mL/g in the linear fit in Figure 2-10 for the refractive index increment $(\mathrm{dn/dc})$ in the concentration range of 10-50 mg/mL to calculate the optical constant K_0. A plot of the Rayleigh ratio as a function of Span 85 concentration is shown in Figure 2-11. The inversed value of Rayleigh ratio is linearly dependent on the concentration of Span 85 where the x-axis is the surfactant concentration subtracting CMC from the total Span 85 concentration, and the limiting value for the concentration approaching the CMC of Span 85 in hexane is the inverse of molecular weight of the Span 85 micelle.

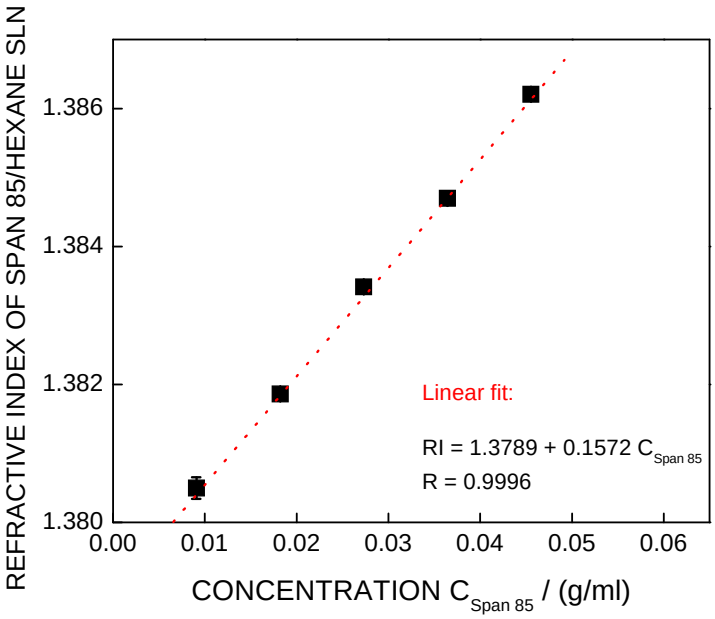

Figure 2-10 Refractive index of Span 85 in hexane solution.

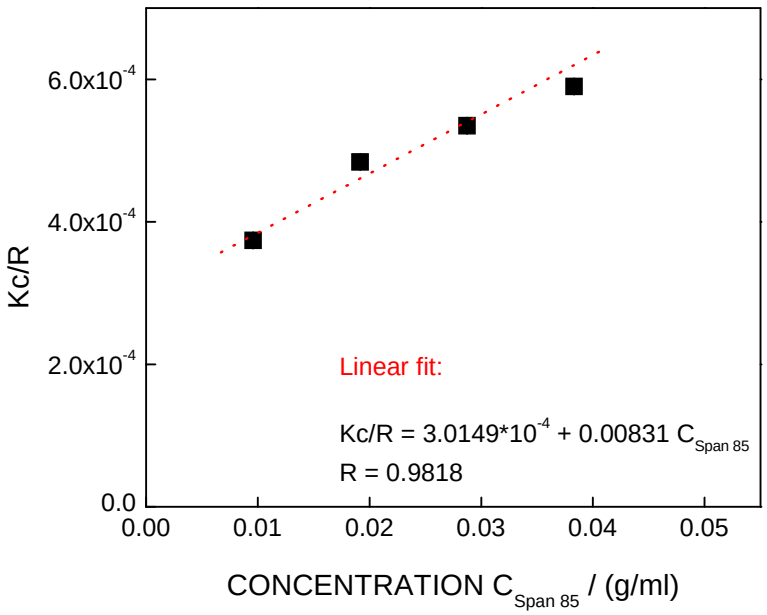

Figure 2-11 The angular dependent Rayleigh ratio obtained by SLS. The x-axis is the surfactant concentration subtracting CMC from the total Span 85 concentration.

In Figure 2-11, the inversed value of molecular weight of the Span 85 micelle is the intercept of the linear fit, 3.0149×10^{-4}. Thus, the molecular weight is around 3400 g/mol, which gives the aggregation number around 3.5 based on the molecular weight of single Span 85 molecule 957.5 g/mol.

According to SLS measurement a Span 85 micelle in hexane thus contains only 3.5 surfactant molecules on average (each with typically 3 – 4 hydrocarbon chains [46]).

2.3.2 Microemulsions

2.3.2.1 Hydrodynamic size of swollen micelles or micro-emulsions

Once there is solubilized water in the surfactant/alkane solution, it will be located in the hydrophilic core of the micelle. The amount of solubilized water will affect the size of reverse micelle. Published schematics like the ones of Figure 2-1 and Figure 2-2 suggest an important role for the "ion reservoir" in the core of reverse microemulsion droplet, which for ionic surfactants arises naturally from the surfactant counterions [29]. In the case of nonionic surfactant one might speculate that ions introduced by added water will play a similar role and affect the ability of such "swollen micelles" to acquire a net electric charge in nonpolar oils. Therefore, in order to understand the electrostatic effects induced by water swollen reverse micelles, we here characterized the systems with swollen micelles or microemulsions, the size and shape of which were measured by DLS.

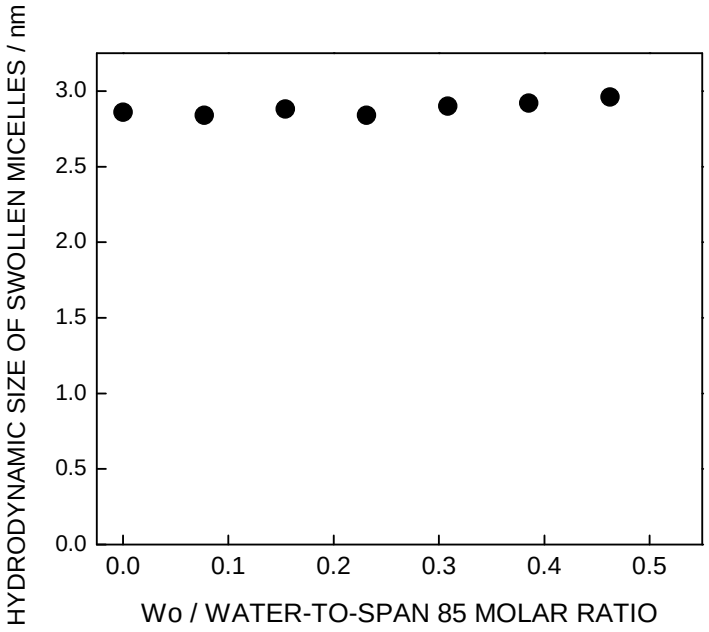

Figure 2-12 Hydrodynamic diameter of the water swollen Span 85 micelles with water-to-Span 85 molar ratio at 50 mM Span 85 in hexane.

Figure 2-12 shows the results of hydrodynamic size of water swollen Span 85 micelle with increasing amount of added water into 50 mM Span 85 in hexane. The maximum of water-to-Span 85 molar ratio is around 0.46, above which there is clearly phase separation between surfactant solution and added water. It is clear that the hydrodynamic diameter of swollen micelles is not significantly increased. Thus, we conclude that Span 85 can only solubilize very little amount of water.

2.3.2.2 Water content

We don't work specifically to get rid of the water existing in the commercial surfactant sources, but determine the precise water content using volumetric Karl Fischer titration (TitroLine KF, SCHOTT), which achieves a resolution of ~10 ppm in the entire

range of 0-100% water.

We confirmed that water content is below 0.003 wt % (30 ppm) for the pure solvent and found that very little water is introduced with the nonionic surfactant, with a molar water-to-surfactant ratio in their micellar solution below 0.05.

Knowing how much water is contained in the solvent and original surfactant, the total amount of water content in water swollen micro-emulsion solution can be calculated by summing with the added water. From the results shown in Figure 2-12, little water can be accepted by Span 85 in hexane solution. In contrast, nonpolar solutions of AOT can involve significant amounts of water. More details on this point will be given in Chapter 4 on particle charging in nonpolar dispersions and charge screening mediated by surfactants.

2.3.3 Conductivity of nonpolar oils increased by surfactants

We measured the conductivity of hexane in the presence of different surfactants, using a high precision conductometer (Emcee Electronics, Model 1154) to monitor electrical conductivity in the range of 0.01 – 20,000 pS/m.

The conductivity results of AOT/hexane solution are shown in Figure 2-13. Each data point is plotted by taking average of three parallel measurements. The standard deviation of the results is considered to be the error introduced by both handling and instrument. The x- and y- error bars are also shown in Figure 2-13, some of which may not be seen when covered by the data markers.

We compared our conductivity values in Figure 2-13 with the results of

AOT/hexadecane solution in Sainis' work in Figure 2-3 [34], the increasing trend of conductivity as a function of AOT concentration is similar, and the conductivity data are in the same order of magnitude for the entire range of AOT concentration. Therefore, we verified the validation of the measurements by our high precision conductometer. The exact values of the conductivity in our AOT work have a little difference from the results in Sainis' work [34] because of either the system error from different instrument or the water content that dissolved in different types of solutions.

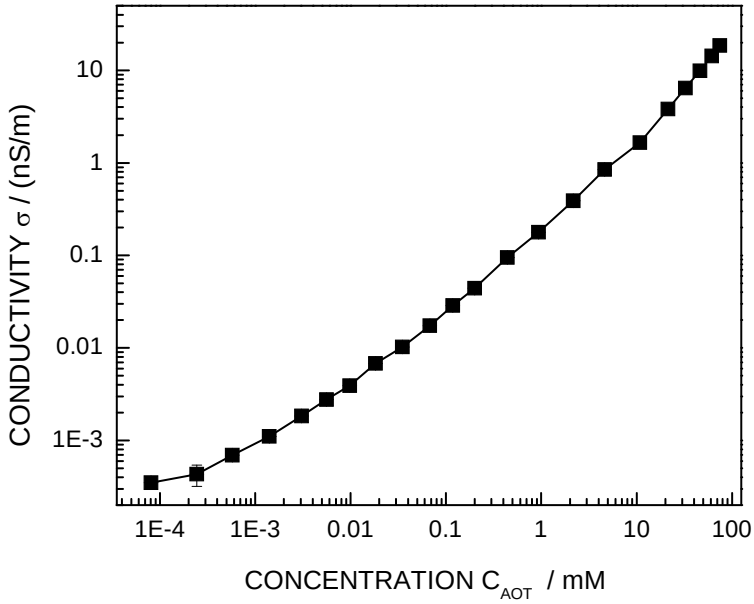

Figure 2-13 Conductivity of AOT/hexane solution.

There appears to be different AOT concentration regions for individual molecule dissolution and micelle formation as shown in Figure 2-3. And the dissociation and disproportionation pathway are suggested as the charge formation mechanism respective for sub and above the CMC for the AOT/hexadecane system in Sainis' work [34]. It

motivates us to study the conductivity of the whole range nonionic surfactant concentration from very dilute to concentrated solutions, and we are interested in observing charged induced even before the micelles formed.

Although Duhkin and Goetz [45] found that nonionic surfactant can surprisingly raise the conductivity of nonpolar liquids acting as common ionic charge control agent, they did not build a connection with the surfactant molecular complex or micellar formation. In addition, they were not able to explain where the charge came from Span 85, the only one surfactant in Figure 2-5 with an analogous structure to AOT, which showed almost no effects in forming charged species in alkanes.

Open questions are raised whether we can confirm that nonionic surfactants show strong charging effects as the ionic ones do, and if so, how the nonionic surfactants below the CMC can induce charge in nonpolar solutions when ionic surfactants like AOT are believed to dissociate and Spans clearly cannot do. We focused on the typical nonionic surfactants without ionizable groups Span family (Span 80 and Span 85) and studied the conductivity raise induced by Spans in nonpolar media.

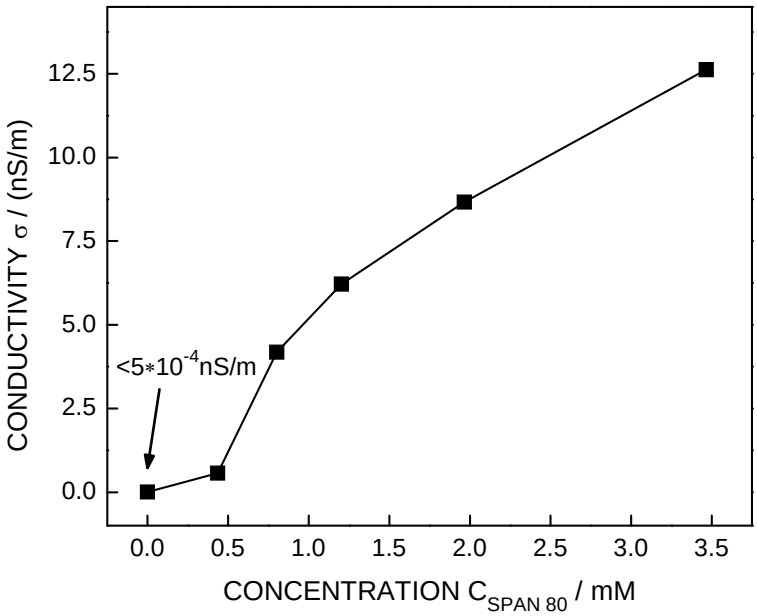

Figure 2-14 Conductivity of Span 80/hexane solution.

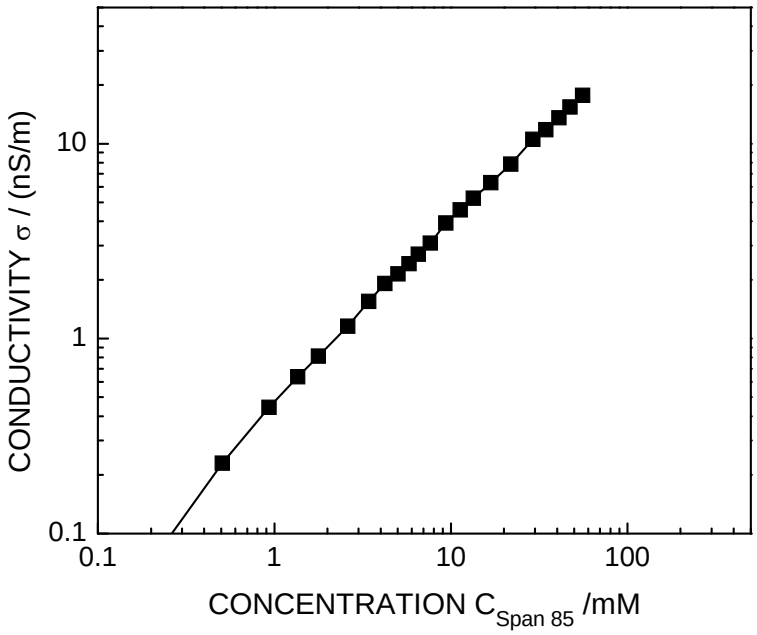

Figure 2-15 Conductivity of Span 85/hexane solution.

The CMC and micellar information of the Spans are obtained in the previous sections, and we show the measured conductivity of surfactant/hexane solutions as a function of Span 80 and Span 85 from sub-CMC to above the CMC, in Figure 2-14 and Figure 2-15, respectively. Nonpolar liquids with high purity have conductivity in the range of 10^{-14}-10^{-12} S/m, which can be resolved by our conductometer.

We confirmed that surfactants without any ionizable groups can raise the conductivity of alkanes as efficiently as AOT can. Impressively, in the addition of less than 1 mM Span 80, the conductivity of Span 80/hexane solution is raised by four orders of magnitude. The observed effect is likely caused by the Span 80 micelles, and the change in slope around 0.5 mM is due to the variation of elongated aggregate structure. Therefore, a quantitative interpretation of the data in Figure 2-14 is complicated by the fact that the micelle size and shape varies with surfactant concentration in the displayed concentration range [56].

The conductivity results show the enhancement of electrical conductivity by different kinds of nonionic surfactants in the very nonpolar liquid hexane. The conductivity is increased significantly by Span 80 and even by Span 85, which was not clear from the data reported by Dukhin and Goetz (Figure 2-4, [45]). Although the effect is somewhat less pronounced for Span 85 because of a higher CMC and smaller micelles, the uniform spherical shape of the Span 85 micelles over a useful concentration range make this surfactant the more suitable surfactant for theoretical modeling. In the following section, we will attempt to rationalize our experimental findings by application of the commonly accepted thermodynamic charge fluctuation model [43,31].

2.3.4 Theoretical fit to charge fluctuation model

In order to better understand the charge formation mechanism by Span 85 and compare the impacts of individually dissolved surfactant molecules and reverse micelles on raising conductivity, we fit the conductivity results in Figure 2-15 as a function of Span 85 concentration in two regimes, below and above the CMC, in Figure 2-16.

Although the conductivity data look "almost but not quite" linear throughout the sampled concentration regime, an even better fit can be obtained by considering the dilute and micellar regime separately. Both below and above the CMC of Span 85, we observe the linear increase in conductivity with surfactant concentration that is usually associated with charge disproportionation. The slope in the two concentration regimes is shown in the insets of Figure 2-16 together with the correlation coefficient R. The correlation coefficient R near 1 attests to the near-perfect linearity of the concentration dependence in these two regimes. Even though the transition is not sharp, the intersection point of the two linear fits is roughly located around 10 mM of Span 85, consistent with the CMC from DLS and IFT data. Thus using a double linear fit in Figure 2-16 (dotted line for dilute regime from Equation 2-12, and dashed line for micelle-dominated regime from Equation 2-13), we can write the conductivity as,

$$\sigma(C) = \sigma_0 + C \times \left(\frac{d\sigma}{dC}\right)_{C<CMC} \text{ for } C < CMC \qquad \text{Equation 2-12}$$

$$\sigma = \sigma_0 + CMC \times \left(\frac{d\sigma}{dC}\right)_{C<CMC} + C \times \left(\frac{d\sigma}{dC}\right)_{C>CMC} \text{ for } C < CMC \qquad \text{Equation 2-13}$$

where σ_0 the is the conductivity of the pure hexane.

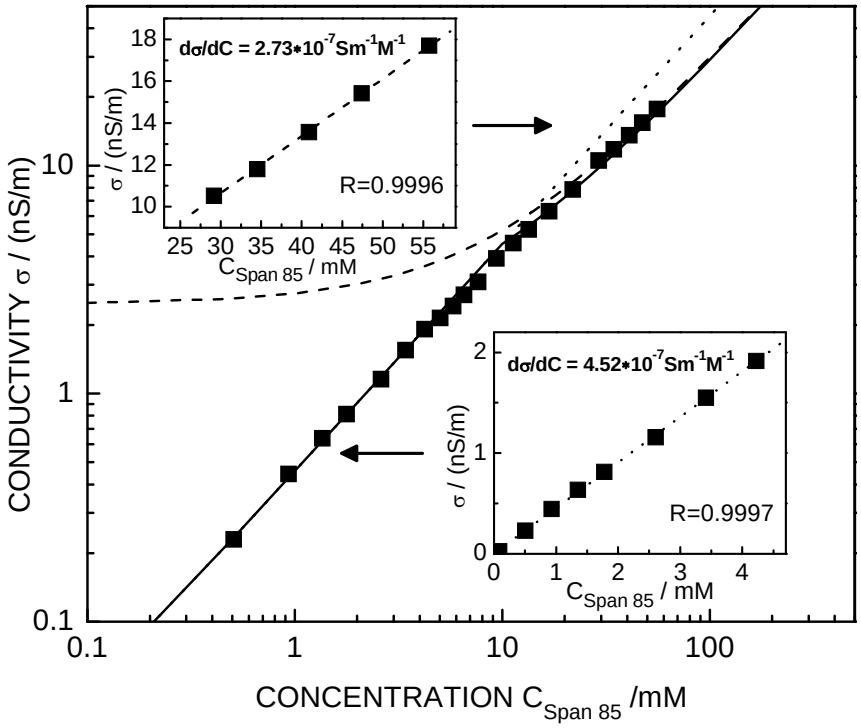

Figure 2-16 Conductivity of hexane as a function of added Span 85. Markers: experimental data. Dashed line: linear fit (with additive offset) for the micelle-dominated regime; dotted line: linear fit for the submicellar regime; solid line: double linear fit described in the text. Insets: linear portions above and below the critical micelle concentration.

In the following discussion, we separately consider the charging processes in the micellar and in submicellar solutions that could explain the two conductivity regimes of Figure 2-16.

2.3.4.1 Conductivity of micellar solution

Above the CMC of our nonionic surfactant nonpolar solutions, just as in the case of ionic surfactants [31], the conductivity is most likely dominated by charged reverse

micelles.

Theoretically, charge fluctuation theory is usually used to describe the conductivity enhancement. Thermodynamics allows the spontaneous disproportionation of two neutral species into oppositely charged ones, as $2M^0 \leftrightarrow M^{Z+} + M^{Z-}$ [31]. According to the theory of equilibrium charge fluctuations, the corresponding concentration of neutral, cationic, and anionic charged species C_0, C_{+Z}, C_{-Z} should satisfy the Boltzmann relation in Equation 2-14,

$$C_{\pm Z} = C_0 exp\left(\frac{-\lambda_B}{2a}\right) \qquad \text{Equation 2-14}$$

Where 2*a* is the Born diameter, in this case the size of the hydrophilic core where charges can reside, and $\lambda_B = e^2/4\pi\varepsilon\varepsilon_0 k_B T$ is the solvent's Bjerrum length.

The expression of conductivity from the reverse micelles charging is given in Equation 2-15 [43]. For $\lambda_B/2a$ as large as in the present system, only the terms for $Z = \pm 1$ are non-negligible, and C_0 is well approximated by the total concentration of micelles.

$$\sigma = \frac{C_0 e^2}{\xi}\sum_{Z=-\infty}^{\infty} exp\left(\frac{-Z^2\lambda_B}{2a}\right) \xrightarrow{Z=\pm 1} \sigma = \frac{e^2(C_+ + C_-)}{\xi} = \frac{e^2 C_0 \chi}{\xi} \qquad \text{Equation 2-15}$$

where the infinite sum excludes the term for *Z=0,*and the friction coefficient ξ for a spherical micelle is related to the micelles' hydrodynamic radius R_H and the solvent viscosity η via the Stokes' equation $\xi = 6\pi\eta R_H$ .The equilibrium fraction of charged micelles$\chi = (C_+ + C_-)/C_0$, according the Boltzmann relation in Equation 2-14, χ can be expressed as

$$\chi = 2exp(-\lambda_B/2a) \qquad \text{Equation 2-16}$$

Here it is important to note that χ is independent of the surfactant concentration, and thus

$\sigma \propto C$, a feature that distinguishes charging by disproprotionation$2M^0 \leftrightarrow M^+ + M^-$from dissociation reactions$AB \leftrightarrow A^+ + B^-$, where the law of mass action implies a square root dependence of σ on concentration instead [31, 34].

Above the CMC, the derivative of the micelle-dominated conductivity with respect to the concentration of added surfactant micelles C_0 is given by

$$\left(\frac{d\sigma}{dC}\right)_{C>CMC} = \frac{e^2\chi}{\xi}\frac{dC_0}{dC} = \frac{e^2\chi}{6\pi\eta R_H}\frac{1}{N} \qquad \text{Equation 2-17}$$

where *N* is the micellar aggregation number obtained from SLS data, and we have made the common assumption that all surfactant in excess of the CMC aggregate into micelles. Equation 2-17 also neglects the concentration dependence of the viscosity, which we have verified to be legitimate for the entire concentration range shown in Figure 2-16.

By comparing the fitted experimental $(d\sigma/dC)_{C>CMC}$ to the prediction of Equation 2-17 and taking the aggregation number (N = 3.5) from SLS measurement and the friction constant $\xi = 6\pi\,\eta\,R_H$ from DLS measurement ($R_H = 1.42\,nm$), we find a tiny fraction of charged micelles, $\chi = 4.86 \times 10^{-7}$ to account for the observed conductivity increase above the CMC. From this fraction, we can infer a Born radius of $a = 0.98\,nm$, which does not seem an entirely unreasonable magnitude for the hydrophilic micellar core compared to the hydrodynamic radius for the whole reverse micelle.

2.3.4.2 Conductivity in the sub-micellar regime

Below the CMC, the observed linear scaling of conductivity with added Span85

in Figure 2-16 represents a sharp contrast to the square root scaling that was reported for AOT solutions and explained by the dissociation of individual AOT molecules[34]. For Span 85 the charging mechanism must obviously be different.

One conceivable pathway again involves the complexation of ionizable impurities with surfactant molecules, followed by a charge disproportionation of the resulting complexes. Note, for instance, that a hypothetical complex involving two trioleate surfactant molecules would have six lipophilic arms and might assume conformations that resemble a "miniature micelle". One might therefore imagine that such complexes would mimic the previously discussed charging behavior of Span 85 micelles. Moreover, Span 85 is known to contain not only pure sorbitan trioleate but also other (similarly nondissociable) sorbitan esters, such as tetraoleate [58]. We do not currently know which of the nonionic surfactant species present in Span 85 participate in forming the charged entities.

Whatever the detailed composition and architecture of these complexes may be, their charging tendency might again be captured by charge fluctuation theory. If, for example, all charged complexes had a hydrodynamic radius $R_{H,c}$ and a Born radius a_c, then the conductivity slope in the lower part of Figure 2-16 should be given, in perfect analogy to Equation 2-17, by Equation 2-18,

$$\left(\frac{d\sigma}{dC}\right)_{C<CMC} = \frac{e^2\chi_c}{\xi}\frac{dC_c}{dC} = \frac{e^2\chi_c}{6\pi\eta R_{H,c}}\frac{1}{N_c} \qquad \text{Equation 2-18}$$

where $\chi_c = 2exp(-\lambda_B/2a_c)$ is the fraction of complexes that acquire a net charge and N_c the number of surfactantmolecules per charge carrier. Since we do not know the hydrodynamic radius independently (as we do in the case of micelles), we cannot solve

for χ_c. According to Equation 2-18, the conductivity slope of in the submicellar regime,$(d\sigma/dc)_{C<CMC}$ observed in Figure 2-16, is larger than the one for the micelle-dominated regime$(d\sigma/dc)_{C>CMC}$. This fact does not imply a larger charging tendency χ_c of the submicellar complexes compared to micelles but might be explained by the difference in the number of surfactant molecules N_c contained in the charged species and the difference in hydrodynamic size $R_{H,c}$. The notion that the conductivity below the CMC is caused by charged entities of the different size than the micelles found above the CMC will be supported independently by experimental data on the interaction of charged colloidal particles in Span 85/hexane solutions presented in Chapter 4.

2.3.5 Role of impurities and charge formation mechanisms

The arguments presented above show that charge disproportionation both above and below the CMC regimes would be variable from an equilibrium statistics point of view, but do not offer any explanation regarding the reaction pathway or the actual source of electric charges in the absence of ionizable surfactant head groups for Span 85. Given the small fraction of charged micelles created, the presence of trace amounts of ionizable impurities incorporated in the micelle core would suffice to explain the availability of separable charges. Good reproducibility of the experimental results with different batches of surfactant and hexane, however, suggests that the charging reaction is not limited by the amount of impurities present in the micelle core, but instead by the size and number of micelles. The most likely ionizable impurities are courterions contained in water contamination and the excess ionic reactant to produce Span 85, which will be discussed in the following sections.

2.3.5.1 Water content and ions in the hydrophilic micelle core

As suggested in Figure 2-2, the aqueous core of swollen micelles or microemulsion droplets is commonly viewed as an ion reservoir [42, 43]. With the assumption of disproportionation [29] two overall neutral micelles react into oppositely charged ones by exchanging an ion between their internal reservoirs.

Hence, by controlling ion content in the hydrophilic core of the micelles, it is possible to study the effects of these reservoirs on the net electric charging of the micelles. One might speculate that particularly large amounts of ions in the reservoir would promote micelle charging and lead to larger conductivity.

In order to study the effect of the micelle core composition on the formation of charged species, we solubilized small aliquots of either pure water (solid squares) or 0.1 M NaCl solution (open triangles) in the micellar solutions (30 mM Span 85 or 20 mM AOT in hexane) and measured the conductivities shown in Figure 2-17. For each case, the amount of water incorporated in the micelle cores was determined by Karl Fischer titration and translated, for better comparison with literature data, into the molar ratio W_0 of water to surfactant molecules. As one might expect from Equation 2-15 and Equation 2-16, swelling reverse micelles with aqueous solution increases the conductivity, which depends sensitively on the core radius a.

The conductivity results shown in Figure 2-17 indicate no significant difference between the reverse micelles swollen with DI water and those swollen with 0.1M NaCl solution. This leads us to the surprising conclusion that only the size of the micelle core, but not its precise ion content, determines the micelles' tendency of acquiring a net

charge. It would be wrong to infer from this that impurities play no role at all; their presence in the micelle core may well be crucial for the generation of charged micelles. It rather appears that ionizable impurities always provide enough ions to accommodate the extent of net micelle charging consistent with the charged micelles' Born energy $U = k_B T\,(\lambda_B/2a)$. This energetic constraint for a given core size, according to $\chi = 2exp(-\lambda_B/2a)$, cannot be removed by raising the concentration of ionizable molecules in the core even further. Hence, the similarity between the conductivity of nonpolar surfactant solutions with solubilized water and solubilized salt solution seen in Figure 2-17.

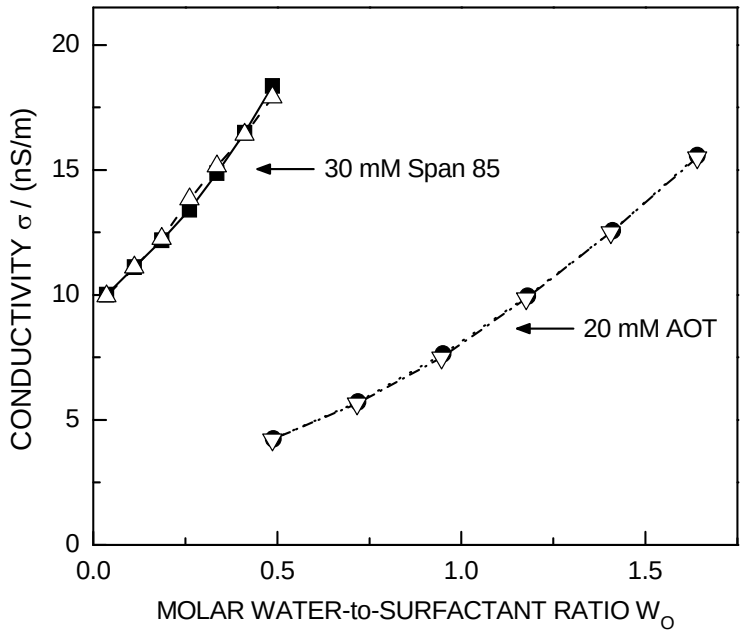

Figure 2-17 Conductivity of hexane solutions containing either 30 mM Span 85 or 20 mM AOT as a function of solubilized DI water (solid markers) or solubilized 0.1 M NaCl solution (open markers).

It is not surprising, considering the above arguments, that the micelles of ionizable and nonionizable surfactants show the same qualitative behavior and are well described by the same statistical model for charge fluctuations [42, 43, 59]. Although this well established model does not explicitly account for the ionic character of the surfactant, its application has practically been reserved to micelles of ionic surfactants.

Conductivity measurements on swollen micelles of AOT are also included in Figure 2-17. Again, the conductivity appears completely insensitive to salt ions in the swelling solution. The ionic surfactant AOT is much more hygroscopic than Span 85; the lowest indicated water content of $W_0 \approx 0.5$ for this surfactant was determined before addition of any swelling solution. Since even in the unswollen state AOT micelles are a little larger [60, 61] than Span 85 micelles, it takes a slightly larger Span 85 concentration to obtain a comparable conductivity. Conversely, Span 85 micelles can only solubilize very small amounts of water and are so small, even in the swollen state, that their size variation upon swelling could not be resolved by light scattering as shown in Figure 2-12.

2.3.5.2 Ionic impurities from unreacted educts of the surfactant synthesis

Further solubilization experiments with various ionic compositions of the solubilizate, larger extents of micelle swelling, and different surfactant compositions shall be carried out in order to understand the insensitivity to the free ions content. One popular dispute concerning the ability of nonionic surfactant to introduce charge in nonpolar liquids relates to likely ionizable organic impurities. Span 85 is known to contain not only pure sorbitan trioleate, but also other non-ionic sorbitan esters, such as tetrooleate [62]. The most likely ionizable impurity in Span 85 is unreacted oleic acid.

We purposely add oleic acid into pure alkanes and surfactant solutions with fixed Span 85 concentration, the conductivity results Figure 2-18 can tell us quantitatively the effect of the ionizable impurity.

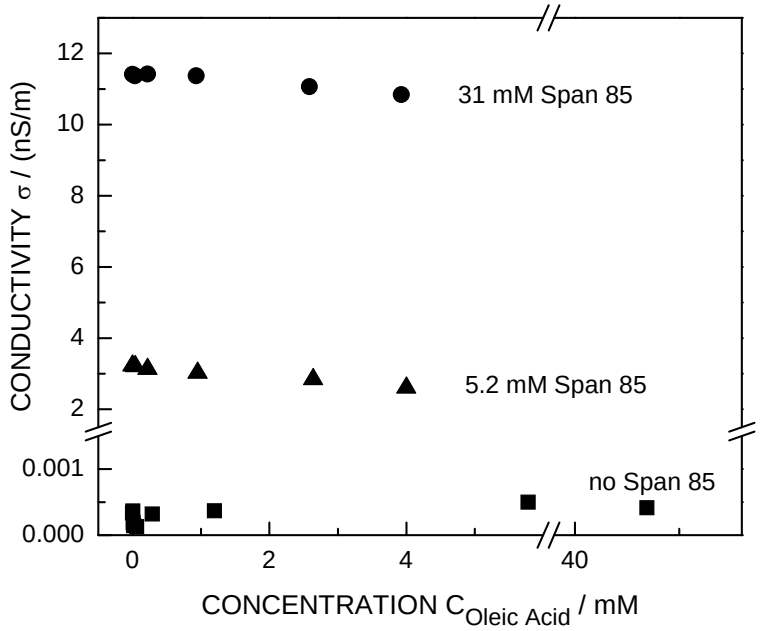

Figure 2-18 Conductivity of Span 85/hexane solutions (pure hexane, hexane solutions with Span 85 below and above the CMC) as a function of added oleic acid.

We verified experimentally that unreacted oleic acid, the most likely ionizable impurity to be found in Span 85, is not responsible for the observed behavior, at least not in the sense of simple contamination acting independently of the surfactant molecules. Increasing amounts of oleic acid were added to Span85/hexane solutions of different surfactant concentrations, including pure hexane and hexane solutions with Span 85 concentration both below and above the CMC. The nonionic surfactant emerges as the determining factor for the conductivity: no raise in conductivity in Figure 2-18 is

observed at all upon addition of the oleic acid; in fact, the conductivity of the surfactant solutions slightly decreases in response to a slight dilution of the surfactant by oleic acid.

2.3.5.3 Charge formation mechanism

The general insensitivity to the salt content and the existence of different conductivity regimes below and above the CMC speaks against the notion that the observed conductivity merely stems from the solvation of ionic impurities. Complexes of ionizable impurities with surfactant dimers or even with single amphiphilic molecules with several hydrophobic arms could resemble a small reversed micelle, and such "pre-micellar complexes" might well be the charge carriers in the dilute regime. Their disproportionation into pairs of charged complexes would explain the conductivity below the CMC just like the disproportionation of micelles with ionic impurities in their core would account for the conductivity above the CMC (Figure 2-19). Importantly, it would be the charge disproportionation step, not the initial complexation of the impurity with the surfactant, that requires overcoming an electrostatic "activation barrier" and limits the overall charging process.

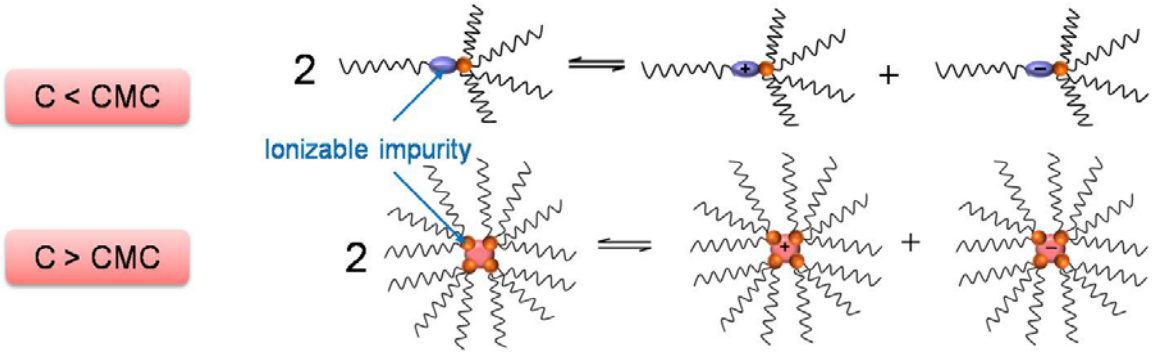

Figure 2-19 Scheme of disproportionation pathway of charge formation in hexane via nonionic surfactant Span 85.

We conclude that, although ionogenic impurities, such as salts, oleic acid, or residual water, may play an important role for the conductivity of our solutions, it appears to be the surfactant, not the impurity, which limits the ionization process. Note that a similar conclusion is reached by Dukhin and co-workers [45] using very different arguments that consider the "steric stabilization of ions" rather than the Born energy associated with introducing an electric charge in the confinement of a hydrophilic region embedded in a nonpolar medium. The conclusion of surfactant limited ionization has an important practical implication: precise control of solution conductivity by nonionizable surfactants should be possible without detailed knowledge or control of impurities.

Besides the electric charging phenomena in nonpolar solvents induced by surfactants, it is also interesting to analyze the effect of surfactants aggregates on the surface charging of dispersed solid particles in nonpolar liquids, which will be discussed in the next chapter.

2.4 Conclusions

Basic properties of surfactants, both ionic and nonionic ones, including hydrodynamic size of self-assembly aggregates, critical micelle concentration (CMC), aggregation number of refined reverse micelles, and ability to solubilize water in hydrophilic micellar cores, are characterized by dynamic light scattering, static light scattering, interfacial tensiometry, and Karl-Fischer titration. The results are used to rationalize the conductivity effects observed when these surfactants are added to nonpolar oils.

Surfactants are found to be able to raise the electric conductivity of nonpolar solvents both above and below the CMC. Data for the nonionizable surfactant Span 85 were chosen for a quantitative analysis because this surfactant forms spherical reverse micelle of a uniform size and cannot contain much water due to branched hydrophobic tails. For Span 85 solutions in hexane, a linear increase of conductivity with surfactant concentration is found both above and below the CMC. It is consistent with a statistical description of equilibrium charge fluctuations, which may arise from charge disproportionation of reverse micelles above the CMC or of surfactant complexes with ionizable impurities below the CMC.

In order to study the effect of ionic impurities in the hydrophilic core of reverse micelle, pure water, salt solution, and organic ionic impurities (oleic acid) were added to the surfactant solutions. The conductivity results show no significant difference between the Span 85 reverse micelles swollen with DI water and those with 0.1M NaCl solution, nor do large additions of oleic acid, the most likely contaminant, enhance the

conductivity in Span 85/hexane solution. Both above and below the CMC, the ionization process appears to be limited by the surfactant, not by ionizable impurities. Our findings suggest that the conductivity of nonpolar solutions can be controlled in a robust way via nonionizable surfactants. We expect that charge screening and conductivity control with nonionic surfactants will prove especially useful for oils in contact with a water phase, which would typically act as a drain for ionic surfactants.

2.5 References

1. Burkitt, S.J., Ottewill, R.H., Hayter, J.B. & Ingram, B.T. Small-angel neutron-scattering studies on micellar systems. 1. ammonium octanoate, ammonium decanoate, and ammonium perfluoroocatanoate. *Colloid and Polymer Science* **265**, 619-627 (1987).

2. Clapperton, R.M., Ottewill, R.H., Rennie, A.R. & Ingram, B.T. Comparison of the size and shape of ammonium decanoate and ammonium dodecanoate micelles. *Colloid and Polymer Science* **277**, 15-24 (1999).

3. Baeurle, S.A. & Kroener, J. Modeling Effective Interactions of Micellar Aggregates of Ionic Surfactants with the Gauss-Core Potential. *Journal of Mathematical Chemistry* **36**, 409-421 (2004).

4. Dominguez, A., Fernandez, A., Gonzalez, N., Iglesias, E. & Montenegro, L. Determination of critical micelle concentration of some surfactants by three techniques. *Journal of Chemical Education* **74**, 1227-1231 (1997).

5. Thorsteinsson, M.V., Richter, J., Lee, A.L. & DePhillips, P. 5-Dodecanoylaminofluorescein as a probe for the determination of critical micelle concentration of detergents using fluorescence anisotropy. *Analytical Biochemistry* **340**, 220-225 (2005).

6. Rodriguez, C. *et al.* Self-Organization, Phase Behavior, and Microstructure of Poly(oxyethylene) Poly(dimethylsiloxane) Surfactants in Nonpolar Oil. *The Journal of Physical Chemistry B* **106**, 22-29 (2002).

7. Shinoda, K., Fukuda, M. & Carlsson, A. Characteristic solution properties of mono-, di-, and triglyceryl alkyl ethers: lipophobicity of hydrophilic groups. *Langmuir* **6**, 334-337 (1990).

8. Liu, M., Fu, Z., Wang, Q., Xu, J. & Fan, Z. Study of amphiphilic poly(1-dodecene-co-para-methylstyrene)-graft-poly(ethylene glycol). Part II: Preparation and micellization behavior of the amphiphilic copolymers. *European Polymer Journal* **44**, 4122-4128 (2008).

9. Turro, N.J. & Yekta, A. Luminescent probes for detergent solutions - simple procedure for determination of mean aggregation number of micelles. *Journal of the American Chemical Society* **100**, 5951-5952 (1978).

10. Infelta, P.P. Fluorescence quenching in micellar solutions and its application to the determination of aggregation numbers. *Chemical Physics Letters* **61**, 88-91 (1979).

11. Wustneck, R., Enders, P. & Fiedler, H. Determination of aggregation numbers and ionization degree of micelles using surface-tension isotherms of maleic-acid mono 2-(4-alkylpiperazinyl) ethyl esters. *Langmuir* **10**, 3955-3958 (1994).

12. Thevenot, C., Grassl, B., Bastiat, G. & Binana, W. Aggregation number and critical micellar concentration of surfactant determined by time-dependent static light scattering (TDSLS) and conductivity. *Colloids and Surfaces a-Physicochemical and Engineering Aspects* **252**, 105-111 (2005).

13. Magid, L. Dynamic Light Scattering: The Method and Some Applications. *Oxford University Press: Oxford, Chapter 13* (1993).

14. Evans, D.F. & Wennerström, H. *The Colloidal Domain: Where Physics, Chemistry, Biology, and Technology Meet*, Edn. 2. (Wiley-VCH, New York; 1999).

15. Eigen, M. & Demaeyer, L. Self-dissociation and protonic charge transport in water and ice. *Proceedings of the Royal Society of London Series a-Mathematical and Physical Sciences* **247**, 505-533 (1958).

16. Damaskin, B.B. & Frumkin, A.N. Potentials of zero charge, interaction of metals with water and adsorption of organic substances. 3. role of water dipoles in structure of dense part of electric double layer. *Electrochimica Acta* **19**, 173-176 (1974).

17. van der Hoeven, P.H.C. & Lyklema, J. Electrostatic Stabilization in Nonaqueous Media. *Advances in Colloid and Interface Science* **42**, 205-277 (1992).

18. Bjerrum, N. A new form for the electrolyte dissociation theory. *Proceedings of the 7th International Congress of Applied Chemistry, Section X, London*, 55-60 (1909).

19. Morrison, I.D. Electrical charges in nonaqueous media. *Colloids and Surfaces A: Physicochemical and Engineering Aspects* **71**, 1-37 (1993).

20. van der Minne, J.L. & Hermanie, P.H.J. Electrophoresis Measurements in Benzene - Correlation with Stability .1. Development of Method. *Journal of Colloid Science* **7**, 600-615 (1952).

21. van der Minne, J.L. & Hermanie, P.H.J. Electrophoresis Measurements in Benzene-Correlation with Stability .2. Results of Electrophoresis, Stability, and Adsorption. *Journal of Colloid Science* **8**, 38-52 (1953).

22. Kitahara, A., Karasawa, S. & Yamada, H. Effect of Water on Electrokinetic Potential and Stability of Suspensions in Nonpolar Media. *Journal of Colloid and Interface Science* **25**, 490-495 (1967).

23. Fowkes, F.M., Jinnai, H., Mostafa, M.A., Anderson, F.W. & Moore, R.J. Mechanism of Electric Charging of Particles in Nonaqueous Liquids. *Acs Symposium Series* **200**, 307-324 (1982).

24. Kornbrekke, R.E., Morrison, I.D. & Oja, T. Electrophoretic Mobility

Measurements in Low Conductivity Media. *Langmuir* **8**, 1211-1217 (1992).

25. Briscoe, W.H. & Horn, R.G. Direct Measurement of Surface Forces Due to Charging of Solids Immersed in a Nonpolar Liquid. *Langmuir* **18**, 3945-3956 (2002).

26. Keir, R.I., Suparno & Thomas, J.C. Charging Behavior in the Silica/Aerosol OT/Decane System. *Langmuir* **18**, 1463-1465 (2002).

27. Ryoo, W., Webber, S.E., Bonnecaze, R.T. & Johnston, K.P. Long-Ranged Electrostatic Repulsion and Crystallization of Emulsion Droplets in an Ultralow Dielectric Medium Supercritical Carbon Dioxide. *Langmuir* **22**, 1006-1015 (2006).

28. Hsu, M.F., Dufresne, E.R. & Weitz, D.A. Charge Stabilization in Nonpolar Solvents. *Langmuir* **21**, 4881-4887 (2005).

29. Strubbe, F., Verschueren, A.R.M., Schlangen, L.J.M., Beunis, F. & Neyts, K. Generation current of charged micelles in nonaqueous liquids: Measurements and simulations. *Journal of Colloid and Interface Science* **300**, 396-403 (2006).

30. Beunis, F., Strubbe, F., Marescaux, M., Neyts, K. & Verschueren, A.R.M. Diffuse double layer charging in nonpolar liquids. *Applied Physics Letters* **91**, 182911-182913 (2007).

31. Roberts, G.S., Sanchez, R., Kemp, R., Wood, T. & Bartlett, P. Electrostatic Charging of Nonpolar Colloids by Reverse Micelles. *Langmuir* **24**, 6530-6541 (2008).

32. Hamada, K., Ikeda, T., Kawai, T. & Kon-No, K. Ionic Strength Effects of Electrolytes on Solubilized States of Water in AOT Reversed Micelles. *Journal of Colloid and Interface Science* **233**, 166-170 (2001).

33. Michel, E., Baur, R. & Macholdt, H.T. Charge stabilizers: properties and applications. *Journal of Electrostatics* **51-52**, 91-96 (2001).

34. Sainis, S.K., Merrill, J.W. & Dufresne, E.R. Electrostatic Interactions of Colloidal Particles at Vanishing Ionic Strength. *Langmuir* **24**, 13334-13337 (2008).

35. Morrison, I.D., Thomas, A.G. & Tarnawskyj, C.J. A method to measure the average charge to mass ratio of particles in low-conductivity media. *Langmuir* **7**, 2847-2852 (1991).

36. Shen, Y. & Duhamel, J. Micellization and Adsorption of a Series of Succinimide Dispersants. *Langmuir* **24**, 10665-10673 (2008).

37. Birkett, K.L. & Gregory, P. Metal complex dyes as charge control agents. *Dyes and Pigments* **7**, 341-350 (1986).

38. Baur, R. & Macholdt, H.T. Charge control agents for triboelectric (friction) charging. *Journal of Electrostatics* **30**, 213-222 (1993).

39. Sainis, S.K., Germain, V., Mejean, C.O. & Dufresne, E.R. Electrostatic Interactions of Colloidal Particles in Nonpolar Solvents: Role of Surface Chemistry and Charge Control Agents. *Langmuir* **24**, 1160-1164 (2008).

40. Nemamcha, M., Gosse, J.P., Gosse, B. & Denat, A. Influence of insulating electrode coatings on the electrical conduction of cyclohexane. *Ieee Transactions on Electrical Insulation* **23**, 529-534 (1988).

41. Denat, A., Gosse, B. & Gosse, J.P. Electrical conduction of solutions of an ionic surfactant in hydrocarbons. *Journal of Electrostatics* **12**, 197-205 (1982).

42. Eicke, H.F., Borkovec, M. & Dasgupta, B. Conductivity of Water-in-Oil Microemulsions - a Quantitative Charge Fluctuation Model. *Journal of Physical Chemistry* **93**, 314-317 (1989).

43. Hall, D.G. Conductivity of microemulsions: an improved charge fluctuation model. *The Journal of Physical Chemistry* **94**, 429-430 (1990).

44. Bumajdad, A. & Eastoe, J. Conductivity of water-in-oil microemulsions stabilized by mixed surfactants. *Journal of Colloid and Interface Science* **274**, 268-276 (2004).

45. Dukhin, A.S. & Goetz, P.J. How non-ionic "electrically neutral" surfactants enhance electrical conductivity and ion stability in non-polar liquids. *Journal of Electroanalytical Chemistry* **588**, 44-50 (2006).

46. Kato, K. *et al.* in Journal of Dispersion Science & Technology, Vol. 27 1217-1222 (Taylor & Francis Ltd, 2006).

47. Wang, Z. & Fingas, N. Analysis of sorbitan ester surfactants. 1. high-performance liquid chromatography. *Hrc-Journal of High Resolution Chromatography* **17**, 15-19 (1994).

48. Stock, R.S. & Ray, W.H. Interpretation of photon-correlation spectroscopy data - a comparison of analysis methods. *Journal of Polymer Science Part B-Polymer Physics* **23**, 1393-1447 (1985).

49. Chu, B. *Laser Light Scattering*, Edn. 2. (Academic Press, New York; 1991).

50. Berne, B.J. & Pecora, R. *Dynamic Light Scattering*. (Wiley, New York; 1976).

51. Zulauf, M. & Eicke, H.F. Inverted Micelles and Microemulsions in the Ternary-System H2o-Aerosol-Ot-Isooctane as Studied by Photon Correlation Spectroscopy. *Journal of Physical Chemistry* **83**, 480-486 (1979).

52. Ekwall, P., Mandell, L. & Fontell, K. *Journal of Colloid and Interface Science* **33**, 215 (1970).

53. Kotlarchyk, M., Huang, J.S. & Chen, S.H. Structure of AOT reversed micelles determined by small-angle neutron scattering. *The Journal of Physical Chemistry* **89**, 4382-4386 (1985).

54. Mukherjee, K., Moulik, S.P. & Mukherjee, D.C. Thermodynamics of micellization of Aerosol OT in polar and nonpolar solvents. A calorimetric study. *Langmuir* **9**, 1727-1730 (1993).

55. Chen, S.H. Small-angel neutron-scattering studies of the structure and interaction in micellar and microemulsion systems. *Annual Review of Physical Chemistry* **37**, 351-399 (1986).

56. Abou-Nemeh, I. & Bart, H.J. Microstructures in the system water/D2EHPA/span-80/n-dodecane. *Langmuir* **14**, 4451-4459 (1998).

57. Opawale, F.O. & Burgess, D.J. Influence of Interfacial Properties of Lipophilic Surfactants on Water-in-Oil Emulsion Stability. *Journal of Colloid and Interface Science* **197**, 142-150 (1998).

58. Kato, K. *et al.* Molecular composition of nonionic vesicles prepared from Span 80 or Span 85 by a two-step emulsification method. *Journal of Dispersion Science and Technology* **27**, 1217-1222 (2006).

59. Kallay, N., Tomic, M. & Chittofrati, A. Conductivity of water-in-oil microemulsions - comparison of the Boltzmann statistics and the charge fluctuation model. *Colloid and Polymer Science* **270**, 194-196 (1992).

60. Eicke, H.F. Surfactants in nonpolar solvents. Aggregation and micellization. *Topics in current chemistry* **87**, 85-145 (1980).

61. Sager, W.F.C. Systematic study on the influence of impurities on the phase behavior of sodium bis(2-ethylhexyl)sulfosuccinate microemulsions. *Langmuir* **14**, 6385-6395 (1998).

62. Chen, Y. *et al.* Electronic paper: Flexible active-matrix electronic ink display. *Nature* **423**, 136-136 (2003).

CHAPTER 3

PARTICLE SURFACE CHARGING AND CHARGE SCREENING IN NONPOLAR LIQUIDS VIA SURFACTANTS

3.1 Backgrounds and theories

3.1.1 Basic properties of particle surface charging in liquids

3.1.1.1 Charged solid surface immersed in a liquid

Charged solid surfaces are very important in many applications, for example, electrophoretic displays, protein studies, coatings, etc. The equilibrium distribution of electric charges at a solid-liquid interface is called an electric double layer. The double layer refers to two parallel layers: the first or "compact" layer comprises immobile positive or negative ions on the particle surface; the second layer is filled with oppositely charged mobile ions in solution attracted to the surface charge via the Coulomb force. This second layer is also called diffuse layer because it is made of ions freely moving in the liquid and loosely associating with the particle.

3.1.1.2 Surface charge and zeta potential

The formation of a double layer on the particle surface leads to the build-up of an electric surface charge, which creates an electrostatic field that affects the ions in the liquid. Figure 3-1 shows the ionic concentration and potential difference as a function of distance from particle surface when suspended in a liquid dispersion.

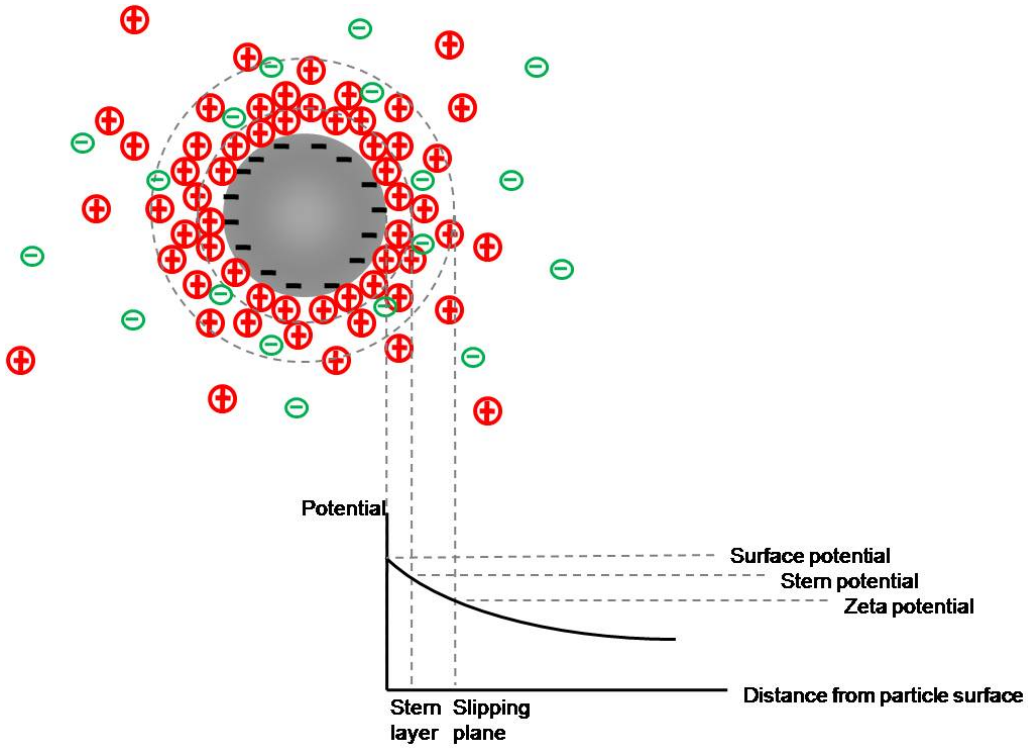

Figure 3-1 Scheme of a negatively charged particle suspended in a liquid medium, showing the ionic concentration and potential difference as a function of distance from the particle surface.

The electric potential difference between the fluid bulk and the surface is called the electric surface potential. The "slipping plane" or "plane of shear" denotes the hydrodynamic boundary between surface-bound fluid and fluid free to move relative to the surface. It is the electrostatic potential at this slipping plane, the so-called electrokinetic potential or zeta potential, which is experimentally accessible and commonly used for estimating the degree of double layer charging. It is worth to mention that zeta potential is not equal to the electric surface potential in the double layer, but zeta potential is often the only measureable parameter to characterize the double layer properties. For particle dispersed in a system with low ionic strength, typical nonpolar

dispersion, the electrostatic potential decays so slowly that the zeta potential and surface potential need not to be distinguished.

The zeta potential cannot be measured directly, but for colloidal particles, it can be calculated from the particles' electrophoretic mobility μ using the standard electrokinetic model [1]. The electrophoretic mobility is defined as the drift velocity *v* of a charged particle in an external electric driving field $\vec{E}$, divided by the field strength, $\mu = \frac{v}{E}$. It can be determined experimentally by applying a known electric field across the dispersion and measuring the induced particle velocities. Modern instruments typically determine this velocity with the help of laser light scattered by the particles, either by intensity frequency analysis of light from particles illuminated by a moving fringe pattern (laser Doppler velocimetry), or by analyzing phase shifts in the scattered light with respect to the incident laser beam (Phase Analysis Light Scattering, PALS).

3.1.2 Particle charging mechanisms in liquids

3.1.2.1 Charging mechanisms of aqueous dispersions

In aqueous colloidal suspension, several mechanisms are proposed to describe the process of charging the immersed solid surfaces which are greatly dependent on the surface chemistry and surrounding phase.

The dissociation of surface bound head groups (for example –OH, –COOH, $-SO_4$, etc.) represents one of the mechanisms for particle surface charging [2-6]; it is similar to the bulk dissociation of salt ions in aqueous solutions. A neutral surface molecule splits into two oppositely charged parts, one remaining on the surface and the other departing

as a free ion. Therefore, a dissociation process is dependent on the bulk electric property which affects the equilibrium of surface molecule's reaction, and on the surface concentration of dissociable surface sites [7].

The colloidal particles dispersed in a liquid can become charged not only by dissociation of surface molecules, which are mostly acid-based, but also due to the preferential adsorption of charged species such as polyelectrolytes and surfactant ions, which depends on the available acceptor sites as well. Sefcik [8], for example, studied surface charging of polymeric latex particles stabilized by sodium dodecyl sulfate (SDS), an anionic surfactant. Lee [9] examined the adsorption of cationic and anionic surfactants on metal oxide surfaces, by sodium nonyl benzene sulfonate (SNBS) and dodecyl or tetradecylpyridinium chloride (DPC/TPC). Iruthayaraj [10] analyzed the effects of ionic strength and pH on the silica surface charging by adsorption of polyelectrolyte containing poly(ethylene oxide) side chains.

Sometimes the chemical composition of the surface gives an indication for the charging mechanism. Water can be incorporated in the metal crystal structure resulting in the formation of responding hydroxides which can dissolve into water to an extent dependent on the solution pH and temperature [11]. When the metal oxide surface (for example Al_2O_3, TiO_2, SiO_2, etc.) is immersed in aqueous solution, the surface reacts with water to produce surface hydroxyl groups [12-16], and partial dissolution can leave the remaining particle surface charged.

3.1.2.2 Charging mechanisms of nonpolar dispersions via surfactants

In non-polar media, according to the studies of the electrophoretic mobility and

colloidal stability of non-aqueous systems firstly carried out by Fowkes [17-19], a charging effect happens only if it can be explained by the particle surface chemistry. The authors gave the credit to competitive acid-base interaction of the surfactant and the solvent with the suspended particle, but did not propose a detailed model of how charge is transferred to or from the particle surface.

More recent studies observe that colloids dispersed in a nonpolar solvent become charged in the presence of reverse micelles. Although there can be no doubt that surfactant additives can promote surface charging of immersed particles, the charging mechanisms remain largely unclear and competing models still await conclusive validation.

Two likely charging mechanisms given by Morrison in his review article [20] involve either preferential adsorption of the charged species (micelles) of one sign over the other, or the surface dissociation of ions which are then incorporated in some lyophilic structure such as the reverse micelles also capable of charging in the absence of a solid surface. Neither of these concepts is universally accepted.

For AOT as the charge control agent, several studies have reported that with increasing surfactant concentration the particle potential either monotonically decreases [21], or (more commonly) displays a maximum [22].

Smith et al. [21] observed the gradual reduction in zeta potential of hydrophobically modified TiO_2 colloids with increasing AOT concentration, and Keir et al. [22] reported a sign reversal of electrophoretic mobility of silica particle in decane as AOT concentration was increased. In marked contrast to these observations, Hsu et al.

[23] found that the surface potential of sterically stabilized PMMA colloids in alkanes was independent of AOT concentration above the CMC, as seen both by electrophoresis and particle interaction measurements, although the presence of reverse micelles appeared to be required for surface charging. They proposed that the surface entropy played an important role for surface charging, which is very different from aqueous systems, where surface entropy effects are typically neglected.

Meanwhile, other researchers believe that asymmetric adsorption of charged reverse micelles formed in bulk liquid phase is the reason why the particles undergo surface charging in surfactant/nonpolar oil solutions.

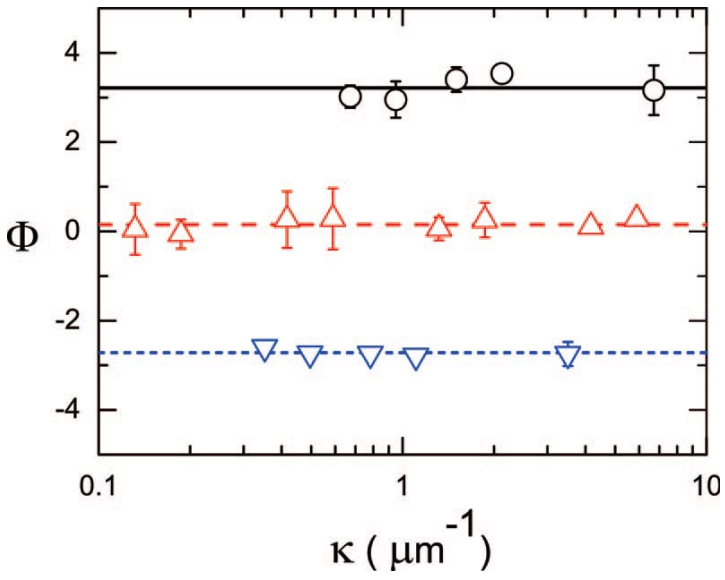

Figure 3-2 Dimensionless surface potential as a function of inverse Debye length (controlled viasurfactant concentration)for 3 different types of surfactants[24].

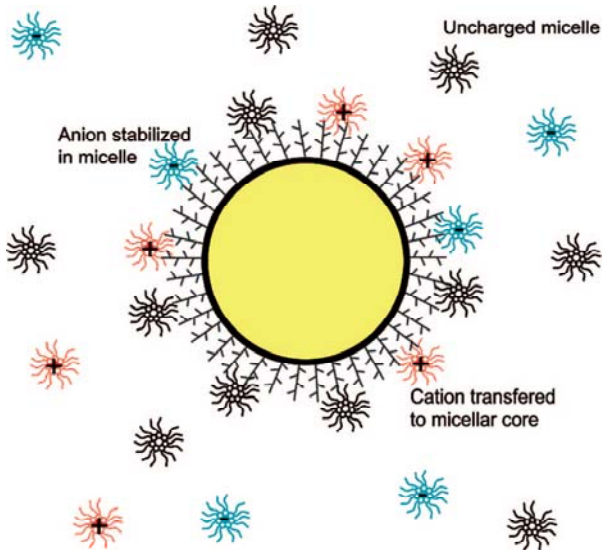

Figure 3-3 Micelle-decorated polymer particle [24]

For example, in Roberts' work [24] different kinds of surfactants, AOT, Zr(Ort)2 and poly(12-hydroxystearic acid) poly(methyl methacrylate) (PHSA-PMMA), promoted negative, positive or no charging of the sterically stabilized poly(methyl methacrylate) particles. They used the technique of single particle optical micro-electrophoresis (SPOM), which allowed the detection of mobility effects in individual colloidal particles caused by just a few elementary charges. In the absence of surfactant reverse micelles, their particles had a very small electrophoretic mobility and were essentially uncharged in dodecane. However, the addition of 1 mM of AOT or 1.7 mM of $Zr(Ort)_2$ affected the electrophoretic mobility and zeta potential dramatically, with AOT reverse micelles causing a large negative charge and $Zr(Ort)_2$ micelles a large positive in the case of added $Zr(Ort)_2$ micelles, as shown in Figure 3-2. However, the colloidal particles remained essentially uncharged upon addition of PHSA-PMMA. Note that for each micellar system, the surface potential was independent of the inverse Debye length or equivalently the

surfactant micellar concentration. Despite the micelles of AOT, $Zr(Ort)_2$ and PHSA-PMMA being chemically different, the oppositely charged species were formed with equal probability. In view of the independence of surface potential on the added surfactant concentration, it was hypothesized that micelles of both signs of the charge adsorb to the particle surface as illustrated in Figure 3-3. The mechanism of dissociation or adsorption of a single species proposed before is inconsistent with their experimental observation of a constant surface potential. However, there is still no model for the respective adsorption isotherms that would explain the experimental data.

In either case, the mechanism of surface charging remains unclear, and there are many open questions. If the notion of the dissociation of surface bound groups is correct, are neutral micelles necessary as counterion acceptors? Or, if asymmetric adsorption of charged micelles explains the different surface charge in the presence of various kinds of surfactant, how does the preference for micelles of one sign of charge arise? Do these proposed mechanisms for surface charging both occur, possibly simultaneously in the same systems, since oppositely charged micelle pairs and neutral micelles always coexist? Can the immersed solid surface get charged in the absence of micelles, due to molecularly dissolved surfactant molecules only? (Previous studies [25, 26] suggest that conductivity effects occur in surfactant solutions below the CMC, surface charging does not.) Finally, is there any other mechanism to describe the charging effect to the non-polar colloidal suspensions?

Besides the two widely debated charging mechanisms, the acid-base interaction between particle surfaces and surfactants pointed out by Fowkes [17-19] is drawing more attention. This mechanism involves the acid-base charge transfer between particle

(surface functional groups or particle materials) and participating surfactant aggregates (complex or micelle). The acid-base interaction to explain the particle charging in nonpolar media will be introduced in more detail in the following section.

3.1.3 Acid-base interactions

The concept of acid-base interaction involves the transfer of protons or electrons between the acid and basic species. The acid species is defined to be a molecular entity (and the corresponding chemical species) that would donate protons or accept electrons, while the basic species is defined as the one that would donate electrons or accept protons. The acid-base properties of interacting molecules as a key to predicting and understanding the formation of an adhesive bond was proposed by Fowkes and coworkers beginning in the 1960s [19, 27, 28].

Some compounds could be both acid and base (in the Bronsted or Lewis sense), such as water, because they are able to either accept or donate protons or electron pairs. In most cases, the proton or electron transfer between interacting molecules is not simply determined by an absolute classification as acid or base, but determined by the comparison of the acid-base properties of the interacting species. For instance, a surface with high basicity (such as the PMMA particles used in the research described below) is most likely to exchange charge with a species of high acidity, where high acidity does not preclude high basicity of the same molecule. Note that it is often unclear whether electron or proton transfer is responsible for the charge exchange [20].

In aqueous dispersion, the acid-base interaction as the driving force for charging is known where the hydroxyl groups on the surface of immersed solid particles are

charged with the surrounding solution. The inherent acidity or basicity of the composition of the particles, surface appending groups, and the pH of the water solution determine the polarity and magnitude of charge on the particle surface.

It is not well understood whether this acid-base interaction can be correlated to surface charging in nonpolar dispersion, more specifically, in the presence of surfactants in the nonpolar solution. Proponents of this idea [26] claim that the polarity and magnitude of surface charge in these systems are determined by the relative acidity (or basicity) of the particle and surfactant in the mechanism of acid-base charge transfer process.

The sign and magnitude of the particle electrophoretic mobility or zeta potential are always used to characterize the surface charging. However, the dependence of zeta potential on surfactant concentration is not settled. The zeta potential is reported as constant [23, 24], monotonically increasing [29] or decreasing [21], switching sign [22], or going through a maximum value as the surfactant concentration increases [30-33]. The inconsistency of these results is partly due to a lack of consistency in the choice particle materials (particle matrix materials and surface groups), charge-stabilizing solutes (surfactants in these cases) and solvents, and to a limited range of surfactant concentration.

Poovarodom and Berg [26] studied surface functionalized silica particles and compared the effects of Span 80 (an acidic surfactant) and PIBS (polyisobutylene succinimide, a basic surfactant) in nonpolar silica particle dispersions. The acid-base properties of surface functionalized silica particles and surfactants had a direct effect on

the magnitude of the resulting surface potential. No particle charging was detected at low surfactant concentrations, but around and above the CMC, Span 80 led to positive particle charging regardless of the surface characteristics, whereas the presence of PIBS invariably resulted in negatively charged particles; this behavior was attributed to the acidic (Span) and basic (PIBS) nature of the surfactants. Furthermore, the degree of acid-base charging is also determined by the relative acid-base properties between the interacting species. In the presence of acid surfactant Span 80, the basic groups functionalized silica particle obtained a large positive surface charge; in contrast, the acidic silica particle only showed a small positive surface charge because compared to Span 80 the acidic silica particle still had a higher ability to donate electrons (or accept protons). This acidic surfactant (electron acceptor or proton donor) conducts an acid-base driven charge transfer, leaving a positive surface charge on the silica particles, and similarly the basic surfactant leaves a negative particle surface charge. From the results of functionalized silica particles, the magnitude of surface charge depended on the relative acidity of the particle compared to the surfactants.

To test the hypothesis of acid-base interactions as the origin of particle charges in nonpolar media, a systematic study accounting for the chemistry of surface headgroups, the nature of the particle material and surfactant, a large range of surfactant concentrations, and a potential influence of the applied electric field is necessary.

The section “Experiments and Discussion” in this chapter describes experiments to compare the acid-base properties of the particles and the surfactants and finds some support for the theory of acid-base driven charging in nonpolar media. Acid-base driven charging could represent a method to predict and control the immersed solid surface

charging in nonpolar dispersions.

3.1.4 Electrostatic particle interactions

For charged particles in dispersion, the interaction depends strongly on both surface potential and ionic concentration in solution. Thus, electrostatic particle interactions provide an opportunity for independent measurements to understand charging phenomenon, besides the conductivity measurements and electrophoresis analysis.

The Derjaguin-Landau-Verwey-Overbeek (DLVO) theory [34, 35] was developed to explain colloidal stability and analyze the electrostatic interactions between the immersed charged surfaces in aqueous solutions. It combines the effect of van der Waals forces and electrostatic double layer forces.

The stability of aqueous colloidal dispersion is controlled by both free ions in the bulk phase and the charge on the particles surface. The pair-particle interaction energy, $u(r)$, between two equally-charged particles immersed in solution can be expressed by the well-know screened-Coulomb interaction potential [36]:

$$u(r) = \frac{(Z^*e)^2}{(4\pi\varepsilon\varepsilon_0)r} \frac{\exp(2\kappa R_{particle})}{(1+\kappa R_{particle})^2} \exp(-\kappa r) \qquad \text{Equation 3-1}$$

where κ is a function of conductivity and $\kappa^{-1}$is known as the Debye-Huckel screening length, e is the elementary charge, Z^* is the (effective) number of elementary charges per particle, r is the distance away from the particle surface, and $R_{particle}$ is the radius of the spherical particle. The first term on the right side of the Equation 3-1, $\frac{(Z^*e)^2}{(4\pi\varepsilon\varepsilon_0)r}$, is the

classical Coulomb term for point charges; the second, $\frac{\exp(2\kappa R_{particle})}{(1+\kappa R_{particle})^2}$, is a correction for the finite particle size; the third, exp $(-\kappa r)$, is the screening term.

Equation 3-1 is derived from a linearized theory accurate only for weakly charged particles, but applicable much more generally if Z^*e is interpreted not as the actual particle charge, but a renormalized lower "effective" charge (hence the asterisk).In particular when the particle size is much larger than the screening length, as it often happens in aqueous media, the effective surface charge can be significantly smaller than the actual surface charge, but for nonpolar dispersions such renormalization effects are typically small and the distinction between true and effective charge is unnecessary.

In the colloidal system, the Debye length is defined as

$$\kappa^{-1} = \sqrt{\varepsilon\varepsilon_0 kT/2N_A e^2 I}, \qquad \text{Equation 3-2}$$

where I is the ionic strength and N_A Avogadro's number, describing the screening of net charge in solution. This Debye length is the decay length of the interaction energy, electrostatic potential, and the ion concentration in the counterion atmosphere. The ionic strength, I, is set by the concentration of ions in the bulk fluid far away from the surface, and affects the Debye length, as can be seen from Equation 3-2, through the scaling, $\kappa^{-1} \propto I^{-1/2}$. A large concentration of ions in the bulk fluid (a small Debye length) effectively "screens" the electrostatic interaction between charged surfaces. The spatial dependence of the electrostatic interaction therefore attracts particular interest.

While the important role of electrostatic interactions in aqueous colloidal dispersions has long been appreciated, their relevance to nonpolar suspensions remains

unclear. Conventionally, it is believed that in nonpolar liquids the electrical double layer and surface charge are not significant, because ions are expected to have very low solubility. Yet, there is solid proof of surface charging in contact with nonpolar liquids in the presence of surfactants [20]. Even if the occurrence of some surface charge is accepted, it is unclear whether this charge leads to significant electrostatic interaction, and if so, how this interaction decays as a function of surface separation. Given the ion paucity of nonpolar solutions, one might doubt that the familiar concepts of charge screening by mobile ions are applicable here, and evidence for both screened [23] and unscreened interaction [31] has been reported.

A good understanding of charge formation in bulk solution and the mechanism of surface charging builds the base of analyzing the electrostatic interaction of colloidal dispersions by controlling the electric properties and modifying the immersed solid surface. The observation of electrostatic repulsion between pair particles via added surfactants should provide solid evidence of surface charging in nonpolar liquids.

As mentioned before, the screened-Coulomb expression of DLVO theory describes the particle interactions very well in aqueous dispersion. We would like to put efforts here to explore whether surface charging and charge screening in nonpolar solutions could also be elucidated in the framework of screened-Coulomb interaction. The measured interactions give information about the surface charge density and concentration of charged species in the solution, as they have done in aqueous systems. More importantly, the measurements under different surface and solution conditions can provide us valuable clues about the charging mechanism in nonpolar media, and the better-understood electrostatic interactions allow us to build a theoretical model

describing the stability of colloidal dispersions. We are going to discuss the electrostatic pair interaction of particles in our nonpolar dispersions and relate it to our surface potential and conductivity measurements.

3.2 Materials and methods

3.2.1 Surfactant solutions

Surfactant solutions are prepared in the same way as the ones described in section 2.2.1. After overnight mixing, the solutions are stable and transparent. All surfactant solutions are allowed to equilibrate for 1 day prior to use. All experiments are performed in a thermostated environment at 22 ± 0.5 ℃.

The surfactants include AOT and Span 85, purchased from Sigma-Aldrich and used without further purification. The nonpolar solvents hexane (BDH, ACS grade) and decane (Sigma-Aldrich, > 99%) were chosen for their very low dielectric constants (ε = 1.9 for hexane and 2.0 for decane) and for their relatively large refractive index mismatch with surfactant solutes and dispersion particles of interest.

3.2.2 Particle dispersions via solvent swap

Nonpolar dispersions were obtained by transferring commercially available particles in Table 3-1 from aqueous dispersions into the target alkanes via a multi-stage solvent swap. Polymethyl methacrylate (PMMA) sulfate particles (Bangs Laboratories; I diameter 0.11 μm: product no. PP02N/5814; II 0.52 μm: PP02N/8813; III 1.08 μm: PP04N/6896), polystyrene (PS) sulfate particles (IV; invitrogen Molecular Probes, Inc.; 1 μm: product no. S37498/456091), PS carboxyl particles (V; invitrogen Molecular Probes, Inc.; 1 μm: product no. C37274/832532), and PS amidine particles (VI; invitrogen Molecular Probes, Inc.; 1 μm: product no. A37322/807567) were originally delivered as a dispersion in deionized water. Ultrapure water with a resistivity of 18.3 $M\Omega \cdot cm$

(Barnstead) and isopropanol (Sigma-Aldrich, >99.5%) were used in the solvent swap step as described below.

Table 3-1 Different types of particles. The diameter of various particles: I – 0.11μm; II - 0.52 μm; III – VI 1μm.

Surface group / Material	Sulfate	Carboxyl	Amidine
PMMA	I, II, III		
Polystyrene	IV	V	VI

In order to transfer these particles into nonpolar solvents, a solvent swap is carried out as follows: an aliquot of aqueous dispersion is diluted with a1:1water/isopropanol mixture and centrifuged at 3500 r/min for 10 minutes. The clear supernatant is discarded, the dense bottom phase collected and diluted with pure isopropanol. After sonication for about 30 seconds, the concentrated particles are again dispersed. Centrifugation, disposal of the supernatant, redispersion of particles, and sonication were repeated three times and the dispersant exchanged for pure isopropanol, 1:1 isopropanol/surfactant in alkane solution, and eventually pure alkane/surfactant solutions. Since isopropanol is miscible with both water and alkanes, transfer through this intermediate circumvented the challenge of crossing a phase boundary without irreversible particle aggregation and reduced the residual water content to a minimum. In the last step, the surfactant concentration is adjusted to its target value by dilution or further addition of surfactant. If particles are transferred into surfactant-free alkane, the resulting dispersion is observed to be unstable and aggregate fast and irreversibly. The presence of surfactant at some fraction of the CMC, however, guarantees the monodispersity and colloidal stability of

the final nonpolar dispersions as confirmed by microscopy and light scattering.

3.2.3 Karl Fischer Titration

This technique was previously introduced in Section 2.2.6. In this part, we use Karl Fischer titration (TitroLine KF, SCHOTT) to determine the water contents of the colloidal dispersions obtained from the solvent swap.

3.2.4 Electrophoretic mobility and zeta potential

Phase analysis light scattering (PALS) [37, 38] was used (Malvern Zetasizer Nano ZS90) to determine the electrophoretic mobility and the respective zeta potential of the dispersed particles [39, 40]. A dip cell provided by Malvern is designed specifically for measurements in nonaqueous environment. It consists of a glass cuvette with square cross-section as the sample container and a unit dipped into the glass cuvette that introduces the external electric field between the two planar palladium electrodes separated by 2 mm. Prior to each measurement, the dip cell electrodes and glass cuvette were sonicated in methanol, carefully cleaned and dried, and rinsed with the target solution. We confirmed that the measured electrophoretic mobility was insensitive to the particle number density in our experiments. In order to observe particle motion in highly nonpolar dispersion, a large electric field is usually required in electrophoresis experiments. As a result, the particles' response to the field can become nonlinear and the apparent electrophoretic mobility a function of the field strength [41], which makes it questionable in our view draw conclusions from the measured raw mobilities about the particle charge in the absence of a field, as is often done in the literature [26, 42]. We indeed found the field-dependent effects in many of our samples by the systematic

mobility variation with the applied electric field. To avoid misinterpretations, we extrapolated the measured electrophoretic mobility to zero field strength, as discussed in the Results section.

3.2.5 Electrostatic interaction measurements

In collaboration with Carlos Espinosa [43], independent evidence of surface charging and charge screening in nonpolar dispersion via surfactants was obtained by measuring the particle interaction through statistical analysis of equilibrium particle configurations. Particle tracking video microscopy as first described by Crocker and Grier [44] is used to locate particle positions, from which the pair interaction energy as a function of particle separation is inferred using an implementation of liquid structure analysis first discussed by Behrens and Grier [45]. In this part of the research, I was in charge of training Carlos and providing the nonpolar dispersions and their characterization, and contributing the conductivity and electrophoresis data. Carlos carried out the interaction measurements and computational modeling. Then we were both involved in interpreting the interaction results for systematic study of particle charging and charge screening in nonpolar media. The scheme of the entire process of pair interaction measurement is shown in Figure 3-4 (below).

The pair interaction of 1.08 μm PMMA particles in nonpolar dispersions was studied by analysis of quasi-2-dimensional equilibrium particle configurations [23]. Dispersions are confined in a narrow gap between two almost parallel glass coverslips (18 mm × 18 mm) spin-coated on their facing surfaces with a thin (0.1 μm) layer of PMMA. The confining gap is created by placing the coverslips together, with a 15 μm

poly(ethylene terephthalate) spacer on one side, and sealing the two contacting sides with a UV-curable epoxy adhesive (NOA 71).This thin, wedge-shaped sample cell is filled, through the open sides, with a nonpolar dispersion of interest and placed horizontally into a glass dish with a thin bottom made from a larger coverslip. The dish is then filled to a level well above the glass wedge with more of the same dispersion (a sample "bath") and covered with a glass lid to prevent solvent loss by evaporation. Particles confined in the wedge, as shown in the upper left of Figure 3-4, are imaged with a long working distance 40×/0.6 NA air objective on an inverted microscope (Nikon Eclipse TE2000-E). [43]

A large number of images (typically 60,000 frames) showing on average 30-80 particles in a 28.8×10^3 μm^2 field of view were recorded with a CCD camera at a rate of 1 frame/s, using the Nikon Perfect Focus system to automatically correct focus drift. Particle positions in two dimensions are obtained from each image with sub-pixel accuracy [44]. From these particle position the ensemble averaged 2-D radial distribution function *g(r)* is computed [45]. This function, which contains valuable information about the particle interaction, is defined as the average (2-D) particle concentration at distance *r* from a randomly chosen central particle, normalized by the average particle concentration of the entire system. The chosen number of frames and overall duration of our measurements (60,000 s=17 h) guarantee that enough independent configurations were sampled to keep the statistical error in *g(r)* below 7.5% when *g(r)* is evaluated at separation intervals of 0.5 μm [45].

The radial distribution function *g(r)* relates to the pair interaction energy *u(r)* in the limit of infinite dilution via,

$$u(r) = -k_B T ln\big(g(r)\big) \qquad \text{Equation 3-3}$$

For finite particle concentration, these two terms are not related in a simple way, but an excellent approximation to describe the long-range interactions can be expected from the Ornstein-Zernike (OZ) integral equation combined with the hypernetted chain (HNC) closure relation [46]. The interpretation of the interaction results and the comparison between the conductivity data and electrophoresis measurements will be discussed in the following section.

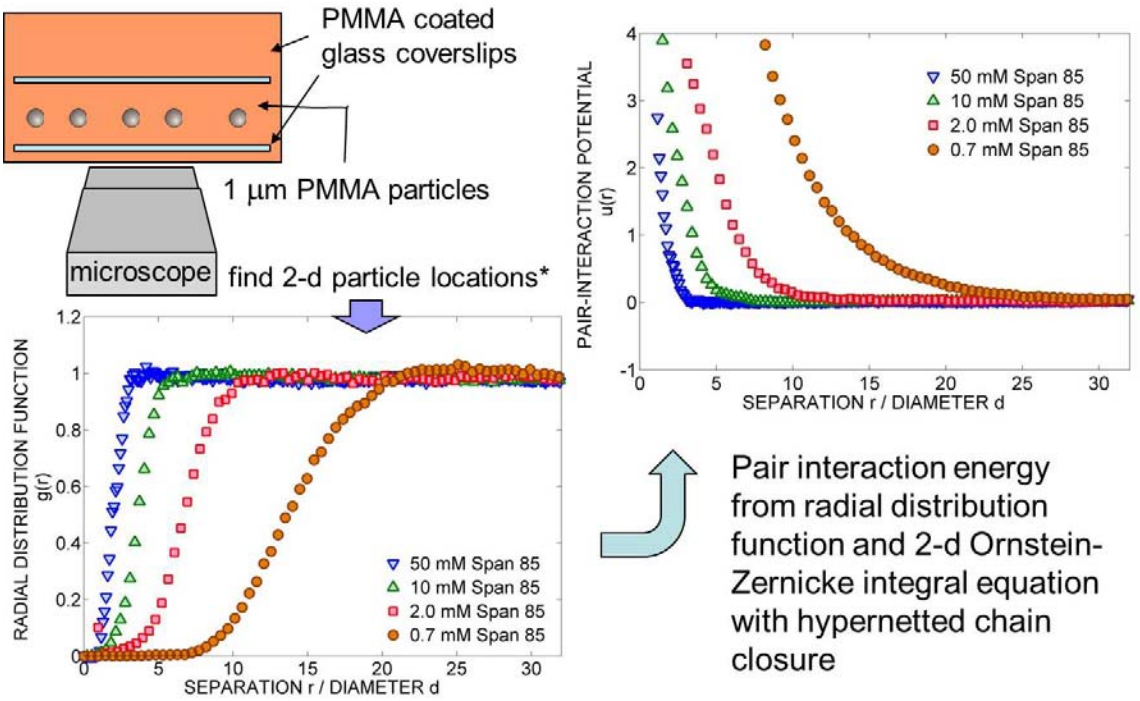

Figure 3-4 Scheme of pair interaction measurement through statistical analysis of equilibrium particle configurations observed by video microscopy. [43]

3.3 Results and discussions

Supported by the proof of charge induced by nonionic surfactant in nonpolar liquids, we studied the electrophoretic mobility of suspended solid particles with the participation of surfactants. The interaction measurements provided independent evidence to further confirm the ability of nonionic surfactants as "charge control agents". In addition, the charging effects from various kinds of surfactants, polymer materials, and particle surface groups were also studied to understand the charging mechanism in nonpolar dispersion.

3.3.1 Particle stabilization mediated by surfactants

Electrophoresis measurements on two different types of PMMA particles (I and II) were carried out both in aqueous solutions of sodium chloride, prepared by direct dilution of the aqueous commercial dispersion, and in hexane solutions of Span 85, prepared by solvent swap from the same dispersion.[43]

3.3.1.1 Electrophoresis in aqueous solutions

Figure 3-5 shows the electrophoretic mobility μ in aqueous dispersions as a function of NaCl concentrations [43]. The observed behavior is typical for polymer particles that retain negatively charged sulfate groups on the surfaces from the initiator used in the polymerization.

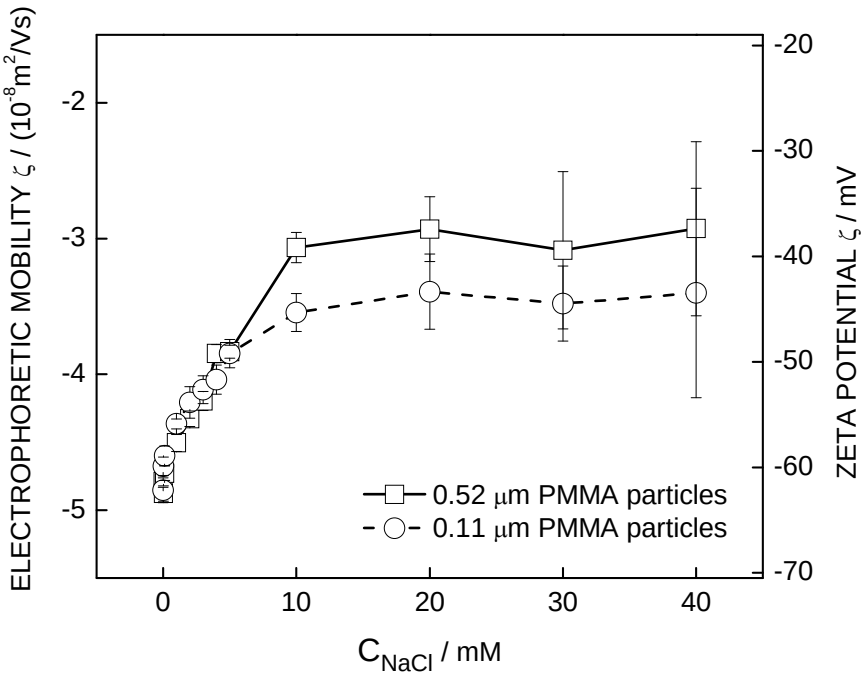

Figure 3-5 Electrophoretic mobility and zeta potential in aqueous dispersions at varied salt concentration for the two particle types with different diameter (I and II). Error bars reflect standard deviations over five measurement runs.[43]

For convenience, Figure 3-5 also indicates the zeta potential ς of the different particles as given by the Smoluchowski expression $\varsigma = \mu\eta/\varepsilon\varepsilon_0$, where η is the dynamic viscosity of the continuous medium. Strictly, this expression is valid only for the limit of strong screening, $\kappa d \to \infty$, where$d$ is the particle diameter, and $\kappa = (4\pi\lambda_B(n_+ + n_-))^{1/2}$ is the inverse Debye length, determined by the number concentration n_+ and n_- of cations and anions in solution. For finite κd, the classic theory by O'Brien and White [1] shows a nonlinear relation between μ and ς, which is not even monotonic for very strongly charged particles [47]. Still, for the system at hand, we can expect the ς-scale shown in Figure 3-5 to correctly capture the qualitative features and the general

magnitude of the zeta potential.

The observed decrease in absolute values in the electrophoretic mobility and zeta potential, less negative and less positive in respective type of surface charge, with added salt is typical of electrostatic screening.

Measured differences between the two particle types in Figure 3-5 may have several origins: apart from the size difference, particles may have a different surface density of sulfate groups, and the 0.52 μm particles come with a small amount of the antimicrobial additive sodium azide, whereas the 0.11 μm particles do not. We shall see below that none of these differences appear to affect the particles' electrophoretic mobility in *nonpolar* solutions.

3.3.1.2 Electrophoresis in nonpolar surfactant solutions

PMMA sulfate particles from the same two original aqueous dispersions were transferred into Span 85/hexane as described before and found to form a stable dispersion above a minimum surfactant concentration of 05.mM. DLS confirmed that the 0.52 μm particles remained fully dispersed, whereas stable clusters around half a micrometer in size were detected and possibly from during the solvent swap. Monitoring over a week after transferring the particles into hexane solutions, no continued aggregate growth was detected by DLS.

The concentrations of the target Span 85 in hexane solutions include the surfactant molecules (or complex)-dominated regime below the CMC and the reverse micelles-dominated regime above the CMC. The particles after solvent swap were fully

and stably dispersed in the hexane/Span 85 solutions despite of their concentrations. We measured the electrophoretic mobility of the two types of PMMA particles (I and II) at different Span 85 concentrations with deliberate variation of the accelerating electric field, shown in Figure 3-6. [43]

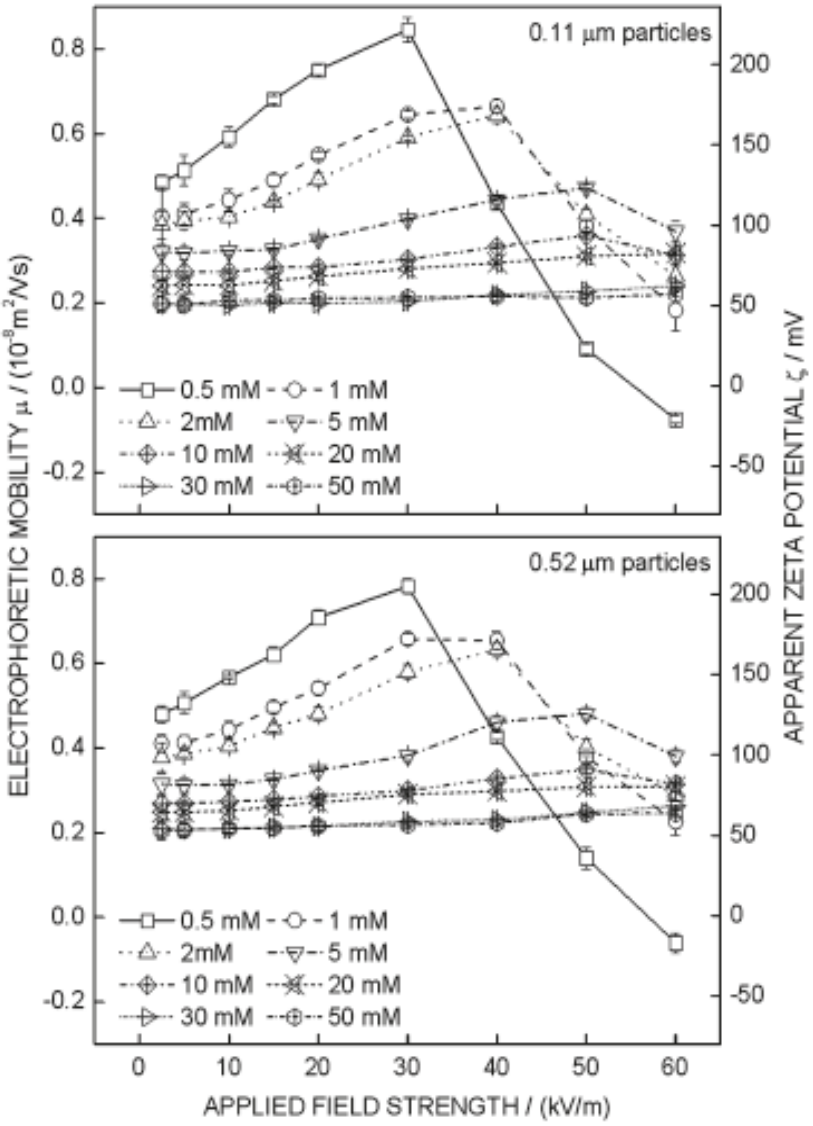

Figure 3-6 Electrophoretic mobility and apparent zeta potential (Huckel limit) of 0.11μm (top) and 0.52 μm (bottom) PMMA particles (I and II) in hexane as a function of field strength and Span 85 concentration. [43]

The distinguished responsive behaviors of PMMA particles as a function of Span 85 concentration and applied field shown in Figure 3-6 indicate that the PMMA particles in nonpolar dispersions have substantial electrostatic surface potentials, which are greatly affected by the added surfactants and external field strength. The interpretation of the results is explained as follows.

3.3.1.3 Voltage dependence and zero field electrophoretic mobility

In aqueous dispersion, a very small electric field is required to create significant particle motion when there are plenty of free charge entities. A linear response of the particle velocity to the applied field, which means a field-independent electrophoretic mobility, is the premise of standard electrokinetic theory relating the induced particle motion to the charging state of the dispersed particles in the absence of external fields.

For nonpolar systems, this premise should not be adopted blindly, because here the electric field strengths necessary to induce measureable electrophoresis can influence both the electrophoretic mobility [48] and solution conductivity [49] and lead to measurement artifacts [41]. Data shown in Figure 3-6 demonstrate that the assumption of a field-independent electrophoretic mobility would indeed be very wrong for our dispersions. Especially at surfactant concentrations below the CMC of 10 mM Span 85, the measured mobilities are seen to vary strongly, even nonmonotonically, with the field strength. At the lowest Span 85 concentration of 0.5mM the mobility of both particle types is field-dependent down to the weakest fields (2.5kV/m) applied in our study, and it even reverses its sign around field strength of 50 kV/m (which is still a moderate value by some standards [22, 41]). At high surfactant concentration, by contrast, the mobility is

seen to be field-independent, in which case the solution environment is more like the one of aqueous dispersions with plenty of free mobile ions. The measured electrophoretic mobilities are also translated, in Figure 3-6, into apparent zeta potentials, using the Huckel expression $\varsigma = 1.5\mu\eta/\varepsilon\varepsilon_0$, which is valid strictly in the limit of vanishing ionic strength ($\kappa d = 0$). [43]

In order to allow conclusions about the particles' charging behavior without applied external fields, we extrapolate the mobility data of Figure 3-6 to zero field strength. Figure 3-7 shows this zero-field electrophoretic mobility and the corresponding zeta potentials (Huckel limit) as a function of surfactant concentration. Some important features are discussed next.

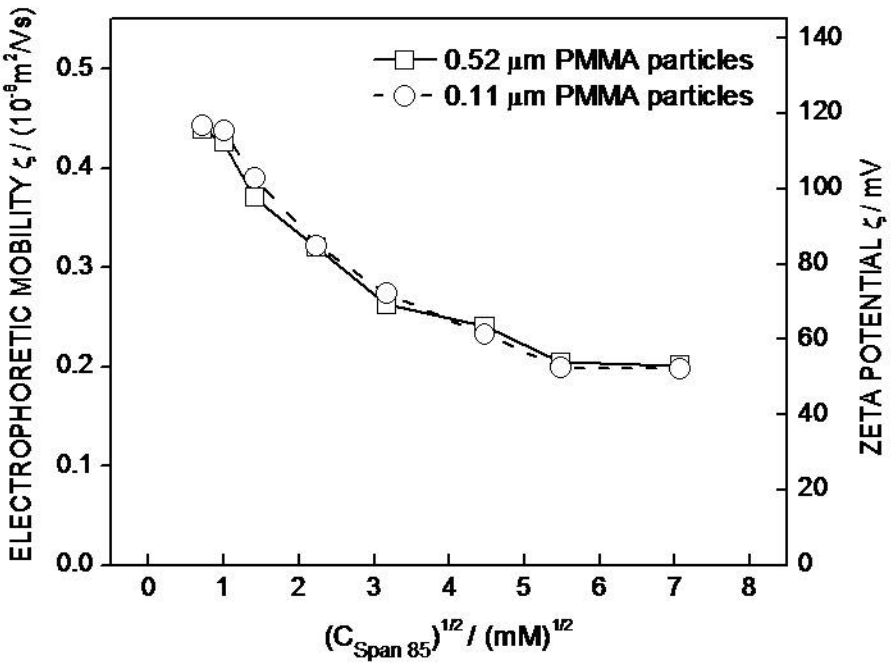

Figure 3-7 Zero field electrophoretic mobility and zeta potential (Huckel limit) of PMMA particles (I and II) in hexane as a function of Span 85 concentration. Confidence intervals are comparable to the marker sizes.[43]

Although the particles I and II are negatively charged in aqueous dispersions (Figure 3-5) the zero-field electrophoretic mobility and thus the particle charge is positive in the entire range of surfactant concentrations (Figure 3-7). It is clear that the positive particle surface charge in Span 85/hexane solution neither stem from the surface sulfate group, nor from the adsorption and dissociation of surfactant molecules since Span 85 is non-dissociable surfactant. Based on the hypothesis of an acid-base interaction between the surfactant and the particle as the source for the charge transfer, PMMA is classified as a basic polymer and Span 85 (sorbitan oleates family) as an acidic surfactant [26]. Relatively strong acid-base interaction between the PMMA particle and Span 85 can occur even in very nonpolar solvents such as hexane. Although it is not clear whether the transferred species is a proton or an electron [20], a charge transfer reaction predicted by the acid-base concept could leave the immersed particle surface positively charged in nonpolar surfactant solutions.

The zero-field mobility obtained (Figure 3-7) in Span 85/hexane solution is one order of magnitude smaller than the mobility in aqueous solution (Figure 3-5). However, the observed mobilities are fairly large compared to values reported for other nonpolar systems [21-23, 26]. For nonpolar dispersions, the zeta potential is considered to represent the electrostatic surface potential. [50] Figure 3-7 indicates the value of zeta potential in the Huckel limit ($\kappa d = 0$) as an approximation of the actual potential in the present condition of small but finite values of κd.

It is important to know that in media of low permittivity substantial surface potentials can be caused by a small number of surface charges. For low values of κd, the particle charge Ze is related to the surface potential via

$$Z\frac{\lambda_B}{d/2} = \frac{e\zeta}{k_B T}\left(1 + \frac{\kappa d}{2}\right) \qquad \text{Equation 3-4}$$

Application of Equation 3-4 with values κd <1 shows that the zeta potentials reported in Figure 3-7 correspond to no more than a few tens of elementary charges per particle because of the large λ_B for the highly nonpolar solvent hexane.

The zeta potential is observed to decrease with increasing ion concentration in both aqueous solution (Figure 3-5) and surfactant/hexane solution (Figure 3-7). The potential drop in aqueous system is a common phenomenon, explained by the screening of the surface charge by a dense atmosphere of indifferent electrolyte ions (NaCl). In nonpolar system, the "ion atmosphere" surrounding the immersed particles is far more extended at all experimental surfactant concentrations and composed of far fewer charged species. The large zeta potential at very low Span 85 concentration below its CMC suggests that individual surfactant molecules or some pre-micellar complexes, rather than regular micelles, are involved in the generation of surface charge and in the initial reduction of surface potential upon further surfactant addition.

Overall, the electrophoresis data for both types of PMMA particles (I and II) in the nonpolar solvent are identical within the experimental uncertainty. Hence, the surface charging in hexane/surfactant solutions appears insensitive to the differences in particle size or surface headgroup density that distinguish the surface charging in aqueous media. The opposite sign of surface charge compared to the aqueous dispersion indicates that the surface charging is dominated by the addition of surfactants.

3.3.2 Particle pair interaction

Electrophoresis and zeta potential measurements confirmed that the surface charging in nonpolar dispersions is closely coupled with the addition of surfactants. Particle interaction measurement provides independent evidence for the presence of particle charge and of charged species in nonpolar solutions. [43]

PMMA particles III in hexane dispersion were obtained by solvent swap with Span 85 concentration ranging from 0.7 mM (below the CMC) to 50 mM (above the CMC). The particles were fully dispersed in the gap between two sandwiched PMMA coated glass plates, and the spatial correlation for the dispersion particles was studied by video microscopy, evaluated in terms of the radial distribution function *g(r)*, and converted into the pair interaction energy *u(r)*.

The pair interaction energy profiles *u(r)* shown in Figure 3-8 were extracted from the radial distribution functions by application of the OZ equation with the HNC closure relation. The results shown in Figure 3-8 indicate a purely repulsive and long-range interaction. The decay is therefore fitted with the screened Coulomb expression

$$u(r) = \frac{(Z^* e)^2}{4\pi\varepsilon\varepsilon_0} \frac{exp(\kappa d)}{(1+\kappa d/2)^2} \frac{exp(-\kappa r)}{r} \qquad \text{Equation 3-1}$$

which constitutes the electrostatic component of the classical DLVO theory [34, 35]. The lines in the inset of Figure 3-8 are best fits to Equation 3-1 and provide strong support for a screened-Coulomb type interaction.

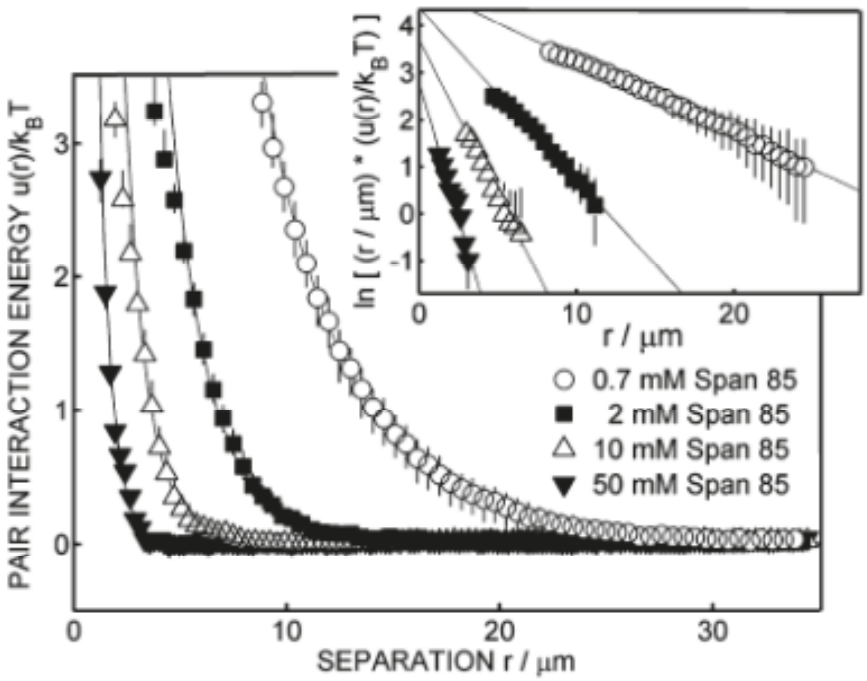

Figure 3-8 Pair interaction energy as a function of inter-particle distance obtained from the experimental radical distribution functions using the OZ/HNC formalism. Inset: logarithmic representation of the data and best fits to the DLVO potential in Equation 3-1.[43]

The fitted parameters, κ and Z^* from the respective slope and interception in the linear fit are listed in Table 3-2 with the sample concentration of Span 85. Here, Z^* is the effective number of particle charges, related to the effective surface potential ζ^* via Equation 3-4.

As seen in Table 3-2, the Debye screening lengths observed in our experiments are several micrometers, similar to those obtained in nonpolar solutions of ionizable surfactants [25], yet far larger than values achievable in aqueous dispersions [51]. The low effective particle charge and nonetheless substantial surface potential are again quite typical of nonpolar dispersions, but the pronounced decrease in these properties with

increasing surfactant concentration is noteworthy. We also note that the measured ζ^* is somewhat lower and its drop even more pronounced than the previously discussed electrophoretic data for smaller but otherwise similar particles (Figure 3-7) would have led us to expect. A similar disagreement between surface potentials obtained through electrophoresis and through interaction measurements has been reported for AOT-stabilized dispersions [23]. In qualitative agreement with the previously discussed electrophoresis measurements on similar particles, our interaction measurements suggest a maximum in the particle charge well below the CMC.

Table 3-2 Fit parameters for the pair potential data presented in Figure 3-8. [43]

Surfactant concentration [mM Span 85]	Screening length κ^{-1} $[\mu m]$	Effective charge number Z^*	Effective surface potential ζ^* [mV]
0.7	7.0 ± 1.4	63 ± 9	82 ± 10
2	2.8 ± 0.7	49 ± 17	58 ± 17
10	1.5 ± 0.2	35 ± 3	36 ± 3
50	0.8 ± 0.1	21 ± 2	18 ± 1

Table 3-3 Conductivity and approximate ion size. [43]

Surfactant concentration [mM Span 85]	Electric conductivity σ [nS/m]	Hydrodynamic diameter d_H [nm]
0.7	0.33 ± 0.05	1.5 ± 0.6
2	0.9 ± 0.08	3.4 ± 1.7
10	4.13 ± 0.15	2.6 ± 0.7
50	16.1 ± 0.5	2.3 ± 0.6

From the fitted Debye lengths, the size of mobile ions in solution can be estimated when combined with the conductivity results reported in Chapter 3. Disregarding, for simplicity, any asymmetry in the size and concentration of the cations and anions, the hydrodynamic ion diameter is calculated as Equation 3-5 and listed in Table 3-3.

$$d_H = \frac{e^2}{12\pi^2\eta\lambda_B}\frac{\kappa^2}{\sigma} \qquad \text{Equation 3-5}$$

The resulting diameters agree, within the experimental uncertainty, with the micelle diameter of 2.8 ± 0.2 nm determined by dynamic light scattering in Chapter 3, in the regime above the Span 85 CMC in hexane. At the lowest surfactant concentration, in the regime below the CMC, the estimated ion size is significantly smaller than a micelle, which is consistent with the idea that the conductivity in this regime is due to a smaller charged species, such as a small pre-micellar complex involving surfactant and an ionizable impurity.

The particle pair interaction measurements show a good agreement of *u(r)* with the DLVO potential down to the lowest concentration of Span 85 that results in robust electrostatic stabilization. The decrease of screening length with the increase of surfactant concentration indicates that Span 85 effectively screens the surface charge of the PMMA particles by introducing more charged species. The estimated hydrodynamic size of charged species in the range both below and above the CMC is consistent with the experimental results from DLS and further confirms the complex role of Span 85 in charging up the immersed particles and screening the surface charge.

3.3.3 Variation of colloidal particles

The surface charging of electrostatic stabilized particles is directly related to the interaction between particles and surfactant solutions in nonpolar media. To test the hypothesis of acid-base interactions as the origin of particle charge, we varied the particle material (using basic PMMA and neutral PS), the surface headgroups (using anionic sulfate or carboxyl groups and cationic amidine groups) and the surfactant. Besides the nonionic (but acidic) surfactant Span 85, we also used the anionic surfactant AOT in the nonpolar solution and explored the similarity and difference between these two types of surfactants in solid surface charging.

The selected particles are listed in Table 3-1. Prior to the comparison of different types of particles in surfactant nonpolar solutions, the original charging states of the particles were characterized in aqueous dispersion (pH around 6.2) in Figure 3-9. The appending negatively (positively) charged sulfate or carboxyl (amidine) groups on particle surfaces account for the negative (positive) particle mobility. For all particle types the addition of ions in the form NaCl salt leads to screening of the particle charge and a drop in the magnitude of the electrophoretic mobility for high salt concentration. Figure 3-9 also shows the occurrence of a maximum in the (absolute) mobility at low salt concentration, which is a well-known feature for large particles in aqueous dispersion. It does not reflect a maximum in the particle charge or zeta potential, but originates from a non-monotonic relation between mobility and zeta potential for large but finite κd [47].

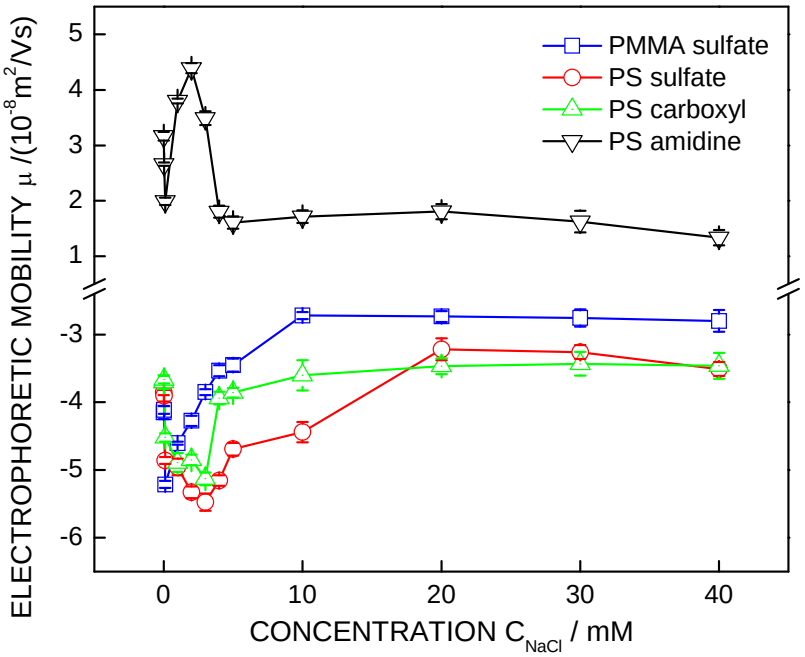

Figure 3-9 Electrophoretic mobility and zeta potential of 1 μm particles in aqueous dispersions at varied salt concentration for the four particle types with different polymer materials (III and IV) and surface groups (IV, V and IV). Error bars reflect standard deviations over five measurement runs.

3.3.3.1 Difference in polymer material

Keeping the surface group (sulfate) and particle size (1 μm) the same, we compared the charging of PMMA particles (III) with the charging polystyrene particles (IV) in Span 85/decane dispersion since polystyrene is considered to be Lewis neutral in contrast with the basic PMMA polymer.

After transfer from the original aqueous dispersion, the particles were confirmed by DLS to be fully dispersed in Span 85/decane solutions at the original size of 1 μm.

The field-dependent electrophoretic mobility of particle III (PMMA sulfate) is

shown in Figure 3-10 and the corresponding zero-field mobility and zeta potential in the Huckel approximation are shown in Figure 3-11. Similarly, the field-dependent electrophoretic mobility and extrapolated mobility results of particle IV (PS sulfate) are shown in Figure 3-12 and Figure 3-13, respectively.

In Figure 3-10 and Figure 3-12, important trends in the dependence of electrophoretic mobility on applied electric field and surfactant concentration are consistent with the previously reported trends for particle I and II (smaller PMMA sulfate particles). At low concentration of Span 85 in decane, the particles' mobility is again strongly dependent on the applied voltage. This dependence gradually disappears when increasing surfactant concentration introduces more mobile charged species and makes the surroundings of the immersed particles resemble more closely the ion bath of an aqueous dispersion.

The electrophoretic mobility obtained by extrapolation to zero field strength reflects the zeta potential and the surface charging in the absence of an applied voltage. The PMMA particles III have positive surface charge in the entire range of surfactant concentrations (Figure 3-11), whereas and the polystyrene particles IV have slightly negative surface charge at the lowest surfactant concentration and switch to positive charge at higher surfactant concentration (Figure 3-13), although both of particles III and IV are negatively charged in aqueous dispersions (Figure 3-9). The electrophoretic mobility of particle III is generally larger than that of particle IV.

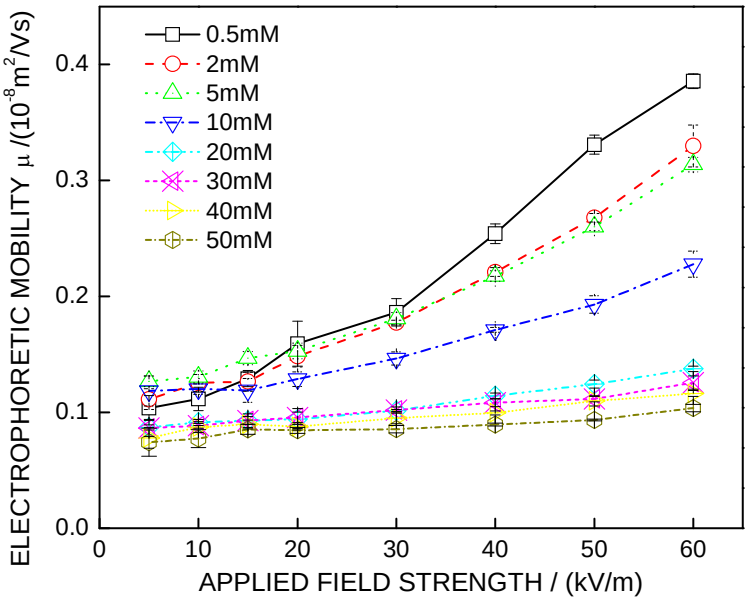

Figure 3-10 Electrophoretic mobility of 1μm PMMA particles with sulfate group (III) in decane as a function of field strength and Span 85 concentration.

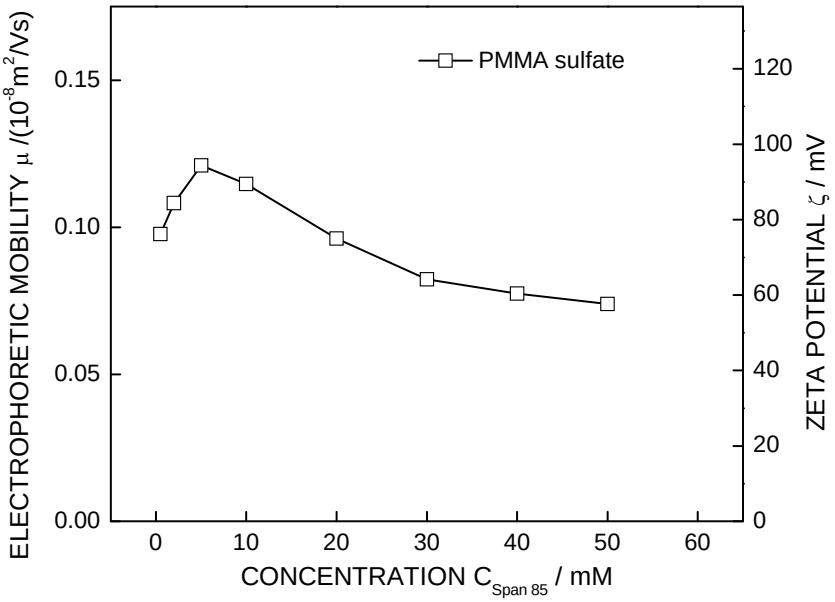

Figure 3-11 Zero field electrophoretic mobility and zeta potential (Huckel limit) of PMMA particleswith sulfate group (III) in decane as a function of Span 85 concentration.

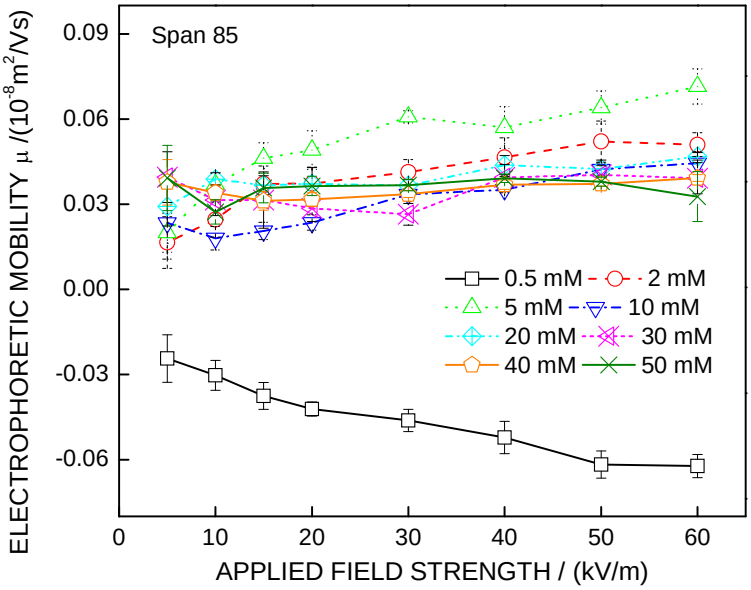

Figure 3-12 Electrophoretic mobility of 1μm polystyrene particles with sulfate group (IV) in decane as a function of field strength and Span 85 concentration.

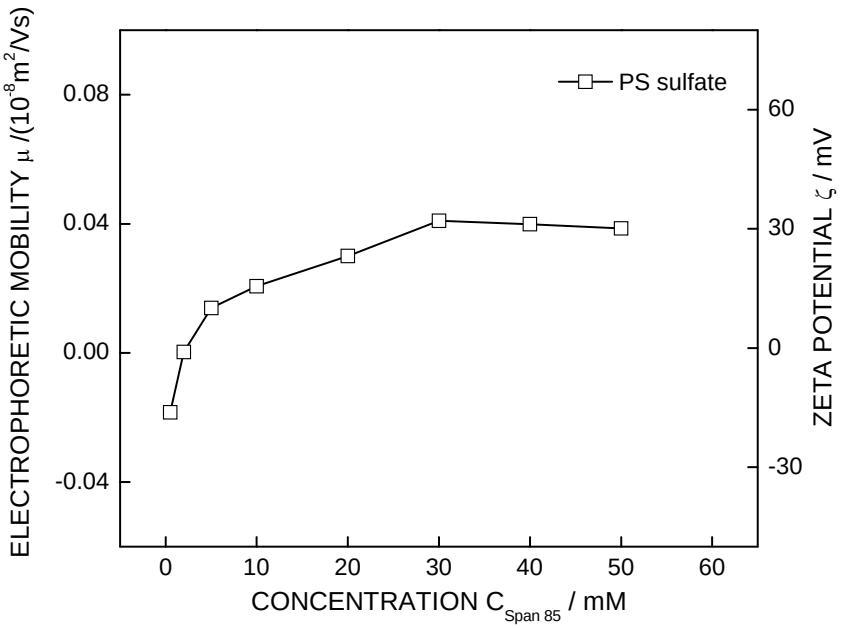

Figure 3-13 Zero field electrophoretic mobility and zeta potential (Huckel limit) of polystyrene particles with sulfate group (IV) in decane as a function of Span 85 concentration.

The observed differences in between these two particle types can be explained by the acid-base properties of the polymer materials. While Span 85 is considered to be a Lewis acid, and PMMA with its electron-rich carbonyl group is a Lewis base, whereas polystyrene has neither strong acidity nor strong basicity. In the dispersion of particle III, Span 85 and PMMA therefore should have stronger acid-base interaction, with PMMA as the electron donor (or proton acceptor) becoming positively charged. By contrast, Span 85 and polystyrene are expected to have weaker acid-base interaction, which would explain the generally weaker positive charging of particle IV in the nonpolar dispersion. The observed evidence of negative charge on these particles at the lowest Span 85 concentration cannot be explained by the acid-base interaction between the surfactant and the polymer, but may suggest an influence of the sulfate headgroups. It has been proposed in the literature that a small number of surface headgroups can dissociate in nonpolar liquids as they would in water, and that even immeasurably small amounts of water at the particles surface might promote this dissociation [20].

We therefore hypothesize that the sign of surface charge is determined by the competition of surface group dissociation and acid-base interaction. According to this hypothesis, at the lowest surfactant concentration, the negative charge on particle type IV (PS) brought about by the dissociation of surface sulfate groups outweighs the positive charge introduced by the acid-base charge transfer at the lowest surfactant concentration, where fewer acidic surfactant molecules are available. At higher surfactant concentration, the charge transfer between surfactant and polymer is more significant, which leaves the surface positively charged. In the dispersion of the basic PMMA particles (type III), however, the stronger acid-base interaction masks the surface group dissociation even at

the lower surfactant concentrations, making the surface positive throughout the entire range of concentrations.

3.3.3.2 Difference in surface group

To further test our hypothesis regarding the influence of particle surface headgroups, we compared the 1 μm polystyrene particle (IV - VI), to maintain similar acid-base interaction, with different surface groups.

In aqueous dispersion (Figure 3-9), sulfate and carboxyl groups dissociate to create a negative particle charge, whereas amidine groups protonate and cause a positive charge. The corresponding behavior in the nonpolar dispersions, obtained by solvent swap, is discussed next.

The field-dependent electrophoretic mobility of particle V (PS carboxyl) is shown in Figure 3-14 and zero-field mobility and zeta potential at Huckel limit are shown in Figure 3-15. Similarly, the field-dependent electrophoretic mobility and extrapolated mobility results of particle VI (PS amidine) are shown in Figure 3-16 and Figure 3-17, respectively.

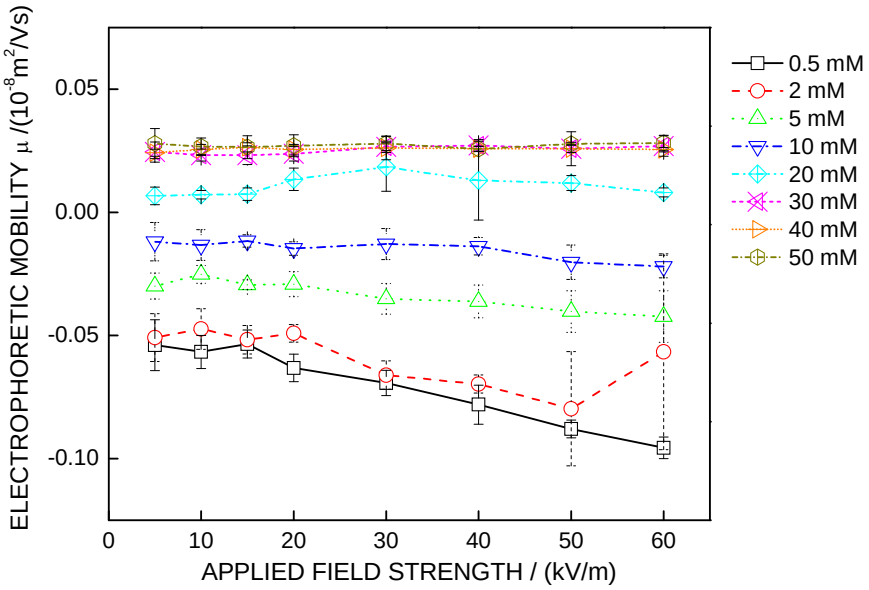

Figure 3-14 Electrophoretic mobility of 1μm polystyrene particles with carboxyl group (V) in decane as a function of field strength and Span 85 concentration.

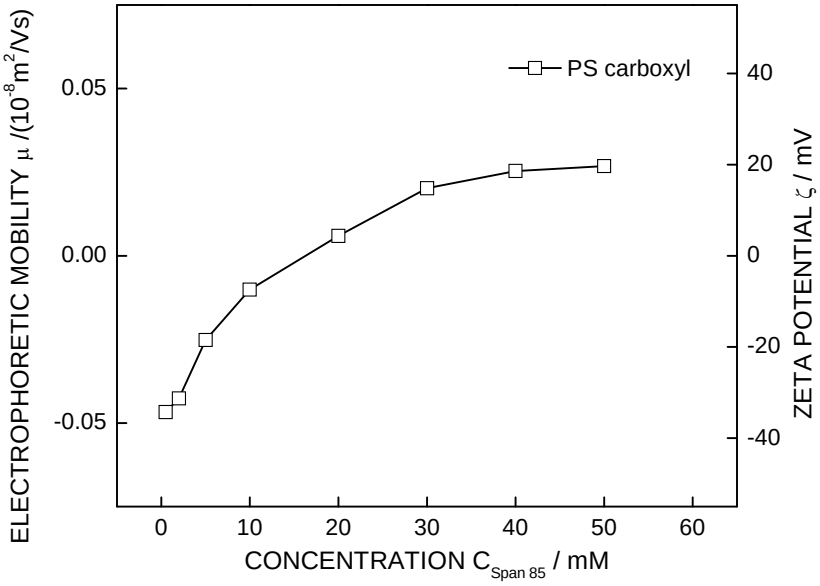

Figure 3-15 Zero field electrophoretic mobility and zeta potential (Huckel limit) of polystyrene particles with carboxyl group (V) in decane as a function of Span 85 concentration.

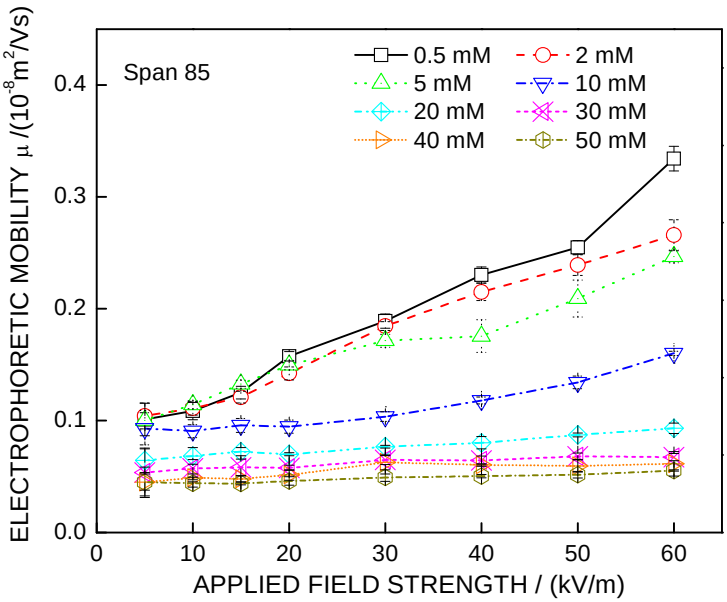

Figure 3-16 Electrophoretic mobility of 1μm polystyrene particles with amidine group (VI) in decane as a function of field strength and Span 85 concentration.

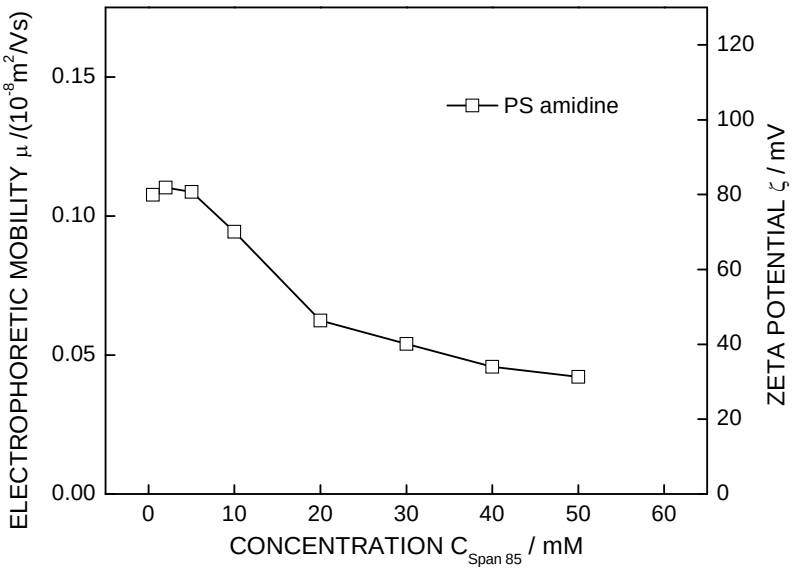

Figure 3-17 Zero field electrophoretic mobility and zeta potential (Huckel limit) of polystyrene particles with amidine group (VI) in decane as a function of Span 85 concentration.

The polystyrene carboxyl particles V (Figure 3-15) have slightly negative surface charge at low surfactant concentration and become positively charge at higher surfactant concentration, in close resemblance to the sulfate particles IV (Fig 3-13). The polystyrene amidine particles VI, by contrast, have positive surface charge in the entire range of surfactant concentrations (Figure 3-17).

The extrapolated electrophoretic mobility results of the four types of particles (III, IV, V, and VI) in decane/Span 85 solutions are summarized to plot in Figure 3-18, by the comparison of aqueous solutions in Figure 3-9.

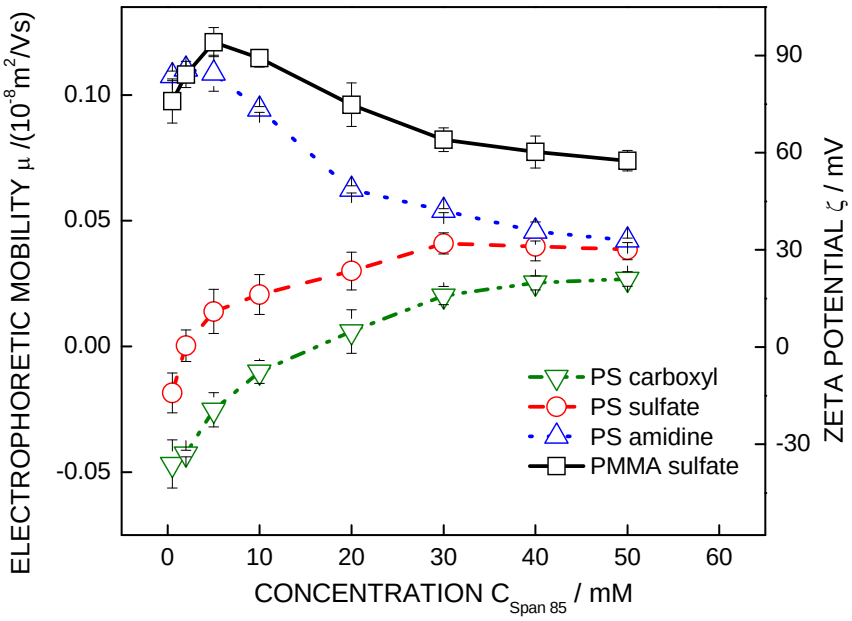

Figure 3-18 Summary of the zero field electrophoretic mobility and zeta potential (Huckel limit) of PMMA particle with sulfate group (III) and polystyrene particles with different surface group (IV, V, and VI) in decane as a function of Span 85 concentration.

We see that in the regime of high surfactant concentration, where we suspect acid-base interactions between the particles' polymer material and the surfactant to dominate particle charging, all the tested particle types are positively charged in decane, and that all PS based particles appear to converge towards the same surface charge as the surfactant concentration increases, whereas the positive charge on the PMMA surface remains larger as one might expect, given the stronger acid-base interaction between PMMA and Span 85. We conclude that the surface charging is likely dominated by the acid-base interaction between the polymer material and surfactant in the presence of high concentration of surfactant.

At lower surfactant concentration in the nonpolar dispersion, the sign of surface charge appears to be determined by a balance of surface group ionization and charge transfer due to acid-base interaction between the surfactant and the particle material. At the lowest surfactant concentrations, surface group ionization can fully account for the sign of charge of the PS particles, and only the PMMA particles remain positively charged despite their sulfate surface groups, suggesting that charging mediated by acid-base interaction with the surfactant still dominates for these strongly basic particles.

While the observed *signs* of charge can tentatively be explained in the interplay of surface group ionization and acid-base charge transfer with the surfactant, variations in the *magnitude* of charge (or zeta potential) with the surfactant concentration must also be influenced by charge screening. In light of the observed surfactant mediated conductivity increase in nonpolar solutions and the screened Coulomb type interaction found in particle dispersions, it seems very reasonable to credit surface charge screening by an increasing number of mobile charges in solution for the mobility decrease with increasing

surfactant concentration observed for the always positively charged PS amidine and PMMS sulfate particles.

We conclude that the sign and magnitude of surface charge can be rationalized qualitatively by a joint consideration of surface group dissociation, charge transfer between the polymer material and surfactant complex due to acid-base interaction, and the screening of surface charges by mobile charges in the surfactant solution. As seen in Chapter 2, such mobile charges are generated even in the absence of particles, presumably by charge disproportionation of reverse surfactant micelles and possibly of smaller surfactant complexes involving ionizable impurities.

Overall, Span 85 a supposedly nonionizable surfactant, is seen to contribute greatly to bulk charging, surface charging and charge screening in nonpolar dispersion.

3.3.4 Variation of surfactants

In Chapter 2, we have confirmed that the mechanism by which nonpolar solutions of the nonionic surfactant Span 85 develop mobile charges is different from the charging mechanism in solutions of the ionic surfactant AOT. While the conductivity of Span 85 solutions shows the scaling with surfactant concentration indicative of charging by a disproportionation reaction both above and below the CMC, the conductivity of AOT is consistent with charge dissociation of AOT molecules below and charge disproportionation of AOT reverse micelle above the CMC.

Aside from the ability to ionize by dissociation, AOT also differs from Span 85 in both the capability to solubilize water in nonpolar solution and the acid-base property as

AOT considered being a neutral surfactant. In this part of the thesis, we investigate the effects of AOT on the charging of particles in nonpolar dispersion and obtain additional clues about the charging mechanism.

We used the same types of PMMA particle (III) and polystyrene particles (IV, V, and VI) introduced previously, and now transferred, by solvent swap, into decane/AOT solutions. Electrophoresis measurements were carried out in complete analogy to the procedure for the Span 85 systems.

The field-dependent electrophoretic mobility of particle III in decane dispersion in the presence of AOT is shown in Figure 3-19; the extrapolated zero-field mobility and zeta potential (in the Huckel approximation) of particle III are shown in Figure 3-20. Similarly, the field-dependent electrophoretic mobility and extrapolated mobility results in decane/AOT solutions are shown in Figure 3-21 and Figure 3-22 for particle IV, in Figure 3-23 and Figure 3-24 for particle V, and in Figure 3-25 and Figure 3-26 for particle VI, respectively.

A general trend of a strongly field strength dependent electrophoretic mobility at low surfactant concentration and field insensitive mobility at high surfactant concentration, seen in Figures 3-19, 3-21, 3-23, and 3-25, is consistent with the previous observations for the same particles in Span 85/decane solution.

In low AOT concentration (low ionic strength) the diffuse part of the electric double layer consists of few, widely spaced counterions, and so the intrinisic electric field near the surface is relatively weak. Therefore, the externally applied field is more than just a weak perturbation and the response to it in terms of particle velocity becomes

nonlinear. At high AOT concentration, by contrast, the excess of charged AOT reverse micelles increases the ionic strength in the solution, and the electrostatic potential drops now from its value at the particle surface over a much shorter Debye length; therefore the intrinsic field strength in the diffuse layer, which is on the order of $\kappa\zeta$, becomes much larger, and the externally applied field only leads to a linear response in particle velocity, i.e. a field independent mobility.

The extrapolated electrophoretic mobility results of the four types of particles (III, IV, V, and VI) in decane/AOT solutions are summarized to plot in Figure 3-27.

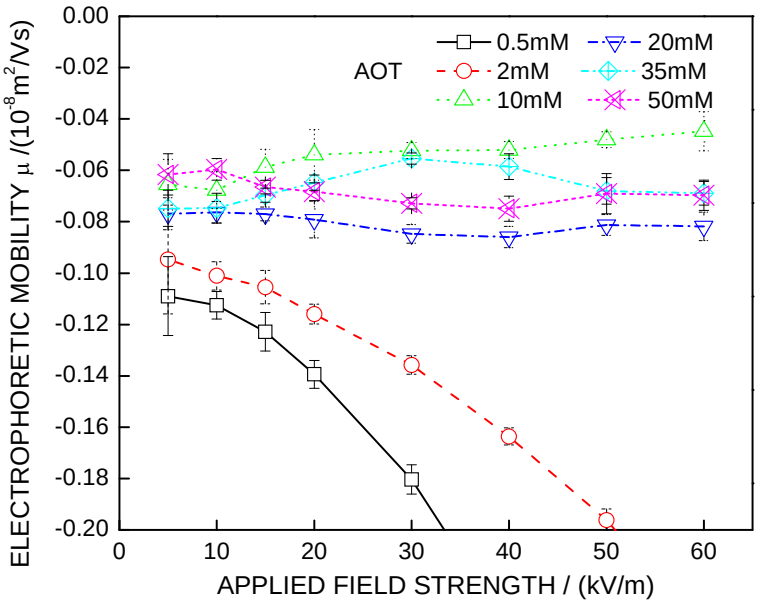

Figure 3-19 Electrophoretic mobility of 1μm PMMA particles with sulfate group (III) in decane as a function of field strength and AOT concentration.

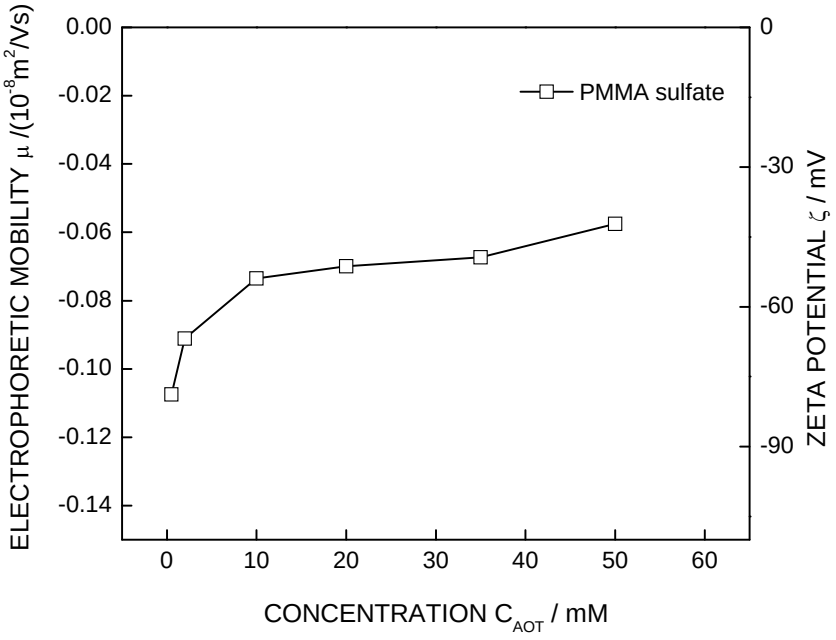

Figure 3-20 Zero field electrophoretic mobility and zeta potential (Huckel limit) of PMMA particles with sulfate group (III) in decane as a function of AOT concentration.

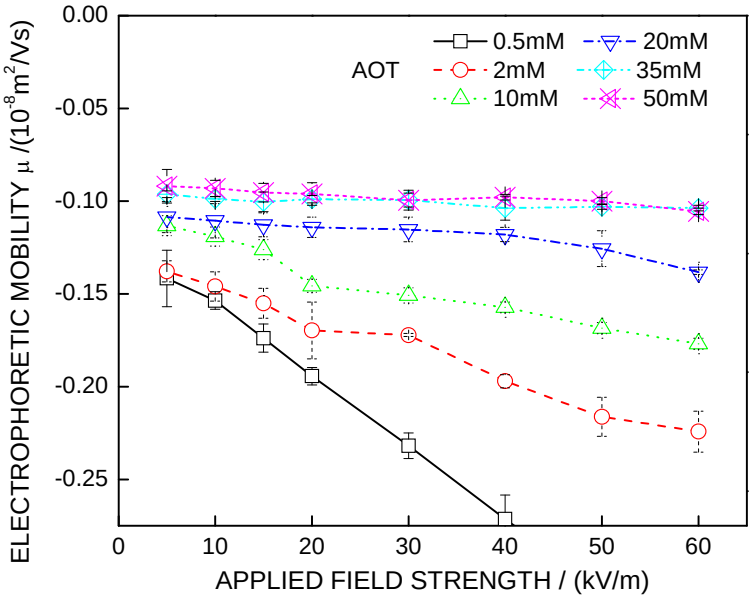

Figure 3-21 Electrophoretic mobility of 1μm polystyrene particles with sulfate group (IV) in decane as a function of field strength and AOT concentration.

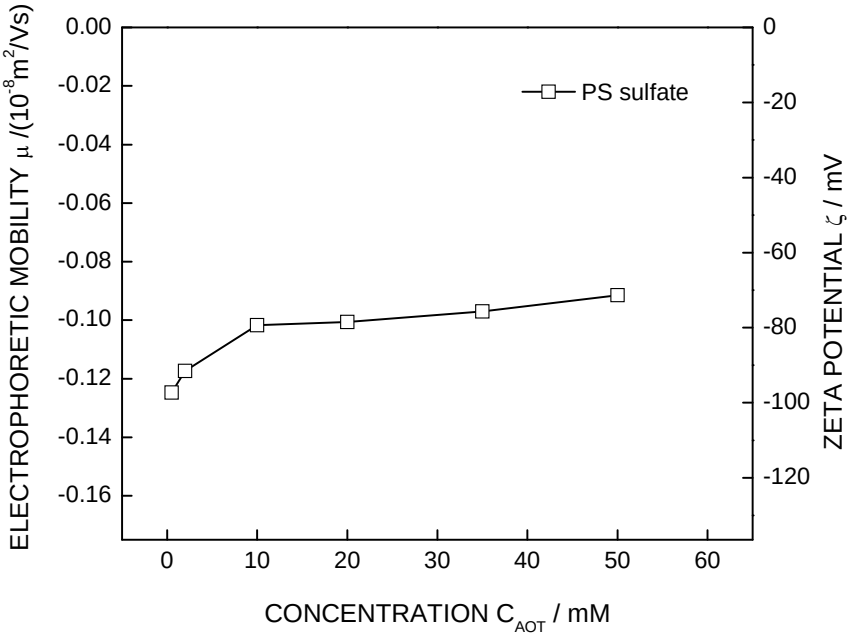

Figure 3-22 Zero field electrophoretic mobility and zeta potential (Huckel limit) of polystyrene particles with sulfate group (IV) in decane as a function of AOT concentration.

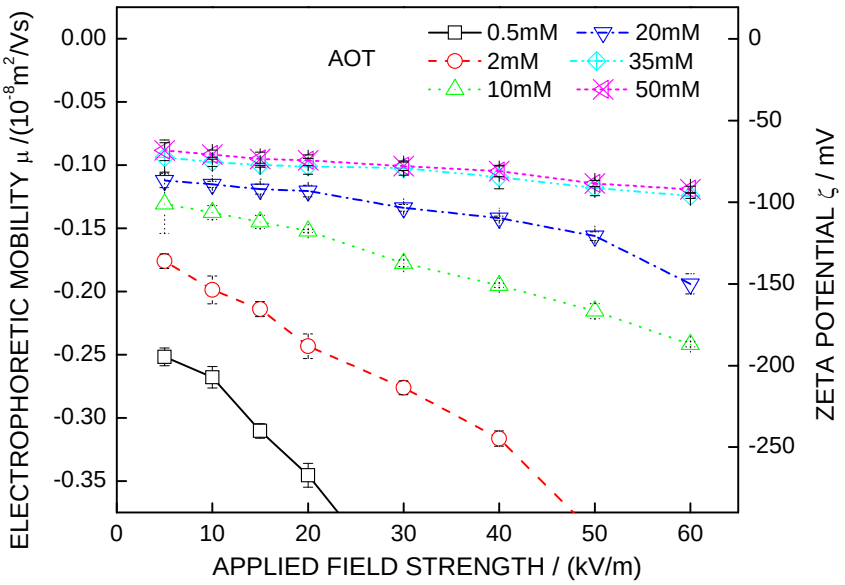

Figure 3-23 Electrophoretic mobility of 1μm polystyrene particles with carboxyl group (V) in decane as a function of field strength and AOT concentration.

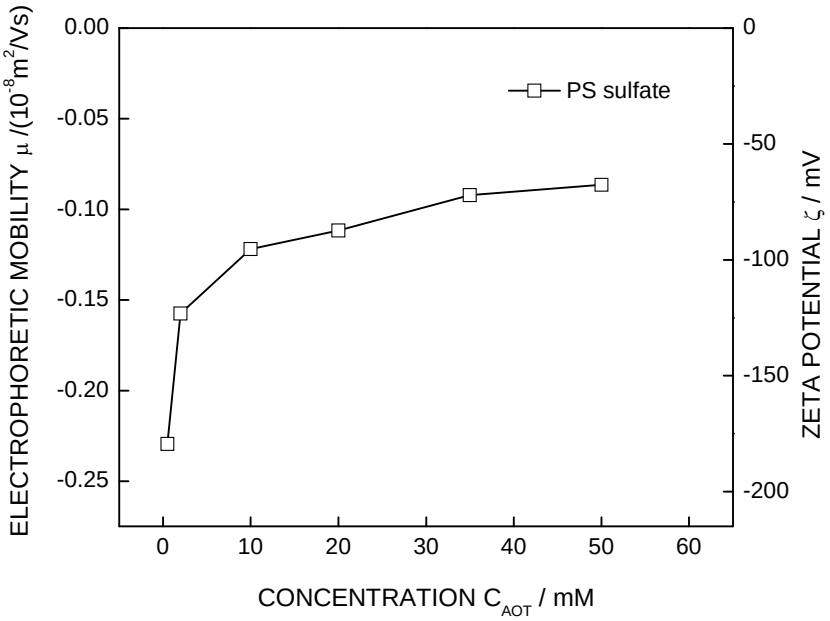

Figure 3-24 Zero field electrophoretic mobility and zeta potential (Huckel limit) of polystyrene particles with carboxyl group (V) in decane as a function of AOT concentration.

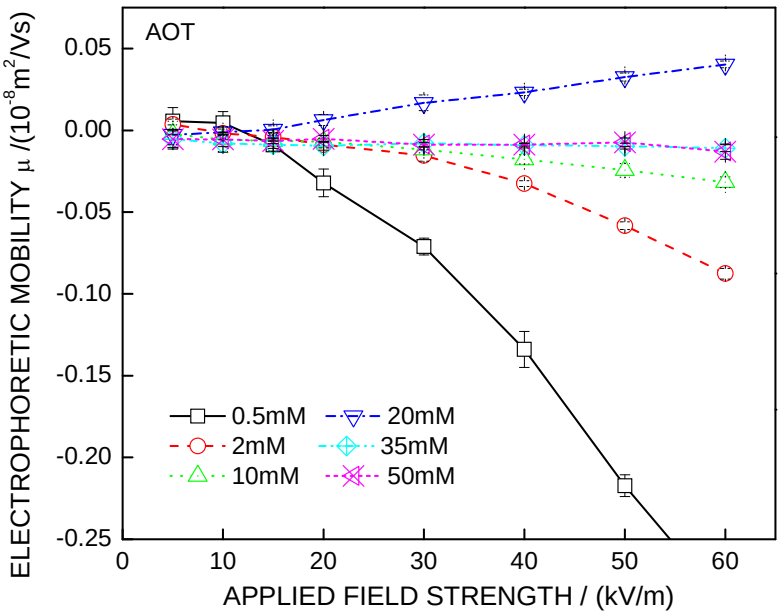

Figure 3-25 Electrophoretic mobility of 1μm polystyrene particles with amidine group (VI) in decane as a function of field strength and AOT concentration.

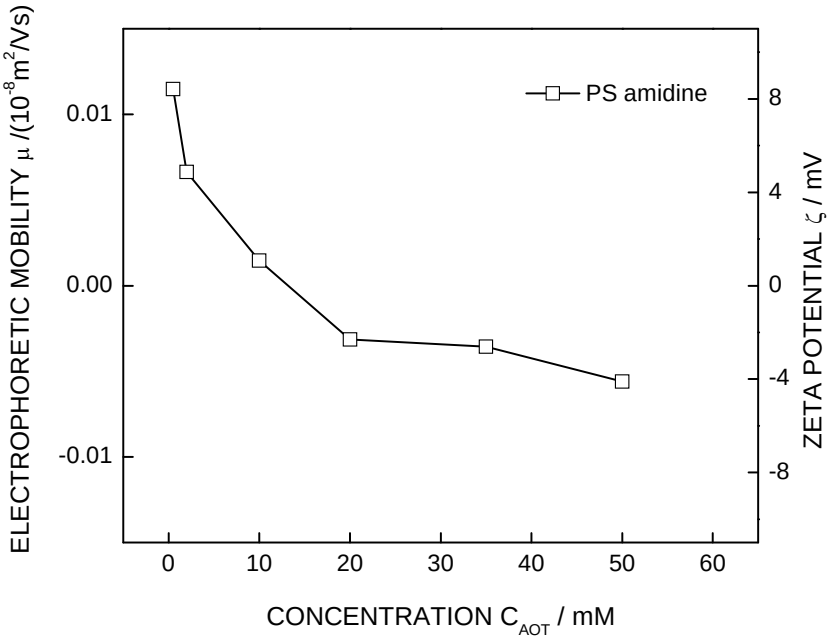

Figure 3-26 Zero field electrophoretic mobility and zeta potential (Huckel limit) of polystyrene particles with amidine group (VI) in decane as a function of AOT concentration

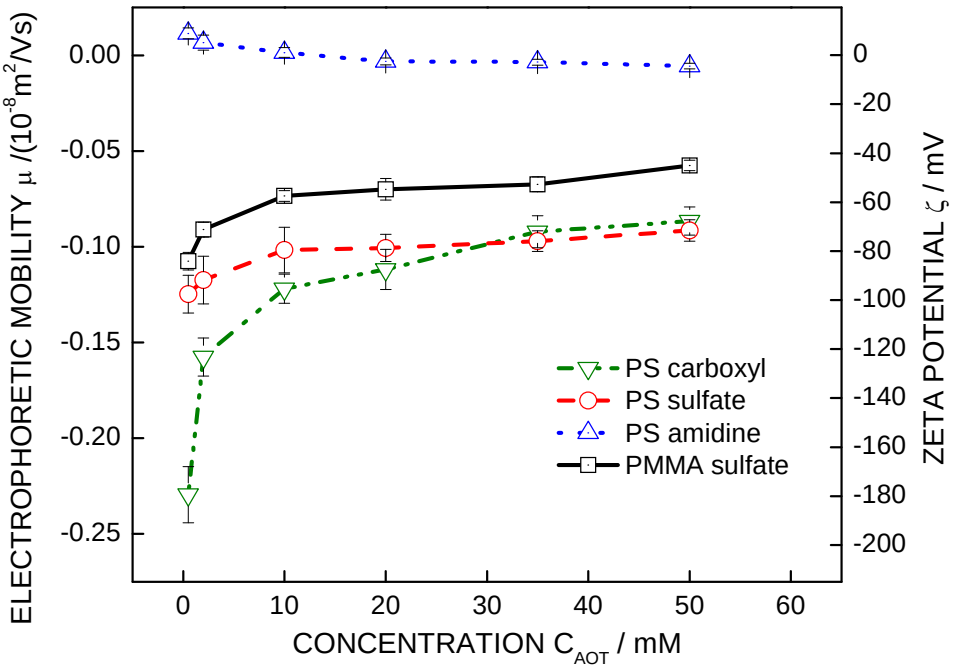

Figure 3-27 Summary of the zero field electrophoretic mobility and zeta potential (Huckel limit) of PMMA particles with sulfate groups (III) and polystyrene particles with different surface group (IV, V, and VI) in decane as a function of AOT concentration.

The PMMA particle III (Figure 3-20) and polystyrene particles IV (Figure 3-22) and V (Figure 3-24) have negative surface charge in the entire range of AOT concentration, as they do in aqueous dispersions (Figure 3-9). However, the polystyrene particle with amidine surface group VI (Figure 3-26), which is positively charged in aqueous solution (Figure 3-9), shows hardly any charging in AOT/decane, with a barely resolved trend indicating a possible transition from weak positive charging at low AOT concentration to very weak negative charging at high AOT concentration.

To explain these results, we considered the combination of three factors including the dissociation of surface group, the dissociation of adsorbed AOT molecules, and acid-

base interaction.

Compared to the acidic surfactant Span 85, AOT is known to be Lewis neutral so that it has weaker acid-base interaction with the basic PMMA particle and negligible acid-base interaction with the neutral polystyrene particles. Thus, acid-base interactions could possibly contribute some positive charge to the PMMA particles, but should have no significant impact on the surface charge of the three polystyrene particles. Charging mechanisms equally plausible for *all particle types* involve the dissociation of either surface groups (anionic for particle IV and V, cationic for particle VI), or of adsorbed AOT (anionic) molecules.

The different acid-base properties of PMMA and polystyrene would indeed explain why the basic PMMA sulfate particle III, systematically acquires less (negative) charge than its (neutral) PS counterparts with anionic surface groups, particles IV and V. For polystyrene particle VI, the very slight positive charge at low AOT concentration presumably comes from the dissociation of surface amidine group.

In addition, AOT, as an ionic surfactant, can dissociate to generate a sodium ion (positive) and a hydrophobic part (negative). As AOT concentration increases in the decane dispersion, the hydrophobic parts from the AOT dissociation adsorb onto the hydrophobic polystyrene particles and bring negative charge onto the particle surface. As a result, the surface charge turns to (very slightly) negative in the regime of higher AOT concentration.

Based on the above arguments, one might expect an even stronger dependence of the PS amidine particle charge on AOT concentration. Moreover, one might expect that

at high AOT concentration, the contribution of adsorbed, negatively charged surfactant should dominate the charging of PS particle in the same way that acid-base interaction with the acidic surfactant appeared to dominate charging at high concentrations of Span 85 in decane, and that differences between PS particles with different surface groups would again become small. Figure 3-27, however, suggests otherwise: the charging of PS amidine (type VI) and PS sulfate (IV) or PS carboxyl (V) particles remains substantially different even at high AOT concentration. The reason, we hypothesize, may be that the addition of the hygroscopic surfactant AOT increases not only the amount of negatively charged surfactant molecules, but also the amount of water, which in turn promotes the ionization of the particle surface groups. In the case of PS amidine particle (VI), the increase in negative surface charges due to adsorbed, dissociated AOT would be partly compensated by an increased number of amidine groups that charge positively thanks to the increased water content. The effect of water is considered more closely in the following section.

3.3.5 Effects of residual water

Since the dissociation of surface group is important in affecting the surface charge, it is important to quantitatively know how much water is dissolved in the nonpolar dispersion. We did not attempt to the notoriously difficult task of eliminating water from our systems, but instead used the Karl-Fischer titration to determine precisely the amount of water left in our samples.

For the pure solvent, hexane or decane, we confirmed that the water content in the purchased solvent is below 0.003 wt%. For the nonpolar dispersion, since all the steps of

the solvent swap were carried out in the same way and by the same person, we considered the operation error to be consistent for all the samples. Water from the addition of surfactants was expected to be proportional to surfactant concentration. The water contents for selected particle dispersion samples after solvent swap are plotted and shown in Figure 3-28 and Figure 3-29 in the presence of Span 85 and AOT, respectively. The comparison between these two surfactants is shown in Figure 3-30.

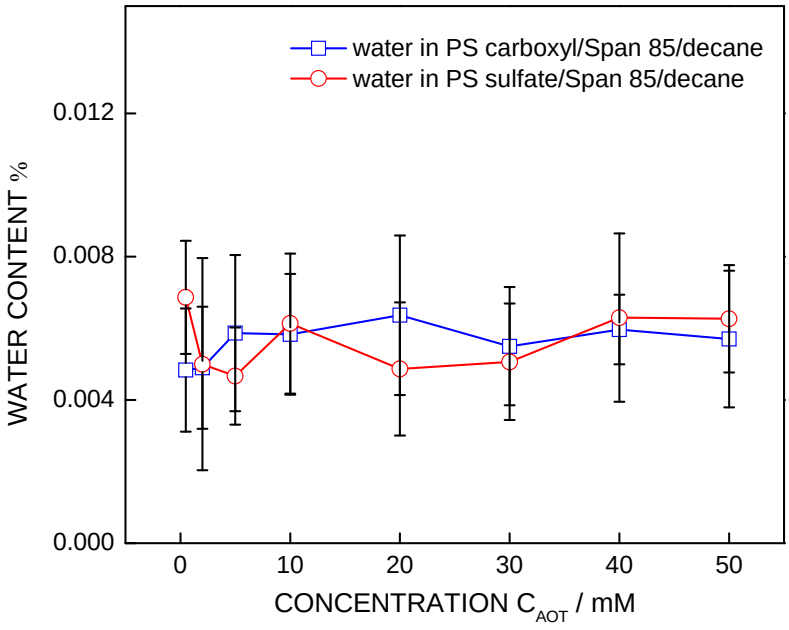

Figure 3-28 Water content (wt. %) in the final sample of particle dispersion after solvent swap as a function of Span 85 concentration.

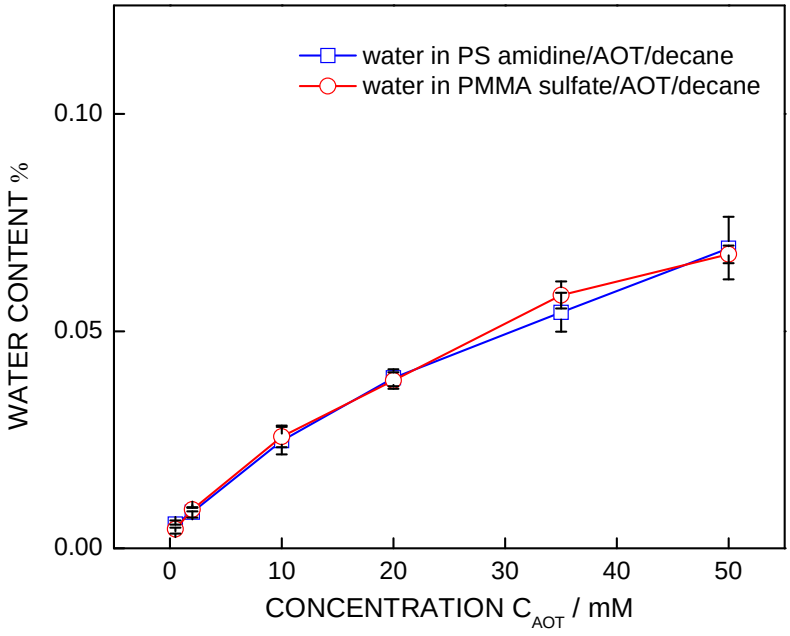

Figure 3-29 Water content (wt. %) in the final sample of particle dispersion after solvent swap as a function of AOT concentration.

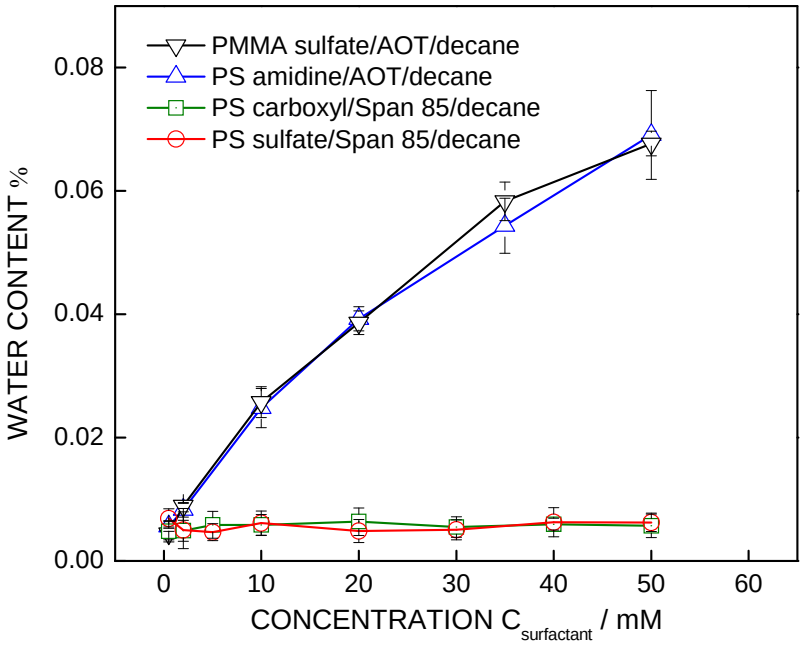

Figure 3-30 The summary of water content (wt. %) in the final sample of particle dispersion after solvent swap as a function of surfactant concentration.

The water contents in the final particle IV and V dispersions in Span 85/decane are roughly constant and below 0.008 wt% in the entire range of Span 85 concentration (Figure 3-28). The average results and standard deviation are from three independent measurements. The independence between water content and Span 85 concentration indicates that Span 85 only introduces very little water, within the combined tolerance of preparation. The small increase of water content compared to the pure solvent decane can be credited to the multiple steps of solvent swap. Thus, we assume that the other types of Span 85/decane dispersion have similar amounts of water left in the final samples, regardless of how much Span 85 is added into the dispersion.

By contrast, the water contents in the final particle III and VI dispersions in

AOT/decane are independent of the particle type, but highly dependent on the AOT concentration (Figure 3-29). Again, the average results and standard deviation are from three independent measurements. The raise in water content with the increase of AOT concentration proves that water is introduced directly by the addition of AOT. We also consider that the other types of AOT/decane dispersion have similar amount of water left in the final samples if the concentration of AOT is the same.

According to Figure 3-30, the amount of water in AOT/decane dispersions is generally much higher than that in Span 85/decane dispersions. This is consistent with the well-known, much larger hygroscopy of AOT. The increased water content upon addition of AOT presumably promotes the dissociation of surface groups, which explains these groups appear more important for particle charging in nonpolar solutions of AOT than in nonpolar dispersions of Span 85. In conclusion the measurements of water content provide further support for the proposed interplay of surface charging mechanisms involving the surfactant, the particle material, and the particles' surface groups.

3.3.6 Other effects

3.3.6.1 Order of contact: surfactant molecules vs. reverse micelles

From the results above, we found that the surface charging and charge screening is closely associated with the addition of surfactants: not only can reverse micelles affect the surface charge on the immersed particle in nonpolar solution, but sub-micellar surfactant concentrations can also contribute to the surface charging. We further investigated, whether a particle's history of surfactant exposure influences its charging state, too. We usually transfer the particles from aqueous dispersion to nonpolar solution

with very low surfactant concentration, and then achieve the target surfactant concentration by dilution of the concentrated particle dispersion with a solution of higher surfactant concentration. One might wonder, in particular for particles in Span 85 below the CMC, whether earlier exposure to Span 85 micelles would make any difference or whether particle charging is due to an equilibrium state that depends only on the particle current environment.

To answer this question we used PMMA particles (type III) transferred into hexane/Span 85 solution by solvent swap. To qualitatively understand the effect and simplify the measurements, we did not vary the applied electric field, but used a fixed field strength of 20 kV/m.

The particles were transferred from original aqueous dispersion directly into the hexane solution with Span 85 concentration of 0.1 – 5 mM, *i.e.* below the critical micelle concentration of 10 mM. The zeta potential results are shown with the solid markers in Figure 3-31. The open markers in Figure 3-31 show the results for particles that were first transferred into the hexane solutions with Span 85 concentration above the CMC and then diluted into the solutions with same final Span 85 concentration the same as the solid markers. The consistence in zeta potential of the particles obtained from the two kinds of procedure indicates no hysteresis whatsoever. In particular, this finding does not support the notion of surface charging by irreversible adsorption of reverse micelles on the particle surface prior to the dilution.

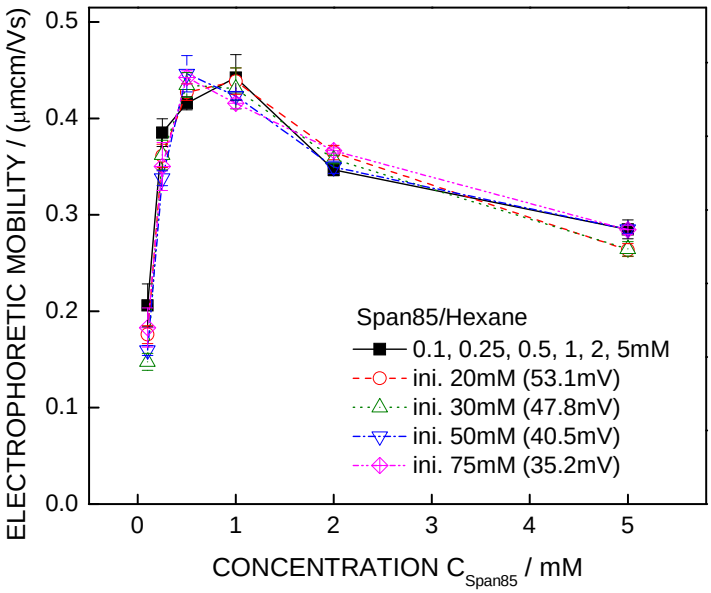

Figure 3-31 The comparison between the particles III that meet surfactant molecules only (solid markers) and that meet reverse micelles first (open markers).

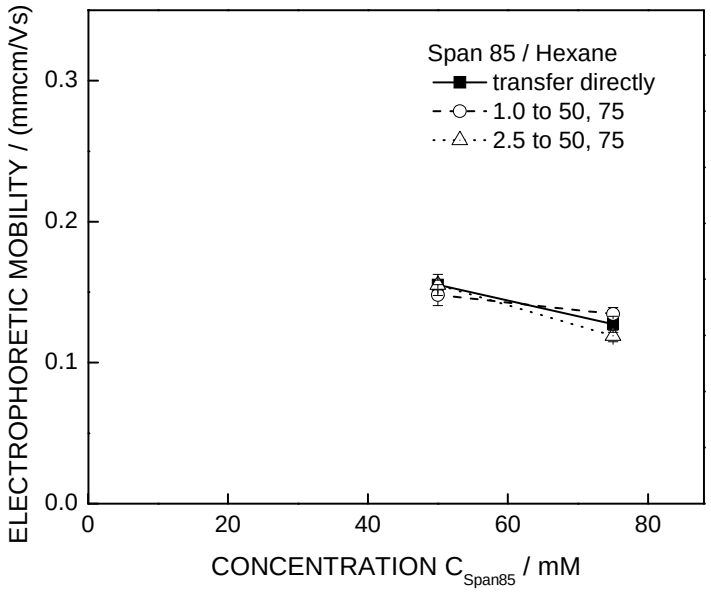

Figure 3-32 The comparison between the particles III that meet reverse micelles only (solid markers) and that meet surfactant molecules first (open markers).

Similarly, the zeta potential results of particles transferred directly into the hexane solution with Span 85 concentration of 50 – 75mM were compared with zeta potentials of particles first exposed to sub-micellar concentrations of Span 85, see Figure 3-32. Again, the results suggest no charging "memory" of the earlier exposure to a different surfactant concentration.

Overall, the particles' charging state in nonpolar dispersions reassuringly appears to depend only on the momentary solution conditions and not on the way in which these conditions were prepared.

3.3.6.2 Surfactant batch difference

Another concern that could bring uncertainty to surface charging in nonpolar dispersion are batch-to-batch variations in the surfactant because we did not purify the commercial surfactants or otherwise control their composition, and Span 85 in particular is known to be a mixture (of different sorbitan oleates) rather than a pure substance.

After obtaining the PMMA particles II in hexane in the presence of Span 85 from a new batch via solvent swap, we re-measured the field-dependent electrophoretic mobility (Figure 3-33) and converted the extrapolated zero-field mobility to zeta potential at different surfactant concentrations (Figure 3-34).

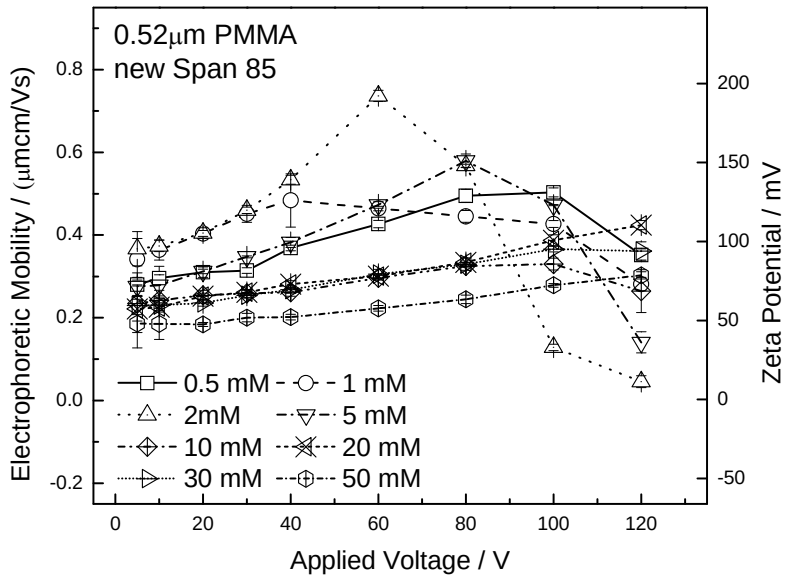

Figure 3-33 Electrophoretic mobility of 0.52μm PMMA particles (II) in hexane as a function of field strength and Span 85 concentration from a new batch.

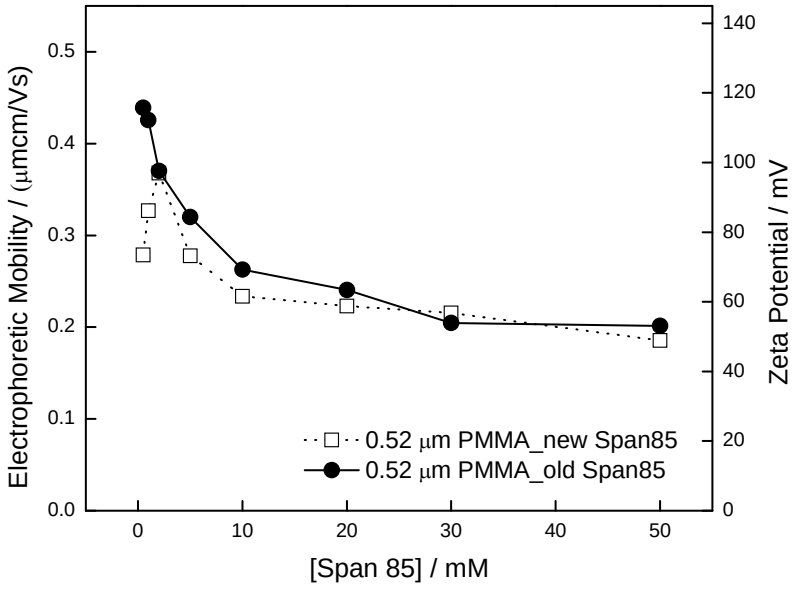

Figure 3-34 Comparison of the zero field electrophoretic mobility and zeta potential (Huckel limit) of PMMA particle (II) in hexane as a function of Span 85 concentration from two different batches.

We compared the zero-field mobility and zeta potential of the PMMA particle II in the presence of Span 85 from the previous batch with the new one in Figure 3-34. The results are very similar, especially in the range with higher Span 85 concentration. The deviation in the very low Span 85 concentration might be due to slight differences in the composition of Span 85.

In order to make sure a new batch of commercial available Span 85 has the same charging effects on particles in nonpolar solutions, we used the PMMA particles II and III and carried out similar electrophoresis experiments with the Span 85 from a new batch.

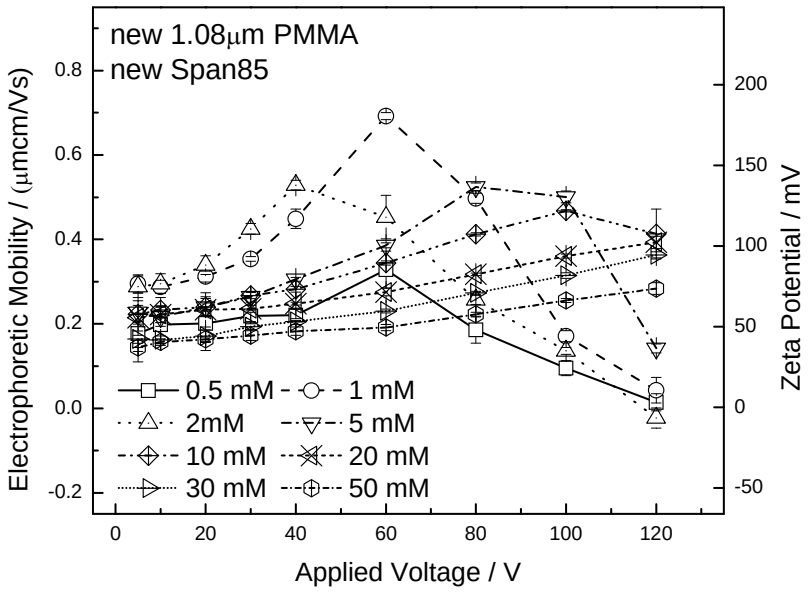

Figure 3-35 Electrophoretic mobility of 1μm PMMA particles (III) in hexane as a function of field strength and Span 85 concentration from a new batch.

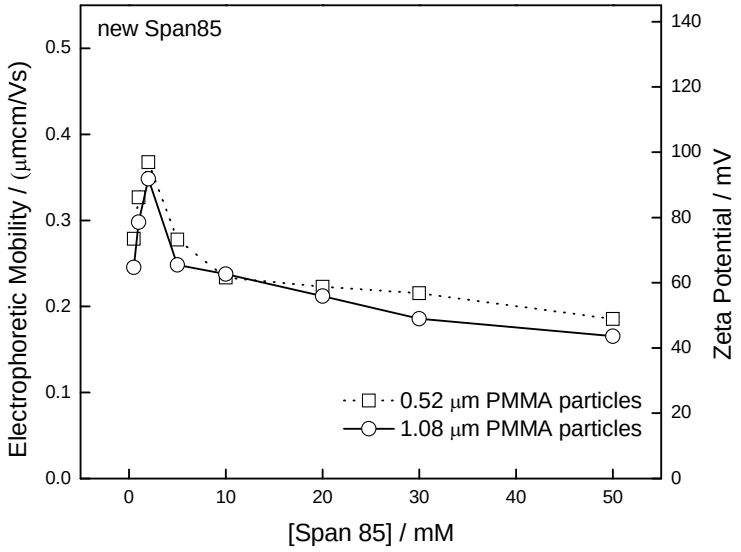

Figure 3-36 Comparison of the zero field electrophoretic mobility and zeta potential (Huckel limit) of PMMA particle (II and III) in hexane as a function of Span 85 concentration from a new batch.

The field-dependent electrophoretic mobility of PMMA particle III is shown in Figure 3-35. Together with the extrapolated mobility and zeta potential results for particle II in Figure 3-34, the comparison between these particles with two different sizes is shown in Figure 3-36 in the presence of a new batch Span 85. The similarity of the charging phenomena on particle II and III with new Span 85, consistent with the comparison between particle I and II in Figure 3-7 with old Span 85, again shows that the surface charging in nonpolar dispersion is independent on the particle size and number density of surface charge in original aqueous dispersion.

For the largely qualitative conclusions drawn in this study, the batch-to-batch variation of surfactants can be considered negligible in particle surface charging and charge screening.

3.4 Conclusions

In this part of the research, we focused on studying the particle charging and surface charge screening in nonpolar oils in the presence of surfactants. Span 85, as a nonionizable surfactant, was previously found capable of raising the electric conductivity of nonpolar solutions. Here it is shown to also induce large electric surface potentials on suspended colloidal particles and provide efficient electrostatic stabilization of (dilute) nonpolar dispersions. AOT, a widely studied ionic surfactant, showed a similar capability of generating significant surface potentials on dispersion particles in nonpolar solvents. The comparison between these two types of surfactants gives valuable insights into the elusive mechanism of charging in nonpolar suspensions.

While earlier studies focused on surface charging in the presence of reverse micelles, we also addressed charging in the sub-micellar regime. Particles of different size and surface groups with different zeta potential in aqueous solutions can acquire very similar zeta potentials in nonpolar dispersions in the addition of surfactants. Special care needs to be taken when measuring the zeta potentials via electrophoresis because at very low surfactant concentration the electrophoretic mobility shows a pronounced dependence on the applied electric field strength. We obtained, therefore, robust and meaningful results on zeta potentials by extrapolating the electrophoretic mobility results to zero field strength.

The surface charging and charge screening in nonpolar dispersion is closely associated with the addition of surfactants. The sign and magnitude of surface charge are rationalized qualitatively by the joint consideration of acid-base interactions between the

particle materials and surfactants, the dissociation of surface groups, and by adsorbed charged surfactant molecules in the case of ionic surfactant. Span 85 as a Lewis acid and a hydrophobic, nonionizable surfactant can dissolve little water in nonpolar solvent and does not have the option to dissociate, but charge transfer due to acid-base interaction between Span 85 and the particle surface provides a mechanism of surface charging that is consistent with our observations. By contrast, the Lewis neutral, ionic surfactant AOT has been confirmed to import relatively large amounts of water into nonpolar dispersions, and the water-assisted dissociation of surface groups and adsorbed surfactant molecules appears as the main pathway towards AOT mediated particle charge. Considering the acid-base property of the surfactant and particle in order to predict and control the surface charge in nonpolar dispersions certainly seems warranted, although it is still unclear whether the transferred species are electrons or protons.

Significant surface charging and charge screening is observed both above and below the CMC of surfactant in nonpolar solution. We can therefore conclude that these effects do not necessarily require the presence of micelles as charge donors or acceptors for the particle surfaces.

Particle pair interaction energy profiles are consistent with a screened Coulomb interaction for the nonpolar dispersion in the presence of Span 85, even at the lowest surfactant concentration far below the CMC. This behavior provides independent confirmation of surfactants' impact on charging at the particle surface and in the nonpolar bulk witnessed by electrophoresis and conductivity measurements.

3.5 References

1. O'Brien, R.W. & White, L.R. Electrophoretic mobility of a spherical colloidal particle. *Journal of the Chemical Society, Faraday Transactions 2: Molecular and Chemical Physics* **74**, 1607-1626 (1978).

2. Diaz, A., Fenzelalexander, D., Wollmann, D. & Barker, J.A. Importance of dissociated ions in contact charging. *Langmuir* **8**, 2698-2706 (1992).

3. de Groot, J., Koper, G.J.M., Borkovec, M. & de Bleijser, J. Dissociation behavior of poly(maleic acid): Potentiometric titrations, viscometry, pulsed field gradient NMR, and model calculations. *Macromolecules* **31**, 4182-4188 (1998).

4. Chatelier, R.C., Hodges, A.M., Drummond, C.J., Chan, D.Y.C. & Griesser, H.J. Determination of the Intrinsic Acid-base Dissociation Constant and Site Density of Ionizable Surface Groups by Capillary Rise Measurements. *Langmuir* **13**, 3043-3046 (1997).

5. Vinod, M.P., Mandle, A.B., Sainkar, S.R. & Vijayamohanan, K. Effect of gelling on the surface structure of a porous lead electrode in sulfuric acid. *Journal of Applied Electrochemistry* **27**, 462-468 (1997).

6. Behrens, S.H., Christl, D.I., Emmerzael, R., Schurtenberger, P. & Borkovec, M. Charging and aggregation properties of carboxyl latex particles: Experiments versus DLVO theory. *Langmuir* **16**, 2566-2575 (2000).

7. Strubbe, F., Beunis, F., Marescaux, M. & Neyts, K. Charging mechanism in colloidal particles leading to a linear relation between charge and size. *Physical Review E (Statistical, Nonlinear, and Soft Matter Physics)* **75**, 031405-031408 (2007).

8. Sefcik, J., Verduyn, M., Storti, G. & Morbidelli, M. Charging of Latex Particles Stabilized by Sulfate Surfactant. *Langmuir* **19**, 4778-4783 (2003).

9. Lee, E.M. & Koopal, L.K. Adsorption of cationic and anionic surfactants on metal oxide surfaces: Surface charge adjustment and competition effects. *Journal of Colloid and Interface Science* **177**, 478-489 (1996).

10. Iruthayaraj, J. *et al.* Adsorption of low charge density polyelectrolyte containing poly(ethylene oxide) side chains on silica: Effects of ionic strength and pH. *Macromolecules* **38**, 6152-6160 (2005).

11. Franks, G.V. & Gan, Y. Charging behavior at the alumina-water interface and implications for ceramic processing. *Journal of the American Ceramic Society* **90**, 3373-3388 (2007).

12. Brown, G.E. *et al.* Metal oxide surfaces and their interactions with aqueous solutions and microbial organisms. *Chemical Reviews* **99**, 77-174 (1999).

13. Brown, G.E. Surface science - How minerals react with water. *Science* **294**, 67-+ (2001).

14. Hiemstra, T., Venema, P. & VanRiemsdijk, W.H. Intrinsic proton affinity of reactive surface groups of metal (hydr)oxides: The bond valence principle. *Journal of Colloid and Interface Science* **184**, 680-692 (1996).

15. Rosenqvist, J., Persson, P. & Sjoberg, S. Protonation and charging of nanosized gibbsite (alpha-Al(OH)(3)) particles in aqueous suspension. *Langmuir* **18**, 4598-4604 (2002).

16. Kosmulski, M. The pH-dependent surface charging and the points of zero charge. *Journal of Colloid and Interface Science* **253**, 77-87 (2002).

17. Fowkes, F.M., Jinnai, H. & Mostafa, M.A. Acid-base Mechanism for Generation Zeta Potentials in Non-aqueous suspensions. *Abstracts of Papers of the American Chemical Society* **182**, 90-COLL (1981).

18. Fowkes, F.M., Jinnai, H., Mostafa, M.A., Anderson, F.W. & Moore, R.J. Mechanism of Electric Charging of Particles in Nonaqueous Liquids. *Acs Symposium Series* **200**, 307-324 (1982).

19. Pugh, R.J., Matsunaga, T. & F.M. Fowkes The dispersibility and stability of carbon black in media of low dielectric constant. 1. Electrostatic and steric contributions to colloidal stability. *Colloids and Surfaces* **7**, 183-207 (1983).

20. Morrison, I.D. Electrical charges in nonaqueous media. *Colloids and Surfaces A: Physicochemical and Engineering Aspects* **71**, 1-37 (1993).

21. Smith, P.G., Patel, M.N., Kim, J., Milner, T.E. & Johnston, K.P. Effect of surface hydrophilicity on charging mechanism of colloids in low-permittivity solvents. *Journal of Physical Chemistry C* **111**, 840-848 (2007).

22. Keir, R.I., Suparno & Thomas, J.C. Charging behavior in the silica/Aerosol OT/decane system. *Langmuir* **18**, 1463-1465 (2002).

23. Hsu, M.F., Dufresne, E.R. & Weitz, D.A. Charge Stabilization in Nonpolar Solvents. *Langmuir* **21**, 4881-4887 (2005).

24. Roberts, G.S., Sanchez, R., Kemp, R., Wood, T. & Bartlett, P. Electrostatic Charging of Nonpolar Colloids by Reverse Micelles. *Langmuir* **24**, 6530-6541 (2008).

25. Sainis, S.K., Germain, V., Mejean, C.O. & Dufresne, E.R. Electrostatic Interactions of Colloidal Particles in Nonpolar Solvents: Role of Surface Chemistry and Charge Control Agents. *Langmuir* **24**, 1160-1164 (2008).

26. Poovarodom, S. & Berg, J.C. Effect of particle and surfactant acid-base properties

on charging of colloids in apolar media. *Journal of Colloid and Interface Science* **346**, 370-377 (2010).

27. Pugh, R.J. & Fowkes, F.M. The dispersibility and stability of coal particles in hydrocarbon media with a polyisobutene succinamide dispersing agent. *Colloids and Surfaces* **11**, 423-427 (1984).

28. Fowkes, F.M. & Pugh, R.J. Steric and electrostatic contributions to the colloidal properties of nonaqueous dispersions. *Acs Symposium Series* **240**, 331-354 (1984).

29. I. Morrison, S.R. *Colloidal Dispersions: Suspensions, Emulsions, and Foams, John Wiley & Sons, New York,* (2002).

30. Jenkins, P. *et al.* The electrochemistry of nonaqueous copper phthalocyanine dispersions in the presence of a metal soap surfactant: A simple equilibrium site binding model. *Journal of Colloid and Interface Science* **211**, 252-263 (1999).

31. Sainis, S.K., Merrill, J.W. & Dufresne, E.R. Electrostatic Interactions of Colloidal Particles at Vanishing Ionic Strength. *Langmuir* **24**, 13334-13337 (2008).

32. Kitahara, A., Satoh, T., Kawasaki, S. & Konno, K. Specific adsorption of surfactants containing Mn or Co on polymer particles revealed by zeta potential in cyclohexane. *Journal of Colloid and Interface Science* **86**, 105-110 (1982).

33. Thwala, J.M., Goodwin, J.W. & Mills, P.D. Electrokinetic studies of colloidal silica particles dispersed in non-aqueous media in the presence of a nonionic surfactant, dodecylhexaethylene glycol monoether (C12E6). *Colloids and Surfaces a-Physicochemical and Engineering Aspects* **335**, 33-42 (2009).

34. Derjaguin, B.V. & Landau, L. Theory of the stability of strongly charged lyophobic sols and of the adhesion of strongly charged particles in solution of electrolytes. *Acta Physicochimica (URSS)* **14**, 633–662 (1941).

35. Verwey, E.J. & Overbeek, J.T.G. *Theory of the Stability of Lyophobic Colloids*. (Elsevier, New York; 1948).

36. Crocker, J.C. & Grier, D.G. Microscopic measurement of the pair interaction potential of charge-stabilized colloid. *Physical Review Letters* **73**, 352 (1994).

37. Schatzel, K. & Merz, J. Measurement of Small Electrophoretic Mobilities by Light-Scattering and Analysis of the Amplitude Weighted Phase-Structure Function. *Journal of Chemical Physics* **81**, 2482-2488 (1984).

38. Miller, J.F., Schatzel, K. & Vincent, B. The Determination of Very Small Electrophoretic Mobilities in Polar and Nonpolar Colloidal Dispersions Using Phase-Analysis Light-Scattering. *Journal of Colloid and Interface Science* **143**, 532-554 (1991).

39. Hunter, R.J. *Zeta Potential in Colloid Science: Principles and Applications*. (Academic Press, New York; 1981).

40. Russel, W.B., Saville, D.A. & Schowalter, W.R. *Colloidal Dispersions*. (Cambridge University Press, Cambridge; 1989).

41. Thomas, J.C., Crosby, B.J., Keir, R.I. & Hanton, K.L. Observation of field-dependent electrophoretic mobility with phase analysis light scattering (PALS). *Langmuir* **18**, 4243-4247 (2002).

42. Poovarodom, S. & Berg, J.C. Effect of alkyl functionalization on charging of colloidal silica in apolar media. *Journal of Colloid and Interface Science* **351**, 415-420 (2010).

43. Espinosa, C.E., Guo, Q., Singh, V. & Behrens, S.H. Particle Charging and Charge Screening in Nonpolar Dispersions with Nonionic Surfactants. *Langmuir* **26**, 16941-16948 (2010).

44. Crocker, J.C. & Grier, D.G. Methods of Digital Video Microscopy for Colloidal Studies. *Journal of Colloid and Interface Science* **179**, 298-310 (1996).

45. Behrens, S.H. & Grier, D.G. Pair interaction of charged colloidal spheres near a charged wall. *Physical Review E* **64**, 050401 - 050404 (2001).

46. Hansen, J.P. & McDonald, I.R. *Theory of Simple Liquids*, Edn. 2. (Academic Press, London; 1986).

47. Borkovec, M., Behrens, S.H. & Semmler, M. Observation of the mobility maximum predicted by the standard electrokinetic model for highly charged amidine latex particles. *Langmuir* **16**, 5209-5212 (2000).

48. Dukhin, A.S. & Dukhin, S.S. Aperiodic capillary electrophoresis method using an alternating current electric field for separation of macromolecules. *ELECTROPHORESIS* **26**, 2149-2153 (2005).

49. Park, J.K., Ryu, J.C., Kim, W.K. & Kang, K.H. Effect of Electric Field on Electrical Conductivity of Dielectric Liquids Mixed with Polar Additives: DC Conductivity. *The Journal of Physical Chemistry B* **113**, 12271-12276 (2009).

50. van der Hoeven, P.H.C. & Lyklema, J. Electrostatic Stabilization in Nonaqueous Media. *Advances in Colloid and Interface Science* **42**, 205-277 (1992).

51. Crocker, J.C. & Grier, D.G. When like charges attract: The effects of geometrical confinement on long-range colloidal interactions. *Physical Review Letters* **77**, 1897-1900 (1996).

CHAPTER 4

REVERSE SURFACTANT MICELLES AS TEMPLATES FOR SYNTHESIZING NANO-SIZED HYDROGELS

4.1 Backgrounds and theories

4.1.1 Hydrogels

4.1.1.1 Basic properties and synthetic methods

Hydrogels are dilute, water-swollen networks of crosslinked hydrophilic polymers. Their degree of swelling can be so high that they consist almost entirely of water, hence the name hydrogel (or"aquagel").

Besides this high water content, hydrogels have tunable chemical properties, flexible three-dimensional physical structures, variable mechanical properties, and biocompatibility. Because of these useful properties hydrogels have drawn great interests in the areas of biomaterials science, biomedical engineering, and pharmaceutical engineering. Applications include medical implants (breast, etc.) [1], sustained-release drug delivery (micro- or nano-sized hydrogels) [2-4], environmentally sensitive "smart" hydrogels [5], tissue engineering (similarity to natural tissue) [6, 7], consumer goods (diapers, contact lenses, etc.) [8], and bio-nanotechnology [5, 9-11].

Physical and chemical pathways can both be utilized to synthesize bulk hydrogels. Some commonly used preparation methods are reviewed here to exhibit the variety of the synthetic approach and provide the clue of preparing nano-sized hydrogels based on the

objective of this thesis.

For the methods of physical crosslinking, Liet al. [12] synthesized biocompatible and thermo-responsive ABA triblock copolymers (A: poly(N-isopropylacrylamide), B: poly(2-methacryloyloxyethyl phosphorylcholine)), which dissolved in dilute aqueous solution at room temperature but separated and formed physical hydrogel at 37 °C due to hydrophobic interactions between A blocks. When temperature droped below the lower critical solution temperature of the PNIPAM block back to room temperature (below the lower critical solution temperature of the PNIPAM block), the hydrogel redissolved. Mi et al.[13] studied the self-assembly of proteins to stable hydrogels when concentration was above the threshold in certain range of temperature and pH. The mechanism of hydrogel assembly was the intermolecular association of the helical domains with unique structures and mechanical properties. In Miyauchi's work [14, 15], supramolecular gels were formed with a helical structure by the host-guest interactions in aqueous solutions. In Dai's work [16], temperature-induced sol-gel transition led to hydrogels which were opaque white at low temperature but became transparent and eventually dissolved as temperature increased. Both optical transition and volume swelling were reversible responding to temperature stimuli. In addition, hydrogen bonding [17], crystallized domains [18], and stereocomplexation [19] can all be utilized to physically form hydrogels. In general, the physically crosslinked hydrogels are able to form and degrade reversibly in response to the external stimuli.

Other methods to the synthesis of hydrogels involve chemical crosslinking with the addition of various types of crosslinkers, including the modification of biopolymers and free radical polymerization of hydrophilic monomers. Murakami et al. [20]

synthesized microbial poly(gamma-glutamic acid) hydrogels in the presence of various saccharides such as glucose, maltotriose, and cyclodextrin. These bio-based hydrogel crosslinked with various saccharides showed different capabilities of water absorption and recovery yields due to their different crosslinker structure and crosslinking density. In Levesque's study [21], a peptide crosslinker was utilized in the development of matrix metalloproteinase sensitive hydrogels derived from dextran in order to separate random hydrolysis and enzymatic digestion. Various water-soluble monomers such as poly(ethylene glycol) (PEG) [22] and its block copolymers [23], poly(amino acid) [24],methacrylates [25], and methacrylate derivatives of sugars [26] have been used in the preparation of synthetic hydrogels via free radical polymerization in aqueous solutions.

4.1.1.2 Nano-sized hydrogels

Although containing a large percentage of water, hydrogels are (soft) solids and show three-dimensional structure. The size of hydrogels varies widely and can be dictated either by the architecture of its constituents or by the dimensions of the container they are formed in. The smallest variants are crosslinked polymeric particles in the colloidal size range of nanometers to microns; they are often referred to as nanogels or microgels [27, 28]. In submicron size dimension, nanogels are developed to provide unique advantages for drug delivery applications by conjugating the polymeric matrix with proteins and drugs [29, 30] and functioning as units of micelles and vesicles [31-34]. In addition to the conjugation of bioactive proteins, drugs, and DNA in the polymer networks, nanogels are also studied for the incorporation of inorganic nano-species such as magnetic nanoparticles [35], metallic nanorods [36], and quantum dots [37].

Meanwhile, new challenges and requirements come up with the developments of nanogel applications to obtain the polymeric networks with more stability, more biocompatibility, and more controllable size and structure. An effective way to achieve these goals is to investigate the synthetic strategies and preparation processes.

Various synthetic methods for the preparation of nano-sized hydrogels will be briefly introduced in the following part, including crosslinking biopolymers, supramolecular assembly of biopolymers, microfluidics, free radical polymerization, and polymerization in reverse microemulsions. Each of the preparation methods has their own superiorities and deficiencies in producing morphology controllable nanogels.

Together with Dr. Murthy and his team in the School of Biomedical Engineering at Georgia Tech, we had the idea of combining our experience in controlling the size of water-swollen reverse micelles with the Murthy's group unique expertise in copper-free click chemistry for a novel approach to nanogels synthesis with clear advantages for biomedical applications: size, biocompatibility, degradability, etc.

4.1.2 Preparation methods of nanogels

4.1.2.1 Modification of biopolymers

In order to utilize the biocompatibility, biodegradability, and low toxicity of biopolymers in micro/nanogels, self-assembled structures composed of biopolymers can be further modified to form particles either by supramolecular assembly or by chemically crosslinking.

Nanogel formation by physical bonding in self-assembly of amphiphilic

biopolymers in aqueous solution have been demonstrated in Akiyoshi's work, such as hydrophobitizied polysaccharide [38, 39] and cholesterol-bearing pullulan [40, 41]. Pullulan, as a hydrophilic polymer, was partly substituted by hydrophobic cholesterol. This modified pullulan was able to form a stable nano-sized hydrogel in water via the supramolecular assembly among the hydrophobic branches. The size and density of the self-aggregation systems were closely related to the substitution degree of the hydrophobic cholesterol. The resulting nanogels, stably dispersed for one week at room temperature, were reported to have the width of 60-200 nm and the height 30-50 nm. [40]

In addition to the participation of hydrophobitized substitution, crosslinking reaction that happens between the active sites in biopolymers and crosslinkers can also help to form size and shape confined nanogels. Chitosan based nanogels were generated by Bodnar et al. [42] from the intramolecular crosslinking the PEG dicarboxylic acid to the chitosan linear chains. The nanogel aqueous dispersion was stable, and the size and structure of the nanogel depended on the ratio of crosslinking and the molecular weight of chitosan. In the study of Shen et al. [43], chitosan was crosslinked with ethylenediaminetetraaceticdianhydride (EDTAA) to form pH-sensitive nanogels. The nanogel composed of EDTA and chitosan, stable in the entire range of pH, achieved reversible surface charge switching upon contact to pH stimuli.

Obtaining nanogels via modification of biopolymers has a great advantage in simplifying the synthetic process; however, results wide size distribution and cannot avoid the participation of free radical in polymerization.

4.1.2.2 Microfluidic preparation

Microfluidic devices have recently been used to prepare monodispersed micro/nanogels. Injecting one liquid with dissolved monomers or oilgomers into the other continuous immiscible phase through microchannels with a tapered junction where the two phases meet. Breaking up the injected phase to droplets and *in-situ* crosslinking the containing monomers to micro/nanoparticles. Considering the design of microfluidic device and gelation process, the dimensions of microchannels, the confinement of droplets, flow rate of the injected phase, and the crosslinking reaction time are the key parameters to prepare nanogels with controllable shape and size. [44]

The unique property of the microfluidic preparation to form nanogels is to apply various gelation methods in a micro-scale environment. De Geest et al. [45] utilized chemical gelation to produce 10 μm monodisperse dextran-modified microgels by emulsifying aqueous droplets stably dispersed in continuous oil phase with the aid of surfactants and crosslinking the monomers to polymer networks. Ionic crosslinking for gelation was carried out by Zhang et al. [44, 46] in microfluidics by controlling the diffusion of crosslinking agents towards the droplets containing the gelling polymer. In addition, Xu et al. [47] achieved physical gelation by temperature change and generated monodispersed microgels by using microfluidics to control the size, shape, and composition. Sugiura et al. [48] obtained calcium alginate gel beads with narrow size distribution via coalescence-induced gelation in microchannels.

The advantages of this method are excellent control over shape, morphology, and size distribution of the resulting nanogels. Microfluidics, however, involve specialty

design and complicated operations.

4.1.2.3 Free radical polymerization

In the presence of crosslinkers, various free radical polymerization reactions of hydrophilic or water-soluble monomers have been utilized to prepare nanogels, usually with the help of amphiphilic stabilizer. In a common process, the monomers, stabilizers, and initiators are soluble in solutions as the continuous phase. Once the free radical polymerization reaction is triggered, the forming polymer networks become insoluble in the continuous medium and stably dispersed in the solution.

Ma et al. [49] successfully obtained spherical nanogels by free radical polymerization from 2-hydroxyethyl methacrylate (HEMA) as monomers, stabilized by poly(ethylene oxide)-b-poly(1,1,2,2-tetrahydroperfluorodecyl acrylate) (PEO-b-PFDA) block copolymer in the supercritical carbon dioxide as the continuous phase. In Jones' work [50], nanogels composed of crosslinked poly(N-isopropylacrylamide) (pNIPAm) was synthesized via free radical polymerization, which were multi-responsive to temperature [51] and pH [52]. Xiong et al. [53] reported a simple one-step ring-opening polymerization to conveniently synthesize poly(ethylene glycol) PEG-armed nanogels. The formation of the core-crosslinked star polymer is surfactant-free; however, the shape and size of the resulting nanogels are associated with the ratio between arm and core materials.

In general, the formation of nanogels via free radical polymerization usually takes a relative long time and the resulting nanogels have irregular shape and non-defined polydispersity. Constraining the polymerization process in a confined space, such as a

reverse micelle or microemulsion in a W/O system, can effectively lead the formed nanogels with controllable size and shape.

4.1.2.4 Polymerization in reverse microemulsions

To avoid multi-steps in the preparation process and to allow precise control of the dimensions and internal structure of the nanogels, reverse micelles and microemulsions are used in this research as containers or templates, which contains the hydrophilic monomers or polymers, crosslinking agents, and initiators if necessary, for the generation of polymeric nano-sized networks.

In some practical applications, drug, DNA, magnetic particles, and cells can be physically bonded inside of the aqueous droplets. The emulsified droplets are stabilized by oil-soluble surfactant such as AOT and Span 80 to form reverse microemulsions. Water-soluble crosslinking agents implement the formation of cargo-loaded micro/nanogels. The resulting crosslinked nanogel particles exist as dispersion in the organic solvent, and can be collected and purified by solvent swap via repeated precipitation, centrifugation, sonication, and washing. For the nanogels obtained from the polymerization in reverse microemulsions, the size and shape can be controlled by the amount of surfactants and degree of swelling, in other words, by the volume of hydrophilic core.

As shown in Figure 4-1, Oh et al. [54] synthesized nanogels in reverse microemulsions by the combination of atom transfer radical polymerization catalyzed by Cu(II). The water-soluble oligo(ethylene glycol) monomethyl ether methacrylate (OEOMA) and disulfide-functionalized crosslinker dissolve in water droplets, which are

stabilized by Span 80 in nonpolar solvent cyclohexane. Going through the polymerization in the hydrophilic core of the reverse microemulsion, the resulting p(OEOMA) networks show the range around 200 nm in diameter with very narrow size distribution. Furthermore, the disulfide linkages can be degraded to destruct the formation of nanogels and lead the crosslinked nanogels back to linear polymer chain.

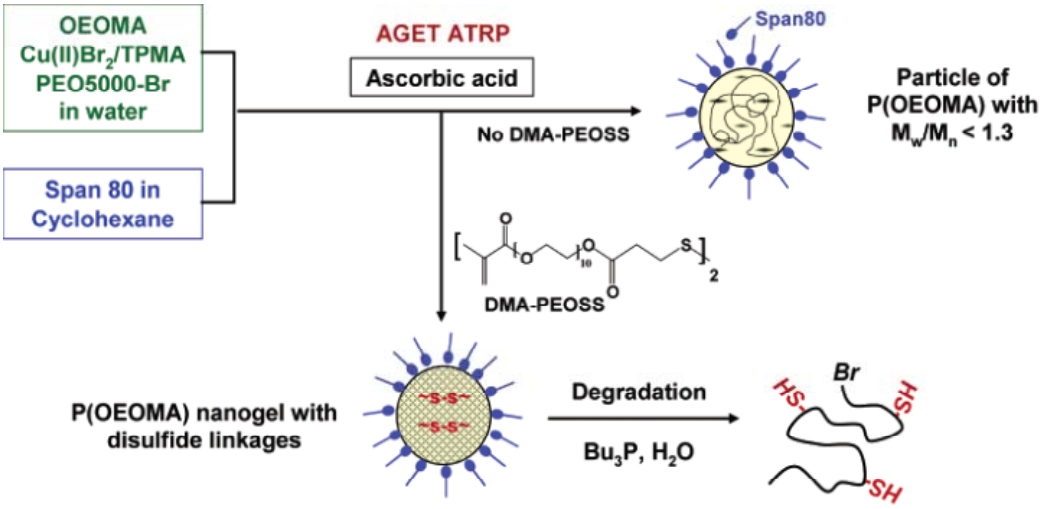

Figure 4-1 Illustration of synthesis and degradation of nanometer-sized colloidal particles of well-controlled water-soluble polymers. [54]

In Mitra's study [55], chitosan nanogels around 100 nm in diameter were prepared in reverse microemlusions stabilized by AOT in hexane. Doxorubicin (Dox)-modified dextran (Dex) also dissolved in the hydrophilic core of swollen AOT reverse micelles. Thus, Dox-Dex encapsulated chitosan-based nanogels were obtained with the crosslinking of glutaraldehyde.

With the stabilization of surfactant mixture of Span 65, Span 80, and Tween 80 in hexane, Lee et al. [56] were able to prepare hyaluronic acid (HA)-based nanogels to

deliver si-RNA. The combination of carbodiimide coupling reaction with reverse microemulsion led to nanogels with a diameter of roughly 200 nm.

McAllister et al. [57] synthesized nanogels via reverse microemulsion polymerization with various types of acrylate monomers. The aqueous droplets were stabilized by laureth-3 in heptane. After free radical polymerization, the acrylate monomers were crosslinked to form nanogels with diameters down to 50 nm. Successful uptake of DNA in the nanogel networks was confirmed by an increase in the hydrodynamic size observed with DLS.

There are some other methods for the preparation of nanogel, for example, precipitation polymerization [58, 59] and micromolding [60, 61]. Chemical reactions to form nanogels usually involve free radicals, toxic catalysts, or heat, under which the bioactives cannot survive. Physical association processes can be more benign, but do not usually offer the desired control over shape, morphology, and size distribution of very small nanogels. Therefore, we propose to combine the reverse microemulsion polymerization with copper-free "click" chemistry avoiding free radicals and metallic catalysts in order to form size, shape, and composition controllable nanogels.

4.1.3 Azide-alkyne cycloaddition in click chemistry

Click chemistry is a powerful and reliable synthetic strategy to explore new molecules by joining small units together through carbon-heteroatom bonds (C-X-C) [62]. Copper(I) catalyzed reactions are known to allow high yields in the regioselective synthesis of triazoles from azide group [63, 64], and thus the copper-mediated azide-alkyne cycloaddition ("click" reaction) has contributed greatly to the development of

polymer synthesis/functionalization and surface modification. [65]

Azides, as mild electrophiles, do not appreciably react with water and oxidation, and require soft nucleophiles for reaction such as alkynes [66]. However, the reactions between azides and terminal alkynes typically require vigorous heating for several hours [67]. The [3+2] azide-terminal alkyne cycloaddition to produce kinetically stable triazole adduct was first described by Huisgen [68]. This reaction is thermodynamically favorable and requires elevated temperature to provide necessary activation energy. Very high temperature is usually not compatible with living systems, therefore alternatively, a copper catalyst was introduced to activate the alkyne groups and drive the reaction going towards the cycloaddition. Fokin&Sharpless and coworkers [64] and Meldal and coworkers [63] concurrently and independently found the significant effects of Cu(I) on accelerating this [3+2] cycloaddition reaction rate, by an impressive 10^6 fold. The copper-mediated reaction can be easily carried out at room temperature and provide excellent regioselectivity. The resulting triazole products are stable to oxidation and acid hydrolysis. Thus, this type of reaction is nowadays used for selectively labeling azide-functionalized biomolecules, such as virus particles and proteins [69, 70].

The fast reaction rate of the catalyzed azide-alkyne cycloaddition is the primary advantage when applying this technique into polymer synthesis; however its disadvantage is that the metal catalyst is toxic and harmful for cellular studies and applications [71]. A more bio-friendly way of introducing the azide-alkyne cycloaddition reaction into living cells is to activate the alkynes via ring strain [72]. In addition to the stability to oxidation and acid hydrolysis, the cycloaddition process and the resulting triazole products are also non-toxic to bioactive, based on the assumption that the harmful azide groups are fully

consumed.

An eight-membered ring (cyclooctyne) is the most appropriate candidate to promote the cycloaddition reaction, because much of the strain energy in the eight-membered ring is released in the transition state [73], but a seven-membered ring is too active and a nine-membered one is not active enough at room temperature. As a consequence, the strain-promoted [3+2] azide-alkyne cycloaddition reaction happens at physiological temperature without the participation of a metal catalyst, and has been used in cellular works without any obvious toxic effects [72]. The simple examples of the heat-generated, copper-catalyzed, strain-promoted azide-alkyne cycloaddition reactions are shown in Figure 4-2. Furthermore, appending electron-withdrawing groups to the cyclooctyne ring can increase the reactivity of alkyne as a nucleophile and thus increase the reaction rate of the strain-promoted cycloaddition [74].

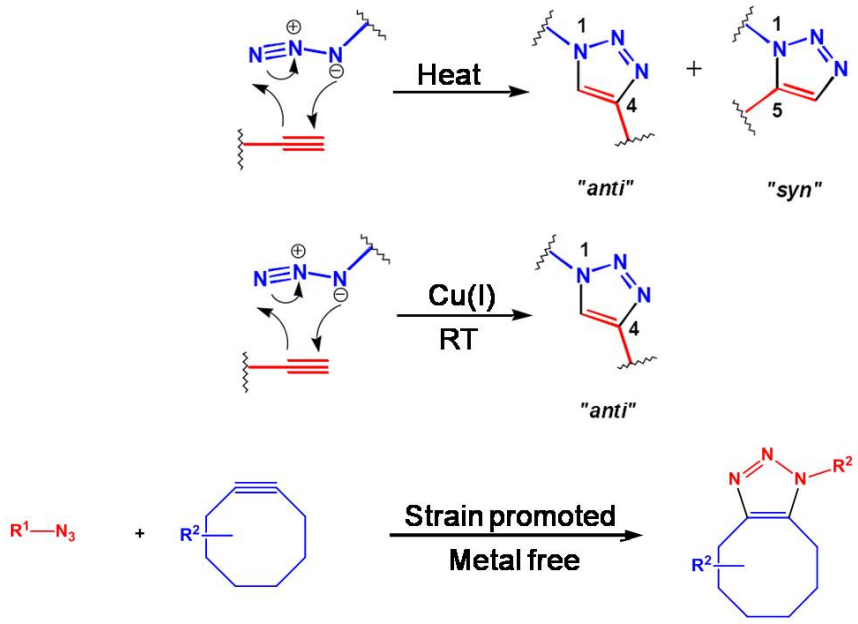

Figure 4-2 Examples of heat-generated, copper-catalyzed, strain-promoted azide-alkyne cycloaddition reactions.

Applying the strain-promoted polymerization of azide-alkyne click components in reverse microemulsions is expected in the following experiments and results parts to allow the synthesis of nano-sized hydrogels with controllable size, shape, composition, and crosslinking density, while avoiding toxic catalysts and free radicals that are considered to be harmful for biomedical applications. We put efforts in studying the chemical composition, size, polydispersity, stability, and swelling behavior of the resulting nanogels from this novel method.

4.2 Materials and methods

4.2.1 Crosslinker synthesis

Microemulsion-templated nanogels were formed via copper-free azide-octyne [3+2] cycloaddition. Both the cyclooctyne-containing poly(ethylene glycol) (PEG)-based crosslinker and azide-containing PEG-based copolymer were generously provided by our collaborators, Dr. Xinghai Ning and Dr. Scott Wilson in Dr. Niren Murthy's Group in the School of Biomedical Engineering at Georgia Tech.

The process to synthesize is as shown in Figure 4-3. The main part of the crosslinker is linear PEG chain to ensure the solubility of the crosslinker in water solution. Both ends of the crosslinker are cyclic-alkyne with two benzyl appending groups to further withdraw electrons. After each step of this process, the target product is separated and purified in a silica gel column.

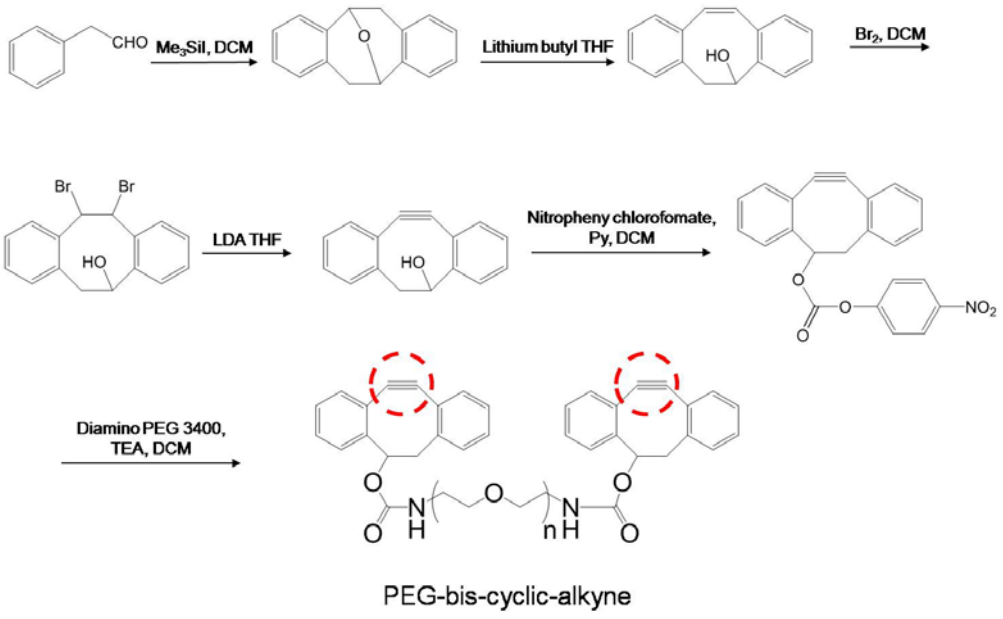

Figure 4-3 Synthesis process of the PEG-bis-cyclic-alkyne crosslinker.

4.2.2 Copolymer synthesis

The azide-containing copolymer is formed via the polymerization from two monomers: a PEG-acrylate and an acrylate-PEG-azide. These two components are combined at a 4:1 molar ratio in a Schlenk flask. With the participation of a micro reversible addition fragmentation chain transfer (RAFT) agent (benzothioylsulfanyl) acetic acid (1:100, uRAFT:total monomer) and azobisisobutyronitrile (AIBN) (1:10000, uRAFT:total monomer) in dimethylformamide (DMF), the reaction flask was degassed by five freeze-pump-thaw cycles, and then immersed in an oil bath magnetically stirring at 70 °C for 20 hours.

After reaction terminated by flash freezing the flask in liquid nitrogen, the products were dissolved in dichloromethane (DCM), and then further diluted in methanol. Since the polymer is not soluble in methanol, it precipitated out after mixing the DCM solution with methanol. The supernatant was decanted and the precipitated polymer was subjected to three more cycles of re-suspension and precipitation. The purified polymer was concentrated under reduced pressure and ready for use.

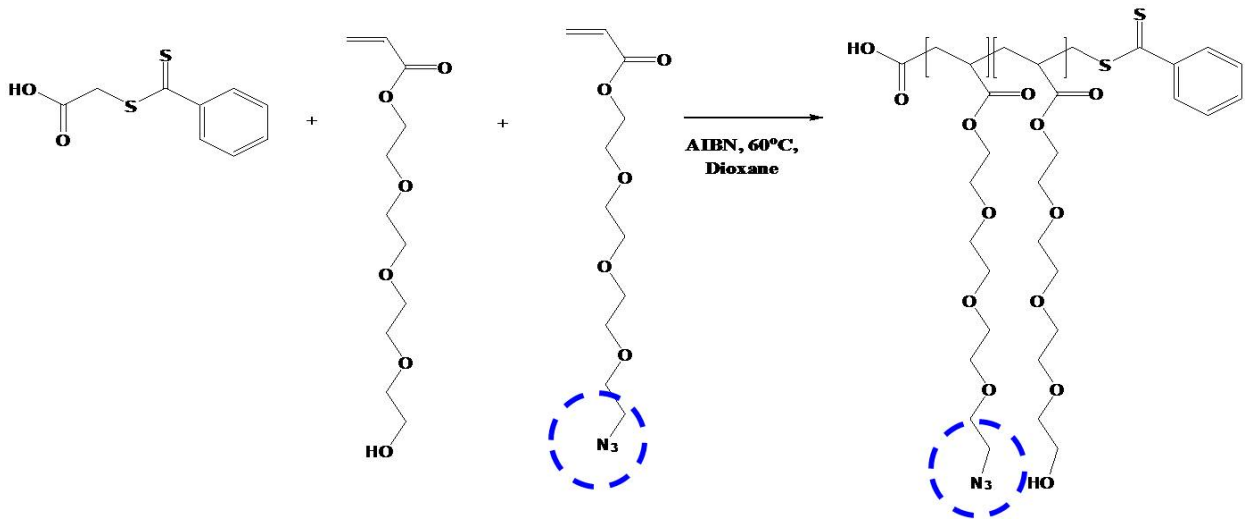

Figure 4-4 Synthesis process of PEG-based heterogeneous copolymer with azide as a side group.

The final heterogeneous copolymer was analyzed by gel permutation chromatography (GPC) and its structure and purity were tested by 1H nuclear magnetic resonance (NMR). It was confirmed that the molecular weight of the copolymer is 22 kDa with a polydispersity of 2.1. On the NMR spectrum, the monomer peaks were almost not visible and less than 1% of the final products, so the polymer concentration is > 99% pure.

4.2.3 Surfactant solutions

Surfactant solutions were prepared just as described in section 2.2.1, by precisely measuring the weight of the surfactants and the volume of the solvents and simply mixing them on a magnetic stirring plate over night. The well dissolved solutions appeared stable and transparent. AOT in hexane solutions were colorless. All surfactant solutions were allowed to equilibrate for 1 day prior to use. All experiments were performed in a

thermostated environment at 22 ± 0.5 ℃.

The surfactant was AOT (Sigma-Aldrich), used without further purification. The solvents included hexane (BDH, ACS grade) and acetone (Sigma-Aldrich, > 99.5%).

Ultrapure water with a resistivity of 18.3 $M\Omega \cdot cm$ (Barnstead) was used for swelling reverse micelles and for dispersing the formed nanogels transferred from the hydrophilic core of the micro emulsions via solvent swap. Besides the crosslinker and copolymer provided by Murthy's group, other dissolved monomers in aqueous swelling solutions were PEG-diacrylate (Sigma-Aldrich, Mw: 575 and 700 g/mol).

4.2.4 Nanogel synthesis

The dissolved AOT molecules self-assembled to form reverse micelles with a core-shell structure in nonpolar solvent such as hexane. Subsequent addition of water into the AOT/hexane solution induced swelling of the hydrophilic micelle cores. Aqueous solution of the crosslinker was then mixed into the microemulsions, whereby the aqueous droplets were further enlarged. In the following step, anaqueous solution of the copolymer was added and also incorporated into the aqueous core. The PEG base of the crosslinker and copolymer were carefully selected to maintain enough aqueous solubility and keep the relaxed-state size small enough to be encapsulated inside the microemulsion droplets because over-sized polymer chain cannot stably stay in the aqueous core and thus cause phase separation.

Once both alkyne crosslinker and azide copolymer co-existed in the same microemulsion, the cycloaddition reaction happened instantaneously. The formed

nanogel particles were then collected transferred into aqueous solution via solvent swap. The entire experimental procedure is described schematically in Figure 4-5. The order of swelling the AOT reverse micelles by crosslinker aqueous solution prior to the copolymer solution made stable swollen microemulsion after mixing the components. Instead, we confirmed that adding copolymer solution to swell the AOT reverse micelles first would cause phase separation.

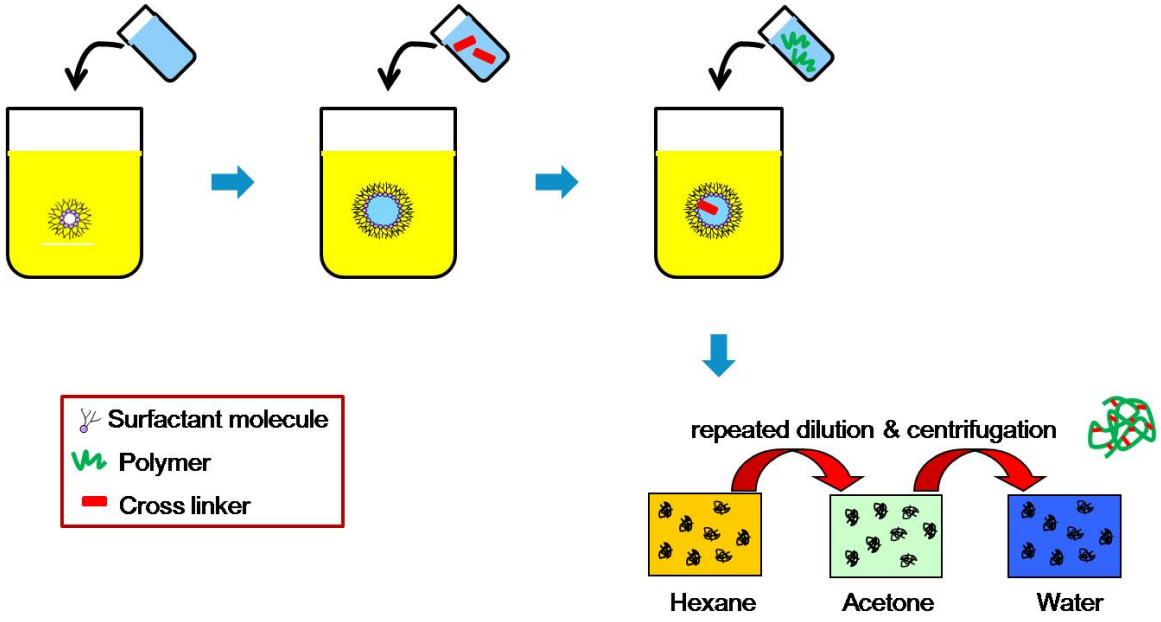

Figure 4-5 Experimental procedure of nanogels preparation.

For comparison with a more conventional method of preparing PEG-based nanogels than azide-alkyne cycloaddition, we also used free radical polymerization of PEG diacrylate to synthesize nanogels in the hydrophilic core of AOT microemulsion in hexane. Free radicals drive a polymerization reaction at both acrylate end groups of short

chains of PEG diacrylate monomers, which thus connect into a crosslinked polymer network. The experiments were carried out in a similar fashion as the ones described by Figure 4-5, except that the monomers and initiator 2,2'-azino-bis(3-ethylbenzothiazoline-6-sulphonic acid) (ABTS) were added in the same step from a single aqueous solution. Continuous exposure to UV light for 12 hours was used to initiate the polymerization. The hydrodynamic size of the resulting PEG diacrylate nanogel was analyzed by DLS and compared with the nanogel formed by "click" components.

4.2.5 Nanogel dispersion via solvent swap

The microemulsion-templated nanogel synthesis yields a dispersion of nanogel particles in AOT/hexane. Transfer of the particles into water was similar to the solvent swap described in section 3.2.2. An aliquot of the nanogel dispersion in hexane is diluted with the same volume of acetone, well mixed, and centrifuged for 20 minutes at 12000 r/min. The supernatant is discarded (and with it most of the surfactants), the concentrated bottom phase is collected and diluted it with pure acetone. After sonication for about 5 minutes, the centrifugation, disposal of the supernatant, dilution, and sonication is repeated for three more cycles. The dispersant is replaced by a 50% acetone/50% water mixture, and then by pure water. After completion of the solvent swap, the resulting nanogels are fully dispersed in the aqueous environment. The size and morphology are then tested by dynamic light scattering and SEM.

4.2.6 Dynamic light scattering

Dynamic light scattering (ALV/DLS/SLS-5022F) was used to measure the

hydrodynamic size of the original reverse micelles, microemulsion droplets, and the synthesized nanogels, dispersed in either hexane or water.

4.2.7 SEM

The nanogels were freeze-dried from the aqueous dispersion under reduced pressure to best maintain the three-dimensional structure. The dried nanogel particles were gently transferred onto carbon SEM sample substrates. Then the size, morphology, and distribution of the nanogels in the dry state were studied by SEM (Zeiss Ultra60).

4.3 Results and discussions

We combined the techniques of reverse microemulsion polymerization and copper-free azide-alkyne cycloaddition to prepare nano-sized hydrogels with controlled size and morphology of the nanogel particles while avoiding free radicals and metal catalysts that would limit biomedical applications

The core of water-swollen reverse AOT micelles serves as a reactor for the investigated nanogel synthesis. Since we are interested in understanding how this reactor controls the size of the generated nanogel particles, we start by systematically studying the micelle size as a function of solubilized water and AOT concentration. We then first discuss the nanogels synthesis by conventional free-radical polymerization of PEG diacrylate in the aqueous micelle cores. Finally we present the results of our attempts to template nanogels crosslinked by the copper-free "click" reaction of azide PEG-based copolymers and cyclooctyne crosslinker. Observed difference between these two types of nanogels is explained by considering the respective rates of the crosslinking reaction and the lifetime of reverse AOT micelles.

4.3.1 Reverse microemulsion stabilized by AOT

We measured and confirmed that the hygroscopic surfactant AOT can introduce a substantial amount of water into nonpolar dispersions and that the water content is directly related to the AOT concentration (Figure 3-29). Here, we studied the water content and micellar size in AOT/hexane solutions for different surfactant concentrations and varying amounts of water added deliberately to swell the micelles. After magnetic stirring, the added water was fully dissolved into the hexane solution, and we used DLS

to measure the droplet size; the results are shown in Figure 4-9.

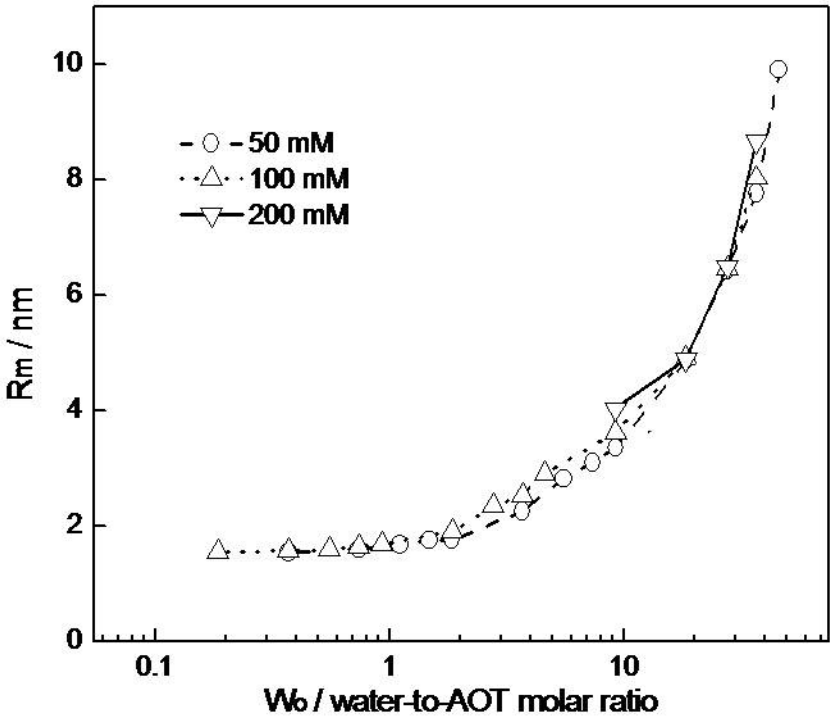

Figure 4-6 Hydrodynamic size of water swollen AOT microemulsions in hexane.

It is not surprising that the hydrodynamic size of water swollen AOT micelles increases with the water content at every given AOT concentration because the added water takes up more space in the surfactant hydrophilic core. From Figure 4-6, we also infer that the swelling degree is a function of the overall water-to-AOT molar ratio only, regardless of the absolute mass of water added into the solution and the absolute surfactant concentration. This observation leads to convenient conclusion regarding the choice of surfactant concentrations when using swollen micelles as reactors for nanogel synthesis: the reactor size can be controlled by varying the water-to-surfactant ratio and is otherwise insensitive to the surfactant concentration. We chose to use the hexane

solutions with 100 mM AOT and vary the volume of added aqueous monomer or crosslinker solution.

4.3.2 PEG diacrylate nanogel

Similar to McAllister's work [57] of preparing acrylate nanogels via free radical polymerization in laureth-3 stabilized reverse microemulsionsin heptane, we used PEG diacrylate to simply prepare nanogels in water/AOT/hexane reverse microemulsions as a reference point for the novel "click" nanogels synthesis discussed later.

In AOT/hexane system, the reverse micelles were swollen by pure water, by aqueous solution containing PEG, or by PEG diacrylate chains (at different molecular weight and different concentration) that serve as potential "monomer" for the crosslinking reaction. Since these organic solutes are different in solution from water molecules, the swelling of reverse micelles by PEG solution must be expected to differ from swelling by pure water. The molecular weight of the PEG "monomer" indicates the length of hydrocarbon chain, and influences the size of swollen microemulsion droplets. In addition, PEG diacrylate is more hydrophobic than PEG chains without the acrylate end groups, which results in a different relaxed size for the same chain length.

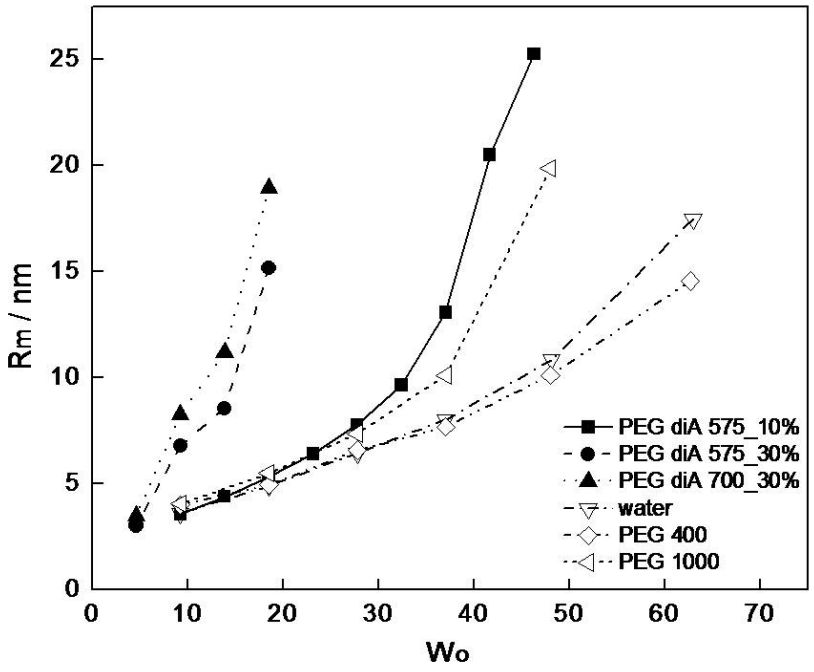

Figure 4-7 Hydrodynamic size of microemulsion swollen by water or aqueous PEG solution in AOT/hexane solution. Numbers in the legend denote the molecular weight of the PEG solute.

The hydrodynamic size of AOT microemulsion swollen by pure water, PEG in water solution at different molecular weight, and PEG diacrylate in water solution at different molecular weight and mass concentration is shown in Figure 4-7. The microemulsions grow with the addition of water and aqueous solutions. The shortest chain of PEG at 400 g/mol shows the most similar swelling capability to pure water. When the molecular weight of PEG increases to 1000 g/mol, the longer PEG chain requires more space in the aqueous droplets of the reverse microemulsion for the same volume of aqueous solution added into the AOT/hexane system. Solutions of larger PEG chains (>4000 g/mol) could not be solubilized, but phase separated from the microemulsion.

Appending acrylate groups to both ends of PEG chain increases the hydrophobicity of the solute, the size of microemulsion droplets shown in Figure 4-7 is found significantly increased when comparing PEG diacrylate 575 with PEG 400, and even compared to PEG 1000 (the number in the solute name always indicating its molecular weight). Moreover, with the addition of the same volume of aqueous solution, concentrated solution further swells the AOT microemulsion when increasing the mass concentration of PEG diacrylate 575 from 10% to 30% in water. Consistently, PEG diacrylate 700 at 30% in water solution confirms the above conclusions that the solute with larger molecular weight (chain length), higher hydrophobicity, and larger concentration in aqueous solution leads to the largest size of swollen reverse microemulsion.

To carry out the free radical polymerization in the hydrophilic core of reverse microemulsion, PEG diacrylate with molecular weight of 575 g/mol at 10% in water was used as monomer to synthesize PEG hydrogels in reverse microemulsions. Together with the water-soluble ABTS as radical initiator, the aqueous mixture was added into 100 mM AOT/hexane solution and fully solubilized without showing any signs of phase separation. UV light was used initiate to the generation of free radicals. With the help of ABTS, the originally transparent microemulsion turns opaque and polymerization is completed.

The resulting nanogels were transferred and re-dispersed into water via solvent swap with acetone as the intermediate solvent. Figure 4-8 compares the hydrodynamic size of microemulsion droplets swollen by aqueous PEG diacrylate monomer solution (triangles) and of the resulting PEG nanogel particles after transfer into water (squares).

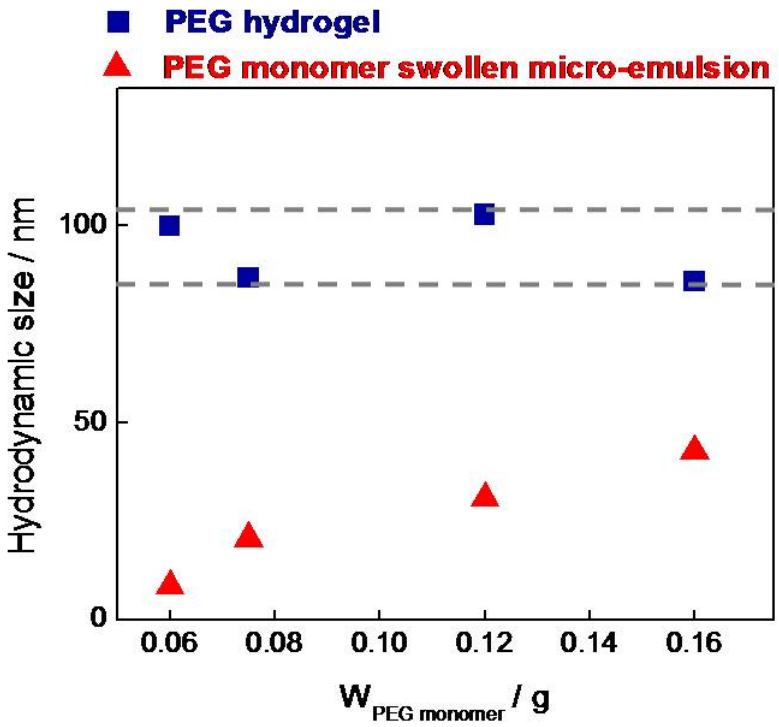

Figure 4-8 Hydrodynamic size of the microemulsions swollen by PEG diacrylate monomer in aqueous solution (triangular markers) and of the PEG nanogels transferred in water dispersion (square markers) as a function of added monomer weight in the PEG diacrylate 575 g/mol at 10 wt.% aqueous solution. Gray dashed lines show the size range of the formed PEG nanogels.

Figure 4-8 shows that the final nanogel particles are significantly larger than the swollen reverse micelles where the nanogels were formed in, and there is no clear correlation between the particle and reactor size.

The click reaction differs from the PEG diacrylate polymerization in many ways, including chain length, molecular size of solutes in aqueous solution, and overall reaction rate. The preparation of nanogel from azide-alkyne cycloaddition using AOT reverse microemulsion as a template will be introduced next to verify the consistency of the formed nanogel size to the aqueous container size in microemulsion.

4.3.3 “Click” nanogel

PEG-bis-cyclic-octyne and heterogeneous PEG-azido copolymer were selected as the crosslinker and polymer material for the nanogel synthesis. The network structure of the crosslinked hydrogel is shown in Figure 4-9, in which the moiety marked by the green circle is formed via [3+2] cycloaddition of the alkyne group marked by the red circle in Figure 4-3 and the azide group marked by the blue circle in Figure 4-4.

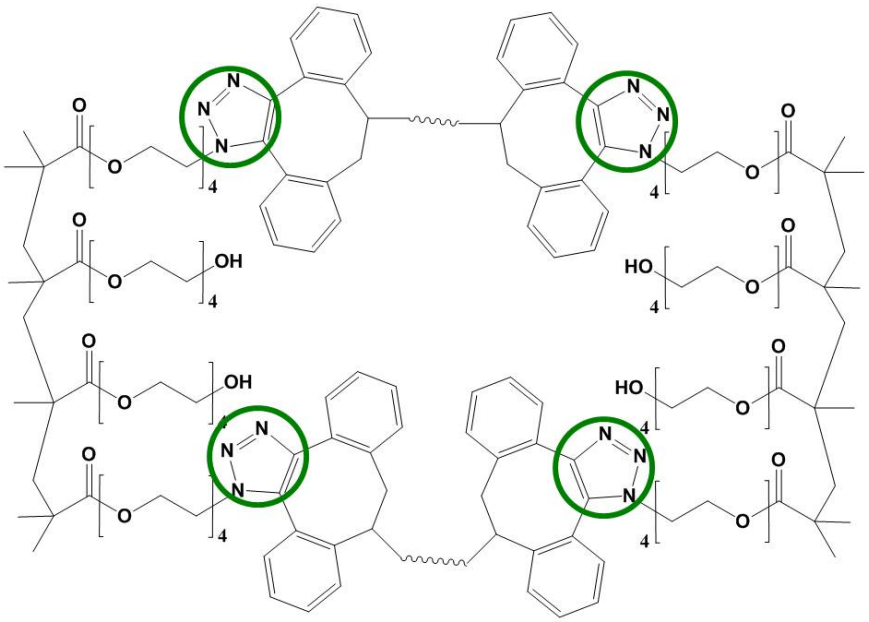

Figure 4-9 Structure of the crosslinked polymer from azide-alkyne cycloaddition.

With the promotion of ring strain in cyclooctyne, the cycloaddition happens spontaneously, without the need for a copper catalyst. The two components react instantaneously upon contact, so we cannot simply mix them together in water before feeding them into the microemulsion droplets; instead aqueous solutions of the crosslinker and the copolymer need to be added into the AOT/hexane solution in

separated steps.

Both the crosslinker and the copolymer are PEG-based to ensure water solubility. Since the cyclooctyne crosslinker has a smaller molecular weight than the copolymer, it is expected to require less space upon inclusion in the microemulsion droplets. Therefore, we added the crosslinker solution first and the copolymer solution second. The other way around was confirmed to cause phase separation.

The hydrodynamic diameter of the reverse microemulsion swollen by aqueous solution of 1 wt.% PEG-bis-cyclooctyne crosslinker is shown in Figure 4-10. According to DLS, the crosslinker solution swells the microemulsion droplets to a size range of 200-300 nm, independently of the absolute amount of crosslinker added into the hexane solution. It is unknown exactly how the incorporation of large aqueous solutes into the microemulsion droplets proceeds, but there clearly is a big difference to swelling by pure water where the total aqueous volume dictates the average droplet size. Here, it seems more as if the space requirement of individual solutes determined the droplet size. A possible explanation to the independency of droplet size in crosslinker amount is that there are crosslinker-filled and unfilled microemulsions existing together upon swelling, although the number of each is not clear. DLS is sensitive to the largest droplets, so the apparent droplet size is insensitive to the total crosslinker concentration.

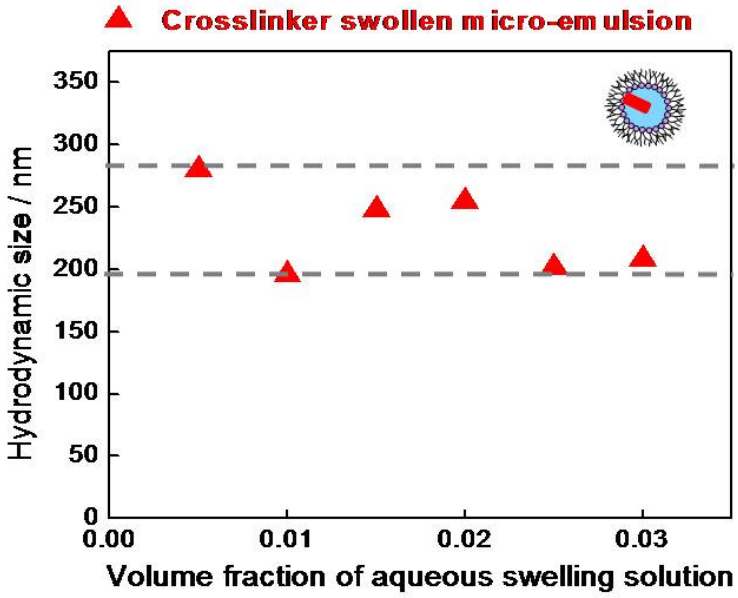

Figure 4-10 Hydrodynamic size of the microemulsions swollen by an aqueous solution of 1 wt.% PEG-based cyclooctyne crosslinker. Gray dashed lines show the size range of the reverse microemulsions.

A fixed volume of PEG-azido copolymer solution in 1 wt.% was added to the mixture next. Magnetic stirring fully dissolved the copolymer solution into the reverse microemulsion. After the spontaneous cycloaddition reaction, the crosslinked nanogels were transferred and re-dispersed into water via solvent swap. The hydrodynamic diameter of the resulting nanogel was measured by DLS and is shown in Figure 4-11.

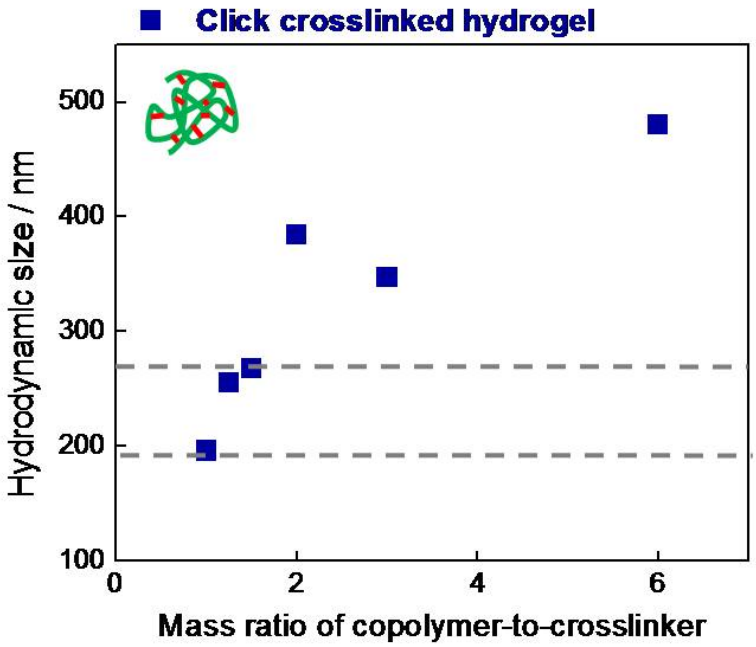

Figure 4-11 Hydrodynamic size of the nanogels from azide-alkyne cycloaddition in reverse microemulsion transferred into water dispersion. Gray dashed lines show the size range of the reverse microemulsions in Figure 4-10.

The grey dashed lines in Figure 4-11 indicate the size range of the crosslinker swollen microemulsion, which is also the container size of the click reaction. As one might expect from a more densely crosslinked network, the nanogels formed at a higher crosslinker-to-copolymer ratio remain more compact when transferred into water. In the range of higher crosslinker concentration, the final nanogel particles have a similar size as the aqueous reactors where they were formed. Thus, we have successfully prepared "click" nanogels with a size dictated by the droplets of a reverse microemulsion. Lower crosslinker density however, leads to nanogel particles above the size range of the templating microemulsion droplets.

We also studied the size and morphology of the formed nanogels after freeze-drying by SEM. Selected SEM images are shown in Figure 4-16. The dry nanogels are around 100-150 nm in diameter, substantially smaller than the ones dispersed in water.

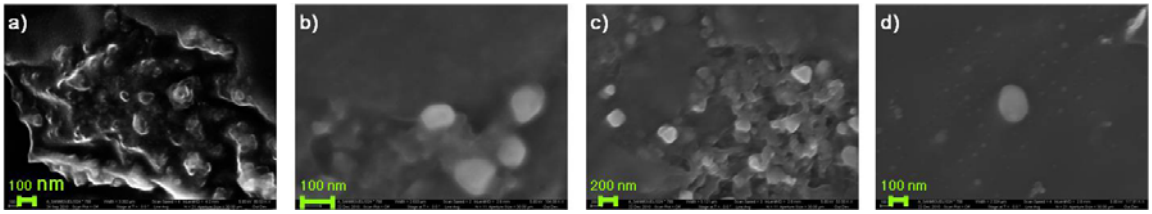

Figure 4-12 SEM images of the crosslinked nanogels formed with "click" components after freeze drying. a) and b) present the SEM images for nanogel formed by the copolymer-to-crosslinker mass ratio at 1.0; c) and d) present the ones at 1.5.

4.3.4 Kinetic analysis in nanogel preparation

The PEG diacrylate nanogels were generally larger than their containers of free radical polymerization, whereas the "click" nanogels stayed in the size range of the templates if they were highly crosslinked. To rationalize this observation, we consider the kinetics involved in the nanogel preparation in reverse microemulsion.

As the container for the nanogel synthesis, the structures of the swollen reverse micelles or microemulsions are at the thermodynamical equilibrium in nonpolar solution. An exchange mechanism explains the coalescence and separation of transient droplets stabilized by AOT. The equilibrium of this dynamic process maintains the size and polydispersity of the microemulsions, when the components involved in the hydrophilic core have chances to expose to others during the exchange.

The surfactant exchange rates were measured using very fast chemical reactions

as indicators for exchange [75] and time-resolved fluorescence probing [76]. For AOT reverse micellar system and corresponding reverse microemulsions, their lifetime are reported to be approximately on a millisecond timescale, dependent in surfactant concentration, hydrodynamic size of microemulsion, aggregation number, and environmental temperature [75-77]. Despite this variation, it is clear that in the case of PEG diacrylate nanogels, the timescale of (free radical) polymerization is much larger than the characteristic time of surfactant exchange between different micelles. The reverse micelles therefore should not be expected to act like a static confinement over the course of the crosslinking reaction that would imprint the reactor size onto the nascent particle. Instead, an exchange of reactants between different micelles during the polymerization is likely and would explain why the resulting nanogels are systematically larger than the templating micelle cores. It would be nice to document the droplet size increase in the microemulsion during the reaction, but that this cannot be done, at least by DLS, because the raising turbidity makes DLS intractable.

By contrast, the reaction rate of the strain-promoted cycloaddition [66, 72, 74] is comparable to the exchange rate in AOT microemulsions. The nanogel synthesis is completed so fast that little or no exchange between the droplets is expected to take place during the reaction, and thus the forming nanogels truly confined by its host droplet, and if highly crosslinked, it cannot expand much further even when the confinement is removed by transfer into water. The formed nanogel, thus, retains a size consistent with the hydrophilic core of the microemulsion.

4.4 Conclusions

As hydrophilic polymer networks, hydrogels have valuable properties including large water content, mechanical flexibility, variable physical and chemical structure, etc. When hydrogels approach sub-micro meter range in dimension, the micro/nanogels have wide and important applications in biomedical areas. However, it is challenging to prepare nanogels with controllable small size and morphology without introducing free radicals or metal catalysts that constitute hazards for biological tissues or sensitive nanogel cargoes. In this chapter, we discussed hydrogel synthesis in the core of water swollen reverse surfactant micelles in nonpolar media. The aqueous core provided the reaction space for nanogel synthesis, and the shell, composed of surfactant molecules, provided some size limitation for the resulting nanogels.

We investigated the nanogels prepared from PEG diacrylate by free radical polymerization and from "click" components by azide-alkyne [3+2] cycloaddition. Nanogels were successfully obtained from polymerization in reverse microemulsion, and their dimensions explained qualitatively by comparing the rate of exchange between reverse surfactant micelles and the reaction rate of polymerization. PEG diacrylate nanogels were generally larger than the microemulsion core size because free radical polymerization proceeds at a much slower pace than the exchange between of AOT micelles, whereas the size of highly crosslinked "click" nanogels is consistent with the micelle size because the cycloaddition reaction can be completed within the micelle lifetime.

To test the nanogels in practical applications, the physical stability of nanogels,

the uptake and release of cargo, and the viability of cells and pharmaceutical actives should be investigated in future studies.

4.5 References

1. Christensen, L.H., Breiting, V.B., Aasted, A., Jørgensen, A. & Kebuladze, I. Long-Term Effects of Polyacrylamide Hydrogel on Human Breast Tissue. *Plastic and Reconstructive Surgery* **111**, 1883-1890 1810.1097/1801.PRS.0000056873.0000087165.0000056875A (2003).

2. Langer, R. Perspectives: Drug delivery - Drugs on target. *Science* **293**, 58-59 (2001).

3. Missirlis, D., Tirelli, N. & Hubbell, J.A. Amphiphilic hydrogel nanoparticles. Preparation, characterization, and preliminary assessment as new colloidal drug carriers. *Langmuir* **21**, 2605-2613 (2005).

4. Huang, G. *et al.* Controlled drug release from hydrogel nanoparticle networks. *Journal of Controlled Release* **94**, 303-311 (2004).

5. Peppas, N.A., Hilt, J.Z., Khademhosseini, A. & Langer, R. Hydrogels in biology and medicine: From molecular principles to bionanotechnology. *Advanced Materials* **18**, 1345-1360 (2006).

6. Langer, R. & Vacanti, J.P. Tissue Engineering. *Science* **260**, 920-926 (1993).

7. Brandl, F., Sommer, F. & Goepferich, A. Rational design of hydrogels for tissue engineering: Impact of physical factors on cell behavior. *Biomaterials* **28**, 134-146 (2007).

8. Jones, L. *et al.* Lysozyme and Lipid Deposition on Silicone Hydrogel Contact Lens Materials. *Eye & Contact Lens* **29**, S75-S79 (2003).

9. Okay, O. & Oppermann, W. Polyacrylamide-clay nanocomposite hydrogels: Rheological and light scattering characterization. *Macromolecules* **40**, 3378-3387 (2007).

10. Miyazaki, S., Endo, H., Karino, T., Haraguchi, K. & Shibayama, M. Gelation mechanism of poly(N-isopropylacrylamide)-clay nanocomposite gels. *Macromolecules* **40**, 4287-4295 (2007).

11. Haraguchi, K. & Song, L.Y. Microstructures formed in co-cross-linked networks and their relationships to the optical and mechanical properties of PNIPA/clay nanocomposite gels. *Macromolecules* **40**, 5526-5536 (2007).

12. Li, C.M. *et al.* Synthesis and characterization of biocompatible thermo-responsive gelators based on ABA triblock copolymers. *Biomacromolecules* **6**, 994-999 (2005).

13. Mi, L.X., Fischer, S., Chung, B., Sundelacruz, S. & Harden, J.L. Self-assembling protein hydrogels with modular integrin binding domains. *Biomacromolecules* **7**,

38-47 (2006).

14. Miyauchi, M., Takashima, Y., Yamaguchi, H. & Harada, A. Chiral supramolecular polymers formed by host-guest interactions. *Journal of the American Chemical Society* **127**, 2984-2989 (2005).

15. Miyauchi, M., Hoshino, T., Yamaguchi, H., Kamitori, S. & Harada, A. A 2 rotaxane capped by a cyclodextrin and a guest: Formation of supramolecular 2 rotaxane polymer. *Journal of the American Chemical Society* **127**, 2034-2035 (2005).

16. Dai, H.J. *et al.* A temperature-responsive copolymer hydrogel in controlled drug delivery. *Macromolecules* **39**, 6584-6589 (2006).

17. Park, H. & Robinson, J.R. Mechanisms of Mucoadhesion of Poly(acrylic Acid) Hydrogels. *Pharmaceutical Research* **4**, 457-464 (1987).

18. Sanabria-DeLong, N., Agrawal, S.K., Bhatia, S.R. & Tew, G.N. Impact of Synthetic Technique on PLA−PEO−PLA Physical Hydrogel Properties. *Macromolecules* **40**, 7864-7873 (2007).

19. de Jong, S.J., van Eerdenbrugh, B., van Nostrum, C.F., Kettenes-van den Bosch, J.J. & Hennink, W.E. Physically crosslinked dextran hydrogels by stereocomplex formation of lactic acid oligomers: degradation and protein release behavior. *Journal of Controlled Release* **71**, 261-275 (2001).

20. Murakami, S. & Aoki, N. Bio-based hydrogels prepared by cross-linking of microbial poly(gamma-glutamic acid) with various saccharides. *Biomacromolecules* **7**, 2122-2127 (2006).

21. Levesque, S.G. & Shoichet, M.S. Synthesis of enzyme-degradable, peptide-cross-linked dextran hydrogels. *Bioconjugate Chemistry* **18**, 874-885 (2007).

22. Lin-Gibson, S., Bencherif, S., Antonucci, J.M., Jones, R.L. & Horkay, F. Synthesis and characterization of poly(ethylene glycol) dimethacrylate hydrogels. *Macromolecular Symposia* **227**, 243-254 (2005).

23. Shah, N.M., Pool, M.D. & Metters, A.T. Influence of network structure on the degradation of photo-cross-linked PLA-b-PEG-b-PLA hydrogels. *Biomacromolecules* **7**, 3171-3177 (2006).

24. Pitarresi, G., Pierro, P., Palumbo, F.S., Tripodo, G. & Giammona, G. Photo-cross-linked hydrogels with polysaccharide-poly(amino acid) structure: New biomaterials for pharmaceutical applications. *Biomacromolecules* **7**, 1302-1310 (2006).

25. Tsou, T.L. *et al.* Poly(2-hydroxyethyl methacrylate) wound dressing containing ciprofloxacin and its drug release studies. *Journal of Materials Science-Materials*

in Medicine **16**, 95-100 (2005).

26. Park, D.W., Haam, S., Lee, T.G., Kim, H.S. & Kim, W.S. Chemoenzymatic synthesis of sugar-containing biocompatible hydrogels: Crosslinked poly(beta-methylglucoside acrylate) and poly(beta-methylglucoside methacrylate). *Journal of Biomedical Materials Research Part A* **71A**, 497-507 (2004).

27. Sahiner, N., Godbey, W.T., McPherson, G.L. & John, V.T. Microgel, nanogel and hydrogel-hydrogel semi-IPN composites for biomedical applications: synthesis and characterization. *Colloid and Polymer Science* **284**, 1121-1129 (2006).

28. Graham, N.B. & Cameron, A. Nanogels and microgels: The new polymeric materials playground. *Pure and Applied Chemistry* **70**, 1271-1275 (1998).

29. Harris, J.M. & Chess, R.B. Effect of pegylation on pharmaceuticals. *Nature Reviews Drug Discovery* **2**, 214-221 (2003).

30. Vicent, M.J. *et al.* Polymer therapeutics designed for a combination therapy of hormone-dependent cancer. *Angewandte Chemie-International Edition* **44**, 4061-4066 (2005).

31. Wu, J. & Eisenberg, A. Proton diffusion across membranes of vesicles of poly(styrene-b-acrylic acid) diblock copolymers. *Journal of the American Chemical Society* **128**, 2880-2884 (2006).

32. Bae, Y., Fukushima, S., Harada, A. & Kataoka, K. Design of environment-sensitive supramolecular assemblies for intracellular drug delivery: Polymeric micelles that are responsive to intracellular pH change. *Angewandte Chemie-International Edition* **42**, 4640-4643 (2003).

33. Harada, A. & Kataoka, K. Supramolecular assemblies of block copolymers in aqueous media as nanocontainers relevant to biological applications. *Progress in Polymer Science* **31**, 949-982 (2006).

34. Nishiyama, N. & Kataoka, K. Nanostructured devices based on block copolymer assemblies for drug delivery: Designing structures for enhanced drug function, in *Polymer Therapeutics Ii: Polymers as Drugs, Conjugates and Gene Delivery Systems*, Vol. 193. (eds. R. SatchiFainaro & R. Duncan) 67-101 (Springer-Verlag Berlin, Berlin; 2006).

35. Gupta, A.K. & Wells, S. Surface-modified superparamagnetic nanoparticles for drug delivery: Preparation, characterization, and cytotoxicity studies. *Ieee Transactions on Nanobioscience* **3**, 66-73 (2004).

36. Das, M., Sanson, N., Fava, D. & Kumacheva, E. Microgels loaded with gold nanorods: Photothermally triggered volume transitions under physiological conditions. *Langmuir* **23**, 196-201 (2007).

37. Fukui, T. *et al.* Intracellular delivery of nanogel-quantum dot hybrid nanoparticles into human periodontal ligament cells. *Drug metabolism letters* **1**, 131-135 (2007).

38. Nishikawa, T., Akiyoshi, K. & Sunamoto, J. Macromolecular complexation between bovine serum albumin and the self-assembled hydrogel nanoparticle of hydrophobized polysaccharides. *Journal of the American Chemical Society* **118**, 6110-6115 (1996).

39. Nishikawa, T., Akiyoshi, K. & Sunamoto, J. Supramolecular assembly between nanoparticles of hydrophobized polysaccharide and soluble-protein complexation between the self-aggregate of cholesterol-bearing pullulan and alpha-chymotrypsin. *Macromolecules* **27**, 7654-7659 (1994).

40. Lee, I. & Akiyoshi, K. Single molecular mechanics of a cholesterol-bearing pullulan nanogel at the hydrophobic interfaces. *Biomaterials* **25**, 2911-2918 (2004).

41. Akiyoshi, K. *et al.* Controlled association of amphiphilic polymers in water: Thermosensitive nanoparticles formed by self-assembly of hydrophobically modified pullulans and poly(N-isopropylacrylamides). *Macromolecules* **33**, 3244-3249 (2000).

42. Bodnar, M., Hartmann, J.F. & Borbely, J. Synthesis and study of cross-linked chitosan-N-poly(ethylene glycol) nanoparticles. *Biomacromolecules* **7**, 3030-3036 (2006).

43. Shen, X.C., Zhang, L.Y., Jiang, X.Q., Hu, Y. & Guo, J. Reversible surface switching of nanogel triggered by external stimuli. *Angewandte Chemie-International Edition* **46**, 7104-7107 (2007).

44. Zhang, H., Tumarkin, E., Sullan, R.M.A., Walker, G.C. & Kumacheva, E. Exploring microfluidic routes to microgels of biological polymers. *Macromolecular Rapid Communications* **28**, 527-538 (2007).

45. De Geest, B.G., Urbanski, J.P., Thorsen, T., Demeester, J. & De Smedt, S.C. Synthesis of monodisperse biodegradable microgels in microfluidic devices. *Langmuir* **21**, 10275-10279 (2005).

46. Zhang, H. *et al.* Microfluidic production of biopolymer microcapsules with controlled morphology. *Journal of the American Chemical Society* **128**, 12205-12210 (2006).

47. Xu, S.Q. *et al.* Generation of monodisperse particles by using microfluidics: Control over size, shape, and composition. *Angewandte Chemie-International Edition* **44**, 724-728 (2005).

48. Sugiura, S. *et al.* Size control of calcium alginate beads containing living cells using micro-nozzle array. *Biomaterials* **26**, 3327-3331 (2005).

49. Ma, Z. & Lacroix-Desmazes, P. Dispersion polymerization of 2-hydroxyethyl methacrylate stabilized by a hydrophilic/CO(2)-philic poly(ethylene oxide)-b-poly(1,1,2,2-tetrahydroperfluorodecyl acrylate) (PEO-b-PFDA) diblock copolymer in supercritical carbon dioxide. *Polymer* **45**, 6789-6797 (2004).

50. Jones, C.D. & Lyon, L.A. Synthesis and characterization of multiresponsive core-shell microgels. *Macromolecules* **33**, 8301-8306 (2000).

51. Serpe, M.J., Yarmey, K.A., Nolan, C.M. & Lyon, L.A. Doxorubicin uptake and release from microgel thin films. *Biomacromolecules* **6**, 408-413 (2005).

52. Bradley, M., Vincent, B. & Burnett, G. Uptake and release of anionic surfactant into and from cationic core-shell microgel particles. *Langmuir* **23**, 9237-9241 (2007).

53. Xiong, M.H. *et al.* Synthesis of PEG-Armed and Polyphosphoester Core-Cross-Linked Nanogel by One-Step Ring-Opening Polymerization. *Macromolecules* **42**, 893-896 (2009).

54. Oh, J.K., Tang, C.B., Gao, H.F., Tsarevsky, N.V. & Matyjaszewski, K. Inverse miniemulsion ATRP: A new method for synthesis and functionalization of well-defined water-soluble/cross-linked polymeric particles. *Journal of the American Chemical Society* **128**, 5578-5584 (2006).

55. Mitra, S., Gaur, U., Ghosh, P.C. & Maitra, A.N. Tumour targeted delivery of encapsulated dextran–doxorubicin conjugate using chitosan nanoparticles as carrier. *Journal of Controlled Release* **74**, 317-323 (2001).

56. Lee, H., Mok, H., Lee, S., Oh, Y.-K. & Park, T.G. Target-specific intracellular delivery of siRNA using degradable hyaluronic acid nanogels. *Journal of Controlled Release* **119**, 245-252 (2007).

57. McAllister, K. *et al.* Polymeric nanogels produced via inverse microemulsion polymerization as potential gene and antisense delivery agents. *Journal of the American Chemical Society* **124**, 15198-15207 (2002).

58. Gan, D.J. & Lyon, L.A. Tunable swelling kinetics in core-shell hydrogel nanoparticles. *Journal of the American Chemical Society* **123**, 7511-7517 (2001).

59. Hoare, T. & Pelton, R. Functional group distributions in carboxylic acid containing poly(N-isopropylacrylamide) microgels. *Langmuir* **20**, 2123-2133 (2004).

60. Yeh, J. *et al.* Micromolding of shape-controlled, harvestable cell-laden hydrogels. *Biomaterials* **27**, 5391-5398 (2006).

61. Franzesi, G.T., Ni, B., Ling, Y.B. & Khademhosseini, A. A controlled-release strategy for the generation of cross-linked hydrogel microstructures. *Journal of*

the American Chemical Society **128**, 15064-15065 (2006).

62. Kolb, H.C., Finn, M.G. & Sharpless, K.B. Click Chemistry: Diverse Chemical Function from a Few Good Reactions. *Angewandte Chemie International Edition* **40**, 2004-2021 (2001).

63. Tornoe, C.W., Christensen, C. & Meldal, M. Peptidotriazoles on solid phase: 1,2,3 -triazoles by regiospecific copper(I)-catalyzed 1,3-dipolar cycloadditions of terminal alkynes to azides. *Journal of Organic Chemistry* **67**, 3057-3064 (2002).

64. Rostovtsev, V.V., Green, L.G., Fokin, V.V. & Sharpless, K.B. A stepwise Huisgen cycloaddition process: Copper(I)-catalyzed regioselective "ligation" of azides and terminal alkynes. *Angewandte Chemie-International Edition* **41**, 2596-+ (2002).

65. Evans, R.A. The Rise of Azide–Alkyne 1,3-Dipolar 'Click' Cycloaddition and its Application to Polymer Science and Surface Modification. *Australian Journal of Chemistry* **60**, 384-395 (2007).

66. Oh, J.K., Drumright, R., Siegwart, D.J. & Matyjaszewski, K. The development of microgels/nanogels for drug delivery applications. *Progress in Polymer Science* **33**, 448-477 (2008).

67. Griffin, R.J. The medicinal chemistry of the azido group. *Progress in medicinal chemistry* **31**, 121-232 (1994).

68. Huisgen, R. 1,3-Dipolar Cycloadditions. Past and Future. *Angewandte Chemie International Edition in English* **2**, 565-598 (1963).

69. Wang, Q. *et al.* Bioconjugation by copper(I)-catalyzed azide-alkyne 3+2 cycloaddition. *Journal of the American Chemical Society* **125**, 3192-3193 (2003).

70. Speers, A.E., Adam, G.C. & Cravatt, B.F. Activity-based protein profiling in vivo using a copper(I)-catalyzed azide-alkyne 3+2 cycloaddition. *Journal of the American Chemical Society* **125**, 4686-4687 (2003).

71. Speers, A.E. & Cravatt, B.F. Chemical strategies for activity-based proteomics. *Chembiochem* **5**, 41-47 (2004).

72. Agard, N.J., Prescher, J.A. & Bertozzi, C.R. A strain-promoted 3+2 azide-alkyne cycloaddition for covalent modification of blomolecules in living systems. *Journal of the American Chemical Society* **126**, 15046-15047 (2004).

73. Turner, R.B., Jarrett, A.D., Goebel, P. & Mallon, B.J. Heats of hydrogenation. IX. Cyclic acetylenes and some miscellaneous olefins. *Journal of the American Chemical Society* **95**, 790-792 (1973).

74. Ning, X., Guo, J., Wolfert, M. & Boons, G.J. Visualizing Metabolically Labeled

Glycoconjugates of Living Cells by Copper-Free and Fast Huisgen Cycloadditions. *Angewandte Chemie International Edition* **47**, 2253-2255 (2008).

75. Fletcher, P.D.I., Howe, A.M. & Robinson, B.H. The kinetics of solubilisate exchange between water droplets of a water-in-oil microemulsion. *Journal of the Chemical Society, Faraday Transactions 1: Physical Chemistry in Condensed Phases* **83**, 985-1006 (1987).

76. Lang, J., Jada, A. & Malliaris, A. Structure and dynamics of water-in-oil droplets stabilized by sodium bis(2-ethylhexyl)sulfosuccinate. *The Journal of Physical Chemistry* **92**, 1946-1953 (1988).

77. Sato, H., Hirai, T. & Komasawa, I. Mechanism of formation of composite CdS-ZnS ultrafine particles in reverse micelles. *Industrial & Engineering Chemistry Research* **34**, 2493-2498 (1995).

CHAPTER 5

CONCLUSIONS AND RECOMMENDATIONS

We find that sorbitan oleate surfactants without dissociable groups can effectively raise the electric conductivity of nonpolar solvents as ionic surfactants usually do, and that they can do this at concentrations both above and below the critical micelle concentration (CMC). For Span 85 solutions in hexane, a linear increase of conductivity as a function of the surfactant concentration is found in both concentration regimes. Based on the statistical theory of equilibrium charge fluctuation, this linear conductivity dependence is expected if the charged species is created by disproportionation of two uncharged entities into a pair of oppositely charged objects. Reverse surfactant micelles are the most obvious species to undergo such a charging reaction above the CMC, and indeed, the hydrodynamic size of the ions, inferred from the experimental conductivity and the Debye length obtained independently (via particle interaction measurements), agrees with light scattering results for the micelle size. It remains unclear, however, exactly where in a charged micelle the electric charge resides. Ionizable impurities like water, simple salt solutions, or organic salts that can lower their ionization energy by incorporation in the hydrophilic micelle core, and may well be involved in the charge formation, but the conductivity appears to be limited by the size and number of host micelles rather than the concentration of impurities. Below the CMC, where no micelles are expected, conductivity and particle interaction measurements suggest a smaller “ion”, which we hypothesize to be a smaller (“pre-micellar”) complex of an ionogenic impurity with one or more surfactant molecules. For both concentration regimes, our findings

suggest that the conductivity of nonpolar solutions can be controlled conveniently and in a robust way via the surfactant concentration, without the need to know or control the impurity level. We expect that nonionic surfactants will prove useful as "charge control agents" especially for oils in contact with a water phase, to which *ionic* surfactants would tend to partition, thus losing their intended effects on the oil phase.

Besides the conductivity raise in nonpolar solvents, large electric surface potentials on suspended colloidal particles and efficient electrostatic stabilization of nonpolar dispersions are also found in association with surfactants. Surface charging and charge screening can be characterized by electrophoresis measurements. Extrapolation of electrophoretic mobility data to zero field strength is required to avoid misinterpretations of the strongly field dependent particle mobility at low surfactant concentrations. Surface charging and charge screening are observed both above and below the CMC, and thus reverse micelles are not necessary to produce strong charging effects. The particle pair interaction energy profiles suggest a "screened Coulomb" interaction with the participation of Span 85, in contrast to the unscreened ("counterion only") interaction reported for particles in dilute solutions of ionic surfactants.

We further investigated the charging mechanism in nonpolar dispersions. A reversal in the sign of particle charge upon transfer from water to Span 85/decane solution suggests that the surfactant's role in particle charging does not simply consist of facilitating the dissociation of the particles' surface groups. Charge transfer driven by acid-base interactions between the surfactants and particle materials appears to play a decisive role in determining the particle charge in the case of Span 85. At low Span 85 concentration without sufficient surfactant molecules, however, the dissociation of

surface groups appears to also contribute to the charge on the particle surface. In the case of AOT, dissociated surfactant molecules at the particle surface might be one more source of the apparent surface charge.

In order to better understand and fully explain the electrostatic phenomena in nonpolar media caused by surfactants, a wider selection of surfactants and better established surfactant solutions/dispersions are needed for further exploration. The targeted synthesis and purification of surfactants with systematically varied architecture and functional groups, resulting in a systematic variation of amphiphilicity and acid-base properties, would greatly facilitate the testing of hypotheses about the charging mechanisms.

Current research also focuses on very dilute particle dispersions, so it is worth working on more concentrated dispersion and studying the associated limitations of charge stabilization provided by surfactants. The stability of nonpolar dispersions in the presence of a contacting aqueous phase is another direction for future research. In this situation, nonionic surfactants should hold an advantage over ionic surfactants, which tend to get extracted by water as explained before.

In addition to the electrostatic charging phenomena, nonpolar surfactant systems are also involved in preparing nano-sized hydrogel. We are able to obtain nanogels from PEG diacrylate by free radical polymerization and from “click” components by azide-alkyne [3+2] cycloaddition, which takes place in the aqueous core of the reverse microemulsion droplets stabilized by AOT. The ring strain energy promoted cycloaddition avoids the toxic metal catalysts, free radicals, and heat, which are

hazardous in most biomedical applications. The size of the resulting nanogels is determined by the comparison of exchange rate between reverse surfactant micelles and the reaction rate of synthesis.

Further investigation in understanding the nanogel formation is recommended, including the potential of swelling and appending functional groups, physical stability, mechanical flexibility, and polydispersity. For instance, a systematic study of the crosslinking degree and its relation to resulting nanogel dimension should yield a better understand of swelling and degradation. Modification of the polymers by appended functional groups helps in studying the recognition of loaded cargo and targeted sites; modification of the crosslinker by designing branch structure would provide further control over the size and morphology of the nanogels. Moreover, the ability of cargo loading and delivery are also necessary for practical application and may introduce new challenges in future research.

VITA

Qiong Guo was born on June 07, 1984 in Zunyi, Guizhou, China. She moved to Dalian, Liaoning, China in 1993 with her family and stayed in Beijing, China for college study since 2002. She received the B.S. degree in Chemical Engineering from Tsinghua University in 2006. In the same year, she came to the US pursuing advanced study and received the M.S. degree in Chemical Engineering from Yale University in 2007.

After completing her M.S. degree, she joined the School of Chemical & Biomolecular Engineering at Georgia Institute of Technology and continued her doctoral research under the supervision of Dr. Sven H. Behrens. Her research focuses on the characterization of surfactant solutions, the electric charging phenomenon in nonpolar solution and dispersion mediated by surfactants, the design and synthesis of size controllable nanogels in surfactant micellar templates, etc.

During the four and a half years she spent at Georgia Tech, Qiong published several articles in peer reviewed journals and presented her work at the ChBE Graduate Student Symposium at Georgia Tech, at the annual meeting of the American Institute of Chemical Engineers (AIChE), at the American Chemical Society (ACS) meeting, and at the Southeast Meeting on Soft Materials. Apart from research, she enjoys playing basketball, swimming, dancing, and travelling,